SECURITY INFORMATION

[redacted]

Copy 218
RM L52A02

[redacted]

NACA RM L52A02

NACA

RESEARCH MEMORANDUM

7307

AN INVESTIGATION AT MACH NUMBERS OF 1.62 AND 1.93 OF THE LIFT EFFECTIVENESS AND INTEGRATED DOWNWASH CHARACTERISTICS OF SEVERAL IN-LINE MISSILE CONFIGURATIONS HAVING EQUAL-SPAN WINGS AND TAILS

By Carl E. Grigsby

Langley Aeronautical Laboratory
Langley Field, Va.

[redacted]

NATIONAL ADVISORY COMMITTEE FOR AERONAUTICS
WASHINGTON
April 11, 1952

[redacted]

Classification cancelled (or changed to UNCLASSIFIED

By Authority of NASA Tech Pub Announcement 124

(OFFICER AUTHORIZED TO CHANGE)

By .....

NAME AND 10 Feb 58

GRADE OF OFFICER MAKING CHANGE)

17 May 61

DATE

NATIONAL ADVISORY COMMITTEE FOR AERONAUTICS

RESEARCH MEMORANDUM

AN INVESTIGATION AT MACH NUMBERS OF 1.62 AND 1.93 OF THE LIFT EFFECTIVENESS AND INTEGRATED DOWNWASH CHARACTERISTICS OF SEVERAL IN-LINE MISSILE CONFIGURATIONS HAVING EQUAL-SPAN WINGS AND TAILS

By Carl E. Grigsby

SUMMARY

An investigation has been made at Mach numbers of 1.62 and 1.93 to determine the lift effectiveness and average downwash characteristics of several in-line missile configurations having rectangular and triangular tail plan forms. Breakdown tests were made for combinations of a body and four wing plan forms and two tail plan forms. For two locations of the wing relative to the tail, tests were made for two values of tail incidence angle so that average effective downwash angles at the tail might be calculated.

A comparison of the experimental lift-curve slopes of the body-wing configurations with the results of Nielsen and Kaattari (NACA RM A51J04) gave satisfactory agreement at both Mach numbers. A comparison of the experimental lift-curve slopes of the rectangular and triangular body-tail configurations with several theoretical results indicated that the best agreement is shown for the rectangular tail configurations. The complete configurations gave a sizable rearward movement in center-of-pressure location at low angles of attack with a leveling off at the higher angles which is a result of the tail moving away from the trailing vortex sheet with resulting lower values of downwash. A systematic decrease in tail efficiency with decreasing wing aspect ratio is shown with the triangular tail configurations indicating lower values of tail efficiency at low angles of attack with little difference between the tail plan forms at the higher angles.

INTRODUCTION

With the development of missile configurations having low-aspect-ratio wings and tails of nearly equal span, wing-tail-body interference has become of increasing importance, especially in the effects upon longitudinal stability. In particular, in-line configurations show considerable loss in stability at angles of attack near zero while interdigitated configurations show similar changes in stability, but at higher angles of attack. The investigation of reference 1 was made to determine some effects of varying wing and tail span upon the aerodynamic characteristics of several in-line missile configurations having rectangular wing and tail plan forms. These results showed that configurations having low-aspect-ratio wings and tails of nearly equal span resulted in nearly 100 percent wing downwash near 0° angle of attack and large changes in downwash and pitching moment as the angle of attack increases and the tail moves away from the trailing vortex sheet.

The calculation of wing downwash has received considerable attention and the results of several theoretical and experimental investigations have been published. In addition, several theoretical methods for predicting the interference between bodies and wings or bodies and tails have been developed. In general, experimental data are necessary to assess these theoretical methods because the complexity of the problem has thus far necessitated the use of restrictive assumptions in the development of most of the theoretical results. As a consequence of this need for experimental data in the assessment and development of theoretical methods, a large number of tests have been made in an investigation of a supersonic missile configuration and its modifications, and the results reported in references 2 to 4. These references present results for a number of missile configurations, both in-line and interdigitated.

As part of a continuing investigation of in-line missile configurations and as an extension of reference 1, a systematic series of tests have been made in the Langley 9-inch supersonic tunnel to determine the tail lift effectiveness of several in-line missile configurations having both straight- and swept-leading-edge-tail plan forms. Configurations having the same wing but with both a rectangular and a triangular tail were investigated in order that the effects of a nonuniform downwash distribution upon the lift of both a straight and a swept leading-edge tail might be determined. Tests with two values of tail incidence angle were made for each of the tail plan forms so that the average effective downwash at the tail might be isolated by the method given in reference 1. A comparison of the average effective downwash angles obtained from the data for the two tail plan forms will thus indicate indirectly the relative effectiveness of the two tails in "strip averaging" the downwash across the tail span. For each of the two tail plan forms, four wing plan forms at two longitudinal locations on the body were tested. The

results of these tests also permit comparison with a number of theoretical methods for predicting body-wing and body-tail interference.

SYMBOLS

A	aspect ratio $\left(b^2/S\right)$
b	wing span
$\bar{c}$	mean aerodynamic chord $\left(\frac{2}{S}\int_0^{b/2} c^2 dy\right)$
S	wing area, includes portion in body formed by extending wing leading and trailing edges
d	body diameter
α	angle of attack
i_t	tail incidence angle
ϵ	average flow angle at tail, positive downward
M	Mach number
ρ	stream density
V	velocity
p_o	stagnation pressure
q	dynamic pressure $\left(\frac{1}{2}\rho V^2\right)$
R	Reynolds number per inch
T_o	stagnation temperature
C_L	lift coefficient $\left(\frac{\text{Lift}}{qS}\right)$
C_D	drag coefficient $\left(\frac{\text{Drag}}{qS}\right)$
C_m	pitching-moment coefficient $\left(\frac{\text{Moment about center of gravity}}{qS\bar{c}}\right)$

c.p. center of pressure, body diameter behind body nose

C_{L_α} lift-curve slope $\left(\frac{\partial C_L}{\partial \alpha}\right)$

η_t wing-wake parameter $\left(\left(\frac{\partial C_L}{\partial i_t}\right)_{bw} \Big/ \left(\frac{\partial C_L}{\partial i_t}\right)_b\right)$

η_t' tail efficiency $\left(\frac{C_{L_{BWT}} - C_{L_{BW}}}{C_{L_{BT}} - C_{L_B}}\right)$

Subscripts:

BWT configuration of body, wing, and tail

BW configuration of body and wing

BT configuration of body and tail

B configuration of body

b in presence of body

bw in presence of body and wing

w due to addition of wing

APPARATUS AND TESTS

Description of Tunnel

The Langley 9-inch supersonic tunnel is a closed-return, direct-drive type in which the pressure and humidity are controlled. The test Mach number is varied by means of interchangeable nozzle blocks forming test sections approximately 9 inches square. Eleven fine-mesh, turbulence-damping screens are provided in the settling chamber ahead of the nozzles. During the tests the amount of water vapor in the tunnel air was kept at sufficiently low values so that the effects of condensation in the supersonic nozzle were negligible.

Description of Model and Tunnel Setup

A drawing of the model showing the relative locations of the wing and tail plan forms is shown in figure 1. The body and rectangular wings and tails are the same as those used in the tests reported in reference 1; however, in the present investigation the vertical tail surface was removed. A detailed drawing of the wing and tail plan forms is given in figure 2, and the principal dimensions and areas are given in table I. The W_2 and W_3 plan forms are flat plates having beveled leading and trailing edges, while W_1 has a 6-percent-thick, circular-arc section and W_4 has a 5-percent-thick, modified double-wedge section.

In these tests, the sting and sting-windshield arrangement was similar to that used in reference 1 except that a different angle-of-attack system (see fig. 3) made the use of a bent sting unnecessary. An angle-of-attack range of approximately $\pm 15^\circ$ was available with the new system. At each angle of attack, the model, sting, and sting windshield were translated across the tunnel so that a fixed point on the model could be kept on the center line of the tunnel. With this arrangement, configurations which at 0° angle of attack were free from shock reflections could be tested up to 15° angle of attack. In fact the most critical condition for these models was at 0° angle of attack. Throughout the tests the gap between the rear of the model and the movable windshield was maintained at less than 0.010 inch.

Test Methods

Measurements of lift, drag, and pitching moment were made using external self-balancing mechanical scales through an angle-of-attack range of approximately -5° to 15°. An optical system employing a small mirror mounted in the rear of the body was used to measure angles of attack. This system gave true angles directly with no correction necessary for model sting deflection.

Measurements of the pressure in the sting-shield-and-balance enclosing box, which tests have shown to be equal to the model base pressure, were made and the drag results were corrected to the condition of base pressure equal to stream pressure.

The test conditions are shown in the following table:

M	T_o (deg F)	p_o (atm)	q (lb/sq ft)	R
1.62	100	1	890	0.348×10^6
1.93	100	1	790	.312

Precision of Data

The precision of the data has been evaluated by estimating the uncertainties in the balance measurements involved in a given quantity and combining these errors by a method based on the theory of least squares.

A summary table of precision estimates is as follows:

Lift coefficient, C_L:	
Based on W_1 area	±0.0018
Based on W_4 area	±0.0007
Drag coefficient, C_D:	
Based on W_1 area	±0.0014
Based on W_4 area	±0.0006
Pitching-moment coefficient, C_m:	
Based on W_1 area and $\bar{c}$	±0.030
Based on W_4 area and $\bar{c}$	±0.005
Angle of attack, α (initial), degree	±0.03
Angle of attack, α (relative), degree	±0.01
Tail incidence angle, i_t, degree	±0.03
Mach number, M	±0.01

RESULTS AND DISCUSSION

The variation of lift, drag, and pitching-moment coefficients with angle of attack are given for the BWT, BW, BT, and B configurations at $M = 1.93$ in figures 4 and 5 and at $M = 1.62$ in figures 6 and 7. All coefficients are based on the individual wing areas including the portion within the body formed by extending the wing leading and trailing edges to the body center line. The pitching-moment coefficients are based on each wing mean aerodynamic chord and are referenced to the center-of-gravity location shown in figure 1. Although the basic data figures are not discussed in detail, it is felt that the data are of sufficient general interest to warrant their inclusion.

Lift and Drag Results

Lift-curve slopes.- The experimental lift-curve slopes at $\alpha = 0^\circ$ are summarized in tables II and III. From theoretical considerations, configurations with W_1 and W_2 are expected to have the highest lift-curve slopes with the W_4 configurations having the smallest slopes. In general this is so, but the trends are greatly exaggerated especially between the W_1 and W_2 configurations. This effect is due to the use of the total wing area as the reference area and to the different proportion of interference lift in the body-wing lift.

In reference 5, a modification to Spreiter's work is given by which the lift-curve slope of a body and triangular wing combination can be obtained. This result has been extended by Nielsen and Kaattari (reference 6) to cover rectangular and trapezoidal plan forms as well as triangular plan forms. These theoretical results are compared with the experimental BW lift-curve slopes where the coefficients are based on exposed wing areas in the following table:

[redacted]

CONFIGURATION	C_{L_α}	
	M = 1.62	M = 1.93
BW_1		
Experimental, wing forward	0.0974	0.0848
Experimental, wing rearward	.0977	.0856
Theoretical, reference 6	.0979	.0818
BW_2		
Experimental, wing forward	.0989	.0929
Experimental, wing rearward	.0984	.0898
Theoretical, reference 5	.1117	.1026
Theoretical, reference 6	.1057	.0969
BW_3		
Experimental, wing forward	.0826	.0796
Experimental, wing rearward	.0880	.0788
Theoretical, reference 6	.0957	.0865
BW_4		
Experimental, wing forward	------	.0574
Experimental, wing rearward	------	.0585
Theoretical, reference 6	------	.0720

In general, the agreement between the experimental lift-curve slopes and the predicted values of Nielsen and Kaattari (reference 6) may be considered good except for the BW_4 configuration. The disagreement between experiment and theory is largest for the BW_3 and BW_4 configurations which have the largest root chords. Thus, if the low Reynolds number of the tests causes separation in the wing-body juncture, these configurations would show the greatest loss in lift. It should be pointed out that in these theoretical methods the theoretical wing-alone lift-curve slopes were used so that differences between experimental and theoretical wing-alone lift-curve slopes are included in the comparison just given.

Morikawa in reference 7 has made calculations of the lift of several body-wing configurations with no afterbody. The lift for the limiting conditions, that is, as the span approaches the body diameter and as the body diameter approaches zero, was established exactly, and approximations were given for the intermediate cases. Dorrance in reference 8 has presented results for similar configurations. These results together

with the results of Nielsen, Katzen, and Tang, and Nielsen and Kaattari can be compared with the BT results of this investigation. It should be mentioned that only comparisons with experiment at small angles of attack are valid since second-order effects and viscous cross-flow effects are not considered in the theoretical methods. A comparison of experimental data with the results of these theoretical methods is made in the following table where the lift-curve slopes are based on the exposed tail areas. In the comparison, the slender-body value of body-alone lift-curve slope is added to the theoretical results of Morikawa and Dorrance.

CONFIGURATION	C_{L_α}	
	M = 1.62	M = 1.93
BT_1		
Experiment	0.0786	0.0655
Theory, reference 7	.0821	.0667
Theory, reference 8	.0762	.0631
Theory, reference 6	.0852	.0705
BT_2		
Experiment	.0801	.0740
Theory, reference 7	.0940	.0845
Theory, reference 8	.0784	.0720
Theory, reference 5	.0957	.0874
Theory, reference 6	.0911	.0820

The result of Dorrance (reference 8) which does not account for any interference lift on the body gives lift-curve slopes lower than experiment. The agreement between experiment and the theoretical results, which include an interference lift on the body (references 5, 6, and 7), is good for the rectangular body-tail configuration with sizable deviations shown for the triangular body-tail configuration. It should be pointed out that the results of Morikawa (reference 7) and Nielsen, Katzen, and Tang (reference 5) do not predict a rearward shift in the interference lift on the body due to the tail. Inasmuch as the body ends at approximately the trailing edge of the tail surface, a sizable portion of this interference lift would not be realized on the body. Thus, the experimental lift-curve slopes should be somewhat lower than theory. Inasmuch as the interference lift on the body is larger for the triangular body-tail configuration than for the rectangular body-tail configuration, the experimental lift-curve slopes would be expected to

deviate more from theory. The effects of separation in the body-tail juncture would also be expected to be largest in the case of the triangular body-tail configuration.

Drag.- It was found in this investigation that extreme care in testing was necessary to achieve systematic drag data especially where interchangeable body and wing sections were used. Any roughness on the body or wing surfaces or any small protuberance was sufficient to alter the flow over the body and, for symmetrical configurations, to increase the minimum drag coefficients over the laminar case with unsymmetrical drag curves at the lower angles of attack. It was found that these effects had negligible effect upon the lift and pitching moments. In view of the low Reynolds number of the tests together with the uncertainties given above, the drag data are presented without analysis.

Pitching-Moment Results

The pitching-moment coefficients are based on the wing area and wing mean aerodynamic chord and are referenced to an arbitrary center-of-gravity location 5.9 diameters from the nose (see fig. 1). The use of a fixed center-of-gravity location results in the large static margins shown in figures 4 and 6 for the rear wing position configurations. The large changes in $\frac{\partial C_m}{\partial \alpha}$ near 0° angle of attack are characteristic of low-aspect-ratio, in-line missile configurations. This change in slope is associated with the large wing downwash near 0° angle of attack. Other data showing similar trends for in-line configurations may be found in references 2 to 4.

The variation of center-of-pressure location with angle of attack for all configurations at $M = 1.93$ is shown in figure 8 and at $M = 1.62$ in figure 9. The results were corrected to the case of $i_t = 0°$ and represent only the center of pressure due to angle-of-attack change.

The center-of-pressure locations for the B and BT configurations are shown only in figures 8(a) and 9(a). The body alone shows a large rearward shift in center-of-pressure location with increasing angle of attack. This shift is about 5 diameters at $M = 1.93$ and about 6.5 diameters at $M = 1.62$. The BT configurations show at both Mach numbers a rearward and then a forward movement of center-of-pressure location with increasing angle of attack. A forward shift with increasing Mach number is also noted.

The BWT configurations show a characteristic rearward shift in center-of-pressure location at low angles of attack with a leveling off

at the higher angles, which is a result of wing downwash effects as discussed previously. Little effect of Mach number was noted.

Integrated Downwash Effects

Average downwash angles.- The average effective flow angle at the tail has been obtained from the lift results by using the method given in reference 1. The results of this calculation are shown for $M = 1.93$ in figure 10 and for $M = 1.62$ in figure 11. A discussion of the results will follow, but a comparison of the results using rectangular tails and triangular tails together with an examination of the procedure indicates that the procedure does not isolate the average wing downwash with sufficient certainty except, possibly, in a few special cases.

The procedure as given in reference 1 for obtaining the average effective downwash angles may be briefly summarized as follows: The lift coefficient of the BT configuration at any angle α_n may be written as

$$C_{L_{BT}} = C_{L_B} + \int_{\alpha=0}^{\alpha_n} \left(\frac{\partial C_L}{\partial i_t}\right)_b d(\alpha - \epsilon_b)$$

or, stepwise,

$$C_{L_{BT}}(\alpha_n) = C_{L_B}(\alpha_n) + \sum_{k=0}^{n} \left(\frac{\partial C_L}{\partial i_t}\,\alpha_{k+\frac{1}{2}}\right)_b \left[\left(\alpha_{k+1} - \alpha_k\right) - \left(\epsilon_{k+1} - \epsilon_k\right)_b\right]$$

where k is the number of steps in the numerical integration from $\alpha = 0$ to α_n. A similar equation may be written for the lift of the BWT configuration and these equations solved for ϵ_b and ϵ_{bw}, respectively. Then, the effective average flow angle due to adding the wing is the difference between the two values; that is,

$$\epsilon_w = \epsilon_{bw} - \epsilon_b$$

The curves of ϵ_b, average effective upwash due to body, (figs. 10(a), 10(c), 11(a), and 11(c)) show little difference between the values for the two tail plan forms up to 5° angle of attack with large differences shown above this angle. Increasing Mach number gave slight increases in $\frac{\partial \epsilon_b}{\partial \alpha}$ for both tail plan forms.

The curves of ϵ_w, the average downwash due to the wing, (figs. 10 and 11) show agreement between the two tail configurations only up to 2° angle of attack with considerable difference shown at the higher angles. Near 0° angle of attack the values of $\frac{\partial \epsilon_w}{\partial \alpha}$ show a systematic increase with decreasing wing aspect ratio for both T_1 and T_2 configurations. At the lowest wing aspect ratio, 1.26 for W_4, $\frac{\partial \epsilon_w}{\partial \alpha}$ approaches one. For each body and wing combination the values of ϵ_w should be identical for both the rectangular and triangular tail plan form if the present method of obtaining average downwash angles is to be regarded as satisfactory. It should be remembered, however, that the experimental average downwash angles contain the effects on the lift of the tail of spanwise and axial velocity gradients as well as vertical velocity gradients. The rectangular tail would act more nearly as a "strip integrator" and tend to minimize the effects of spanwise velocity gradients. In addition, the assumption that the lift increment on the body due to the tail is the same for a change in incidence angle as for a change in angle of attack is made in this analysis. This assumption would be expected to have the largest effect on the triangular tail rather than the rectangular tail as a small chord relative to the body diameter would minimize this effect. Also, at the higher angles of attack an effect of Reynolds number upon the downwash at the tail might be expected in that any change in the separation point on the wings will change the location of the trailing vortex sheet. For the configurations tested, this change in separation point would have small effect on the downwash at the tail since the tail is a considerable distance from the trailing vortex sheet at the higher angles of attack.

From the previous discussion it appears that the method given in reference 1 is satisfactory in the low-angle-of-attack range, but at the higher angles fails to isolate the average wing downwash with sufficient certainty. Therefore, it is felt that the average downwash results do not warrant the time and effort necessary to isolate them by this method.

Experimental wing-wake parameter.- The variation of the wing-wake parameter η_t with angle of attack is shown in figures 12 and 13 for

M = 1.93 and 1.62, respectively. In the low-angle-of-attack range this parameter is about 1 for all configurations except BW_1T_2 at M = 1.93. It should be noted that although the accuracy in η_t with changing angle of attack is about ±0.03, an error of ±0.03° in initial reference angle causes η_t to be in error by about ±0.10. At the higher angles of attack η_t shows sizable but erratic changes for all configurations with no significant effect of wing location shown.

Tail efficiency.- As was pointed out previously, it is difficult to separate the different effects of the addition of a wing to a configuration by the use of force data. Thus, a parameter which expresses the gross effect of the addition of a wing would be valuable in indicating trends in wing downwash. Such a parameter is the ratio of the lift of the tail in the presence of the wing to the lift of the tail in the presence of the body without wing, or the tail efficiency. This may be written as

$$\eta_t' = \frac{C_{L_{BWT}} - C_{L_{BW}}}{C_{L_{BT}} - C_{L_B}}$$

A similar equation may be written using pitching-moment results. Calculations were made using the pitching-moment results, but are not presented since they show the same trends as do the lift calculations and show more scatter due to the greater error in the pitching-moment results.

The variation of η_t' with angle of attack for all configurations is given in figures 14 and 15 for M = 1.93 and 1.62, respectively. These curves have the form characteristic of in-line configurations with the minimum value of η_t' at 0° angle of attack with values approaching 1 at the higher angles of attack. As might be expected from wing downwash considerations, the lowest value of η_t' is found for the lowest aspect ratio, the W_4 configuration, with a systematic increase in η_t' with increasing wing aspect ratio. The lower-aspect-ratio configurations, W_3 and W_4, also require a higher angle of attack before the values of one for η_t' are reached due to the larger $d\epsilon/d\alpha$ for these configurations.

For all wing plan forms, the triangular tail configurations show the lowest values of tail efficiency near 0° angle of attack with little difference shown at the higher angles. In calculating values of tail efficiency, tail incidence angle effects are not included and it is not assumed that the lift increment on the body due to the tail is the same for a change in incidence angle as for a change in angle of attack. Since the wing downwash distribution for these configurations is identical, the differences in tail efficiency or lift effectiveness shown must be associated with the effects on the tail lift of spanwise and

axial velocity gradients at the tail. As the rectangular tail has an approximately constant span loading, it is to be expected that the effects of spanwise and axial velocity gradients would be a minimum for these configurations.

Some effect of Mach number is noted with the minimum values of η_t' at $M = 1.62$ being about 0.08 lower than the corresponding values at $M = 1.93$. No systematic effect of varying wing location is shown.

CONCLUDING REMARKS

Tests at Mach numbers of 1.62 and 1.93 of several in-line missile configurations having several wing and tail plan forms of equal span have indicated the following results:

1. A comparison of the experimental lift-curve slopes of the body-wing configurations with the results of Nielsen and Kaattari (NACA RM A51J04) gave good agreement except for the configuration having trapezoidal plan form. The configurations having the largest root chord gave the greatest disagreements indicating that the experimental lift-curve slopes were reduced due to separation in the body-wing juncture.

2. A comparison of the experimental lift-curve slopes of the rectangular and triangular body-tail configurations with several theoretical results indicated that the best agreement is shown for the rectangular tail configurations. The theoretical result which includes no interference lift on the body due to the tail gave lift-curve slopes lower than experiment while the other theoretical results which include interference lift were higher than experiment.

3. The complete configurations showed in the low-angle-of-attack range a sizable rearward movement in center-of-pressure location and a nearly constant center-of-pressure location at the higher angles which is a result of the large reduction in downwash associated with the movement of the tail away from the trailing vortex sheet. The body alone gave a large shift in center-of-pressure location with increasing angle of attack, having maximum shifts of 6.5 body diameters at a Mach number of 1.62 and 5 body diameters at a Mach number of 1.93.

4. From average effective downwash angles calculated from force data for both the rectangular and triangular tail configurations, it appears that the method where the tail surface is used as a strip integrator is satisfactory in the low-angle-of-attack range, but fails to isolate the average wing downwash with sufficient certainty at the higher angles.

5. The curves of tail efficiency against angle of attack are characteristic of in-line configurations with the minimum value at 0° angle of attack and values approaching 1 at the higher angles. As might be expected from wing downwash considerations, a systematic decrease in tail efficiency with decreasing wing aspect ratio is shown.

6. A comparison of the tail efficiency variations with angle of attack between the rectangular and triangular tail configurations shows the triangular tail configurations to have the lowest tail efficiency near 0° angle of attack with little difference between the tail plan forms at the higher angles.

Langley Aeronautical Laboratory
National Advisory Committee for Aeronautics
Langley Field, Va.

REFERENCES

1. Grigsby, Carl E.: Investigation at a Mach Number of 1.93 to Determine Lift, Drag, Pitching-Moment, and Average Downwash Characteristics for Several Missile Configurations Having Rectangular Wings and Tails of Various Spans. NACA RM L50I08, 1950.

2. Rainey, Robert W.: Langley 9-Inch Supersonic Tunnel Tests of Several Modifications of a Supersonic Missile Having Tandem Cruciform Lifting Surfaces. Three-Component Data Results of Models Having Ratios of Wing Span to Tail Span Equal to 1. NACA RM L9L30, 1951.

3. Rainey, Robert W.: Langley 9-Inch Supersonic Tunnel Tests of Several Modifications of a Supersonic Missile Having Tandem Cruciform Lifting Surfaces. Three-Component Data Results of Models Having Ratios of Wing Span to Tail Span Equal to and Less than 1 and Some Static Rolling-Moment Data. NACA RM L50G07, 1951.

4. Rainey, Robert W.: Langley 9-Inch Supersonic Tunnel Tests of Several Modifications of a Supersonic Missile Having Tandem Cruciform Lifting Surfaces. Three-Component Data Results of Models Having Ratios of Wing Span to Tail Span Less than 1. NACA RM L50I29a, 1951.

5. Nielsen, Jack N., Katzen, Elliott D., and Tang, Kenneth K.: Lift and Pitching-Moment Interference between a Pointed Cylindrical Body and Triangular Wings of Various Aspect Ratios at Mach Numbers of 1.50 and 2.02. NACA RM A50F06, 1950.

6. Nielsen, Jack N., and Kaattari, George E.: Method for Estimating Lift Interference of Wing-Body Combinations at Supersonic Speeds. NACA RM A51J04, 1951.

7. Morikawa, G. K.: Supersonic Wing-Body Lift. Preprint No. 296, Inst. Aero. Sci. Inc., July 1950.

8. Dorrance, W. H.: Body-Tail Interference in Supersonic Flow Including an Example Application. Rep. No. UMM-38, Aero. Res. Center, Univ. of Michigan, Aug. 1949.

TABLE I.- MODEL DIMENSIONS

Configuration / Quantity	Rectangular wing, W_1	Triangular wing, W_2	Diamond wing, W_3	Trapezoidal wing, W_4	Rectangular tail, T_1	Triangular tail, T_2
Area, S, sq in.	1.080	1.456	2.161	2.676	1.141	1.456
Aspect ratio, A	3.11	2.31	1.56	1.26	2.95	2.31
Mean aerodynamic chord, $\bar{c}$, in.	0.590	1.058	1.573	1.651	0.622	1.058

Fuselage ordinates:

Station 0 to 3.125, $r = 1.40 \left[\frac{x}{6.25} - \left(\frac{x}{6.25}\right)^2\right]$

Station 3.125 to 6.625, constant diameter of 0.700 inch

Station 6.625 to 8.750, $r = 0.40 \left[\frac{8.75 - x}{4.25} - \left(\frac{8.75 - x}{4.25}\right)^2\right] + 0.25$

TABLE II.- SUMMARY OF EXPERIMENTAL LIFT-CURVE SLOPES

AT $\alpha = 0^\circ$ FOR BWT AND BW CONFIGURATIONS

Configuration	C_{L_α} (a)			
	M = 1.93		M = 1.62	
	Wing forward	Wing rearward	Wing forward	Wing rearward
BW_1T_1 $i_t = -0.43^\circ$	0.0726 (.1172)	0.0739 (.1193)	0.0810 (.1307)	0.0837 (.1351)
BW_1T_2 $i_t = 0.03^\circ$	.0684 (.1103)	.0722 (.1165)	.0763 (.1232)	.0790 (.1275)
BW_1	.0525 (.0848)	.0530 (.0856)	.0603 (.0974)	.0605 (.0977)
BW_2T_1 $i_t = -0.43^\circ$	.0517 (.1353)	.0513 (.1343)	.0578 (.1513)	.0577 (.1511)
BW_2T_2 $i_t = 0.03^\circ$	.0460 (.1204)	.0464 (.1215)	.0505 (.1322)	.0511 (.1338)
BW_2	.0355 (.0929)	.0343 (.0898)	.0378 (.0989)	.0376 (.0984)
BW_3T_1 $i_t = -0.43^\circ$	.0390 (.1021)	.0390 (.1021)	------- -------	------- -------
BW_3T_2 $i_t = 0.03^\circ$	.0353 (.0924)	.0349 (.0914)	.0361 (.0945)	.0376 (.0985)
BW_3	.0308 (.0796)	.0301 (.0788)	.0316 (.0826)	.0336 (.0880)
BW_4T_1 $i_t = -0.43^\circ$	.0334 (.0711)	.0335 (.0713)	------- -------	------- -------
BW_4T_2 $i_t = 0.03^\circ$	.0316 (.0651)	.0328 (.0698)	------- -------	------- -------
BW_4	.0270 (.0574)	.0275 (.0585)	------- -------	------- -------

[a]In each case the lift-curve slope based on total wing area is given first and the corresponding value based on exposed wing area indicated in parentheses.

TABLE III.- SUMMARY OF EXPERIMENTAL LIFT-CURVE SLOPES AT $\alpha = 0^\circ$ FOR BT AND B CONFIGURATIONS

Configuration	C_{L_α} (a)	
	M = 1.93	M = 1.62
BT_1 $i_t = -0.43^\circ$	0.0465 (.0655)	0.0558 (.0786)
BT_2 $i_t = 0.03^\circ$	.0451 (.0740)	.0488 (.0801)
B	.0119	.0101

[a]For each BT configuration the lift-curve slope based on total wing area of W_1 is given first and the corresponding value based on exposed tail area given in parentheses.

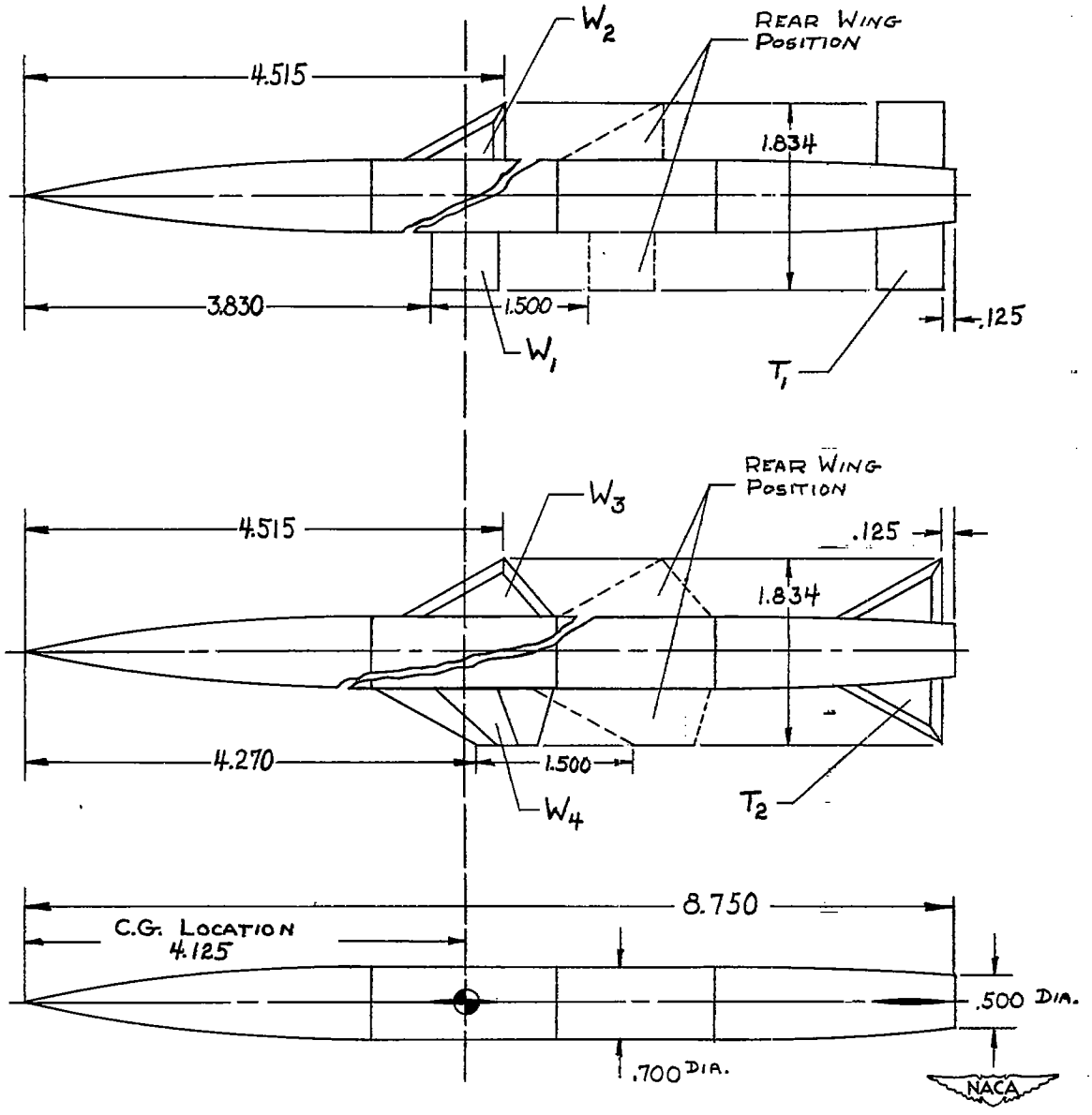

Figure 1.- Detail of models. (All dimensions are in inches.)

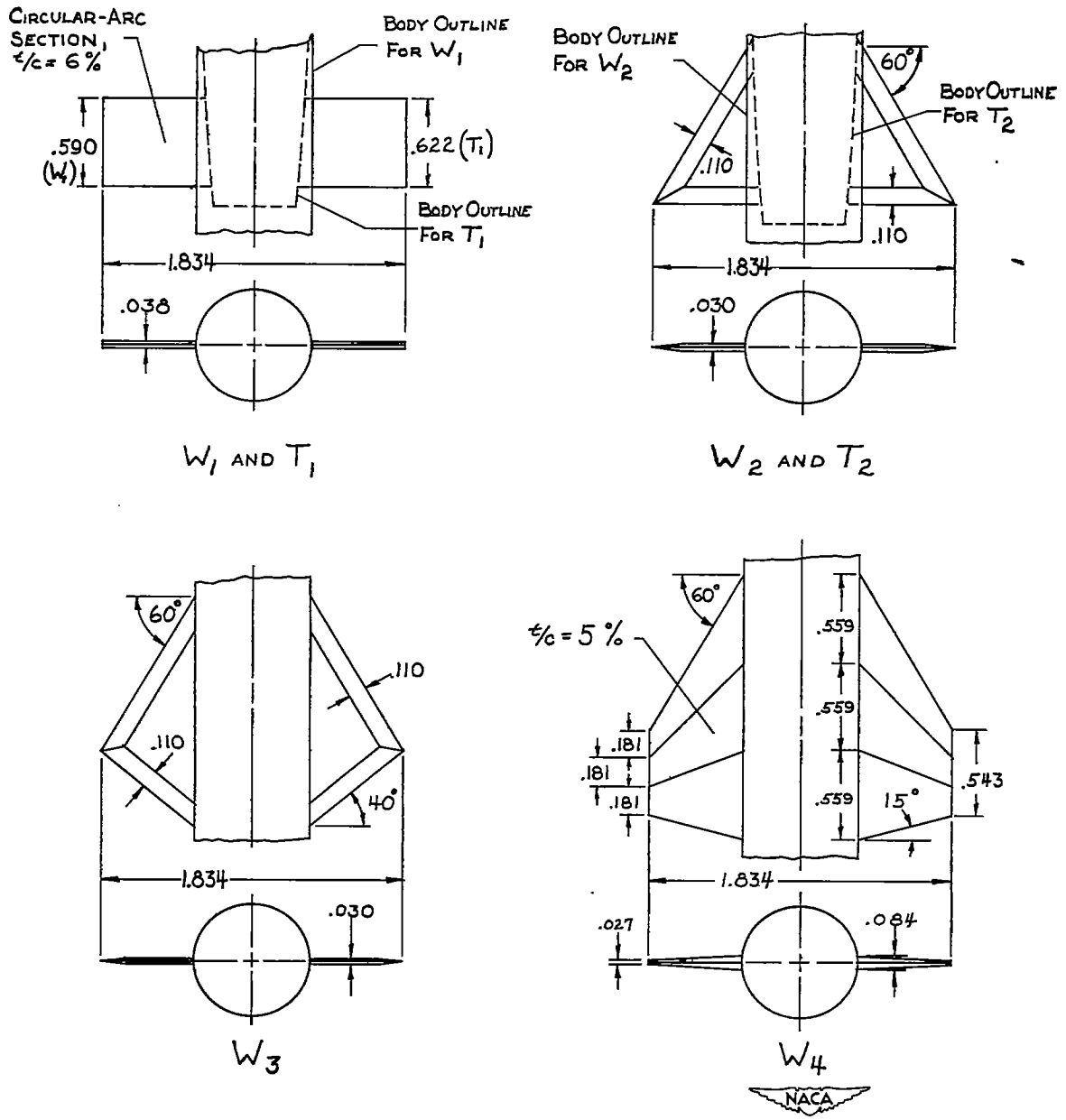

Figure 2.- Detail of wings and tails. (All dimensions are in inches.)

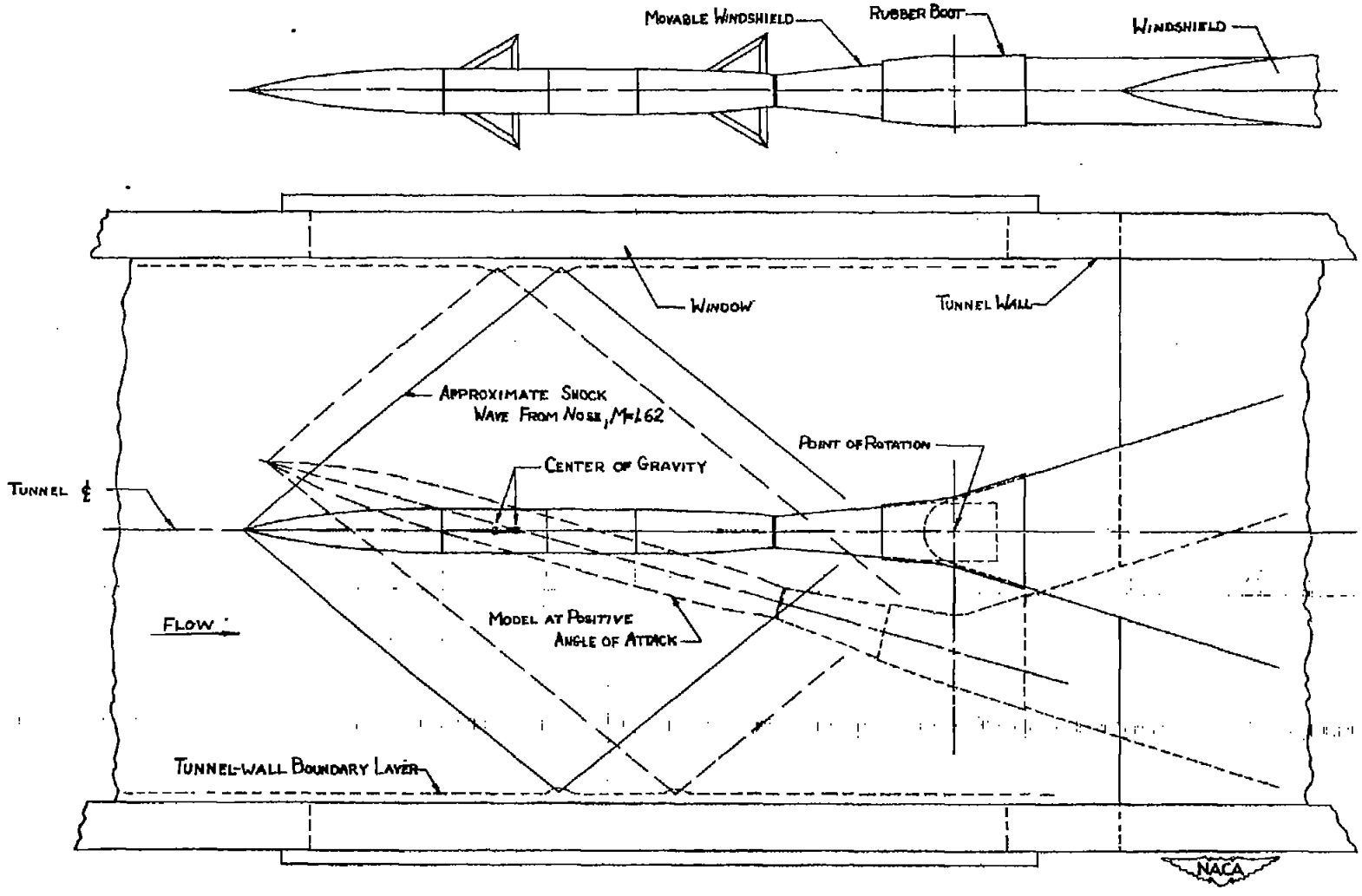

Figure 3.- Model installation in tunnel.

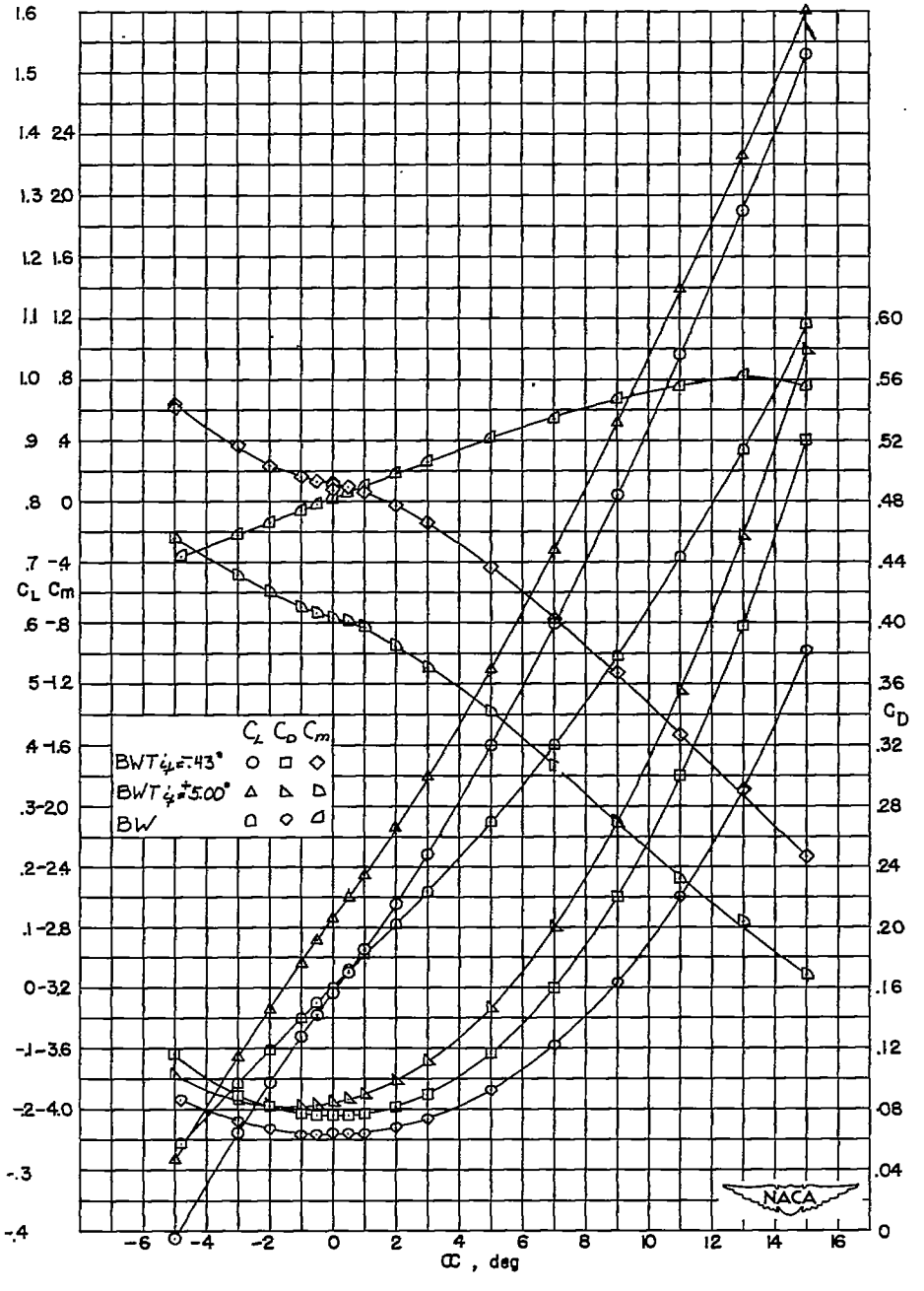

(a) BW_1T_1; wing forward.

Figure 4.- Aerodynamic characteristics of the BWT and BW configurations at M = 1.93.

[redacted]

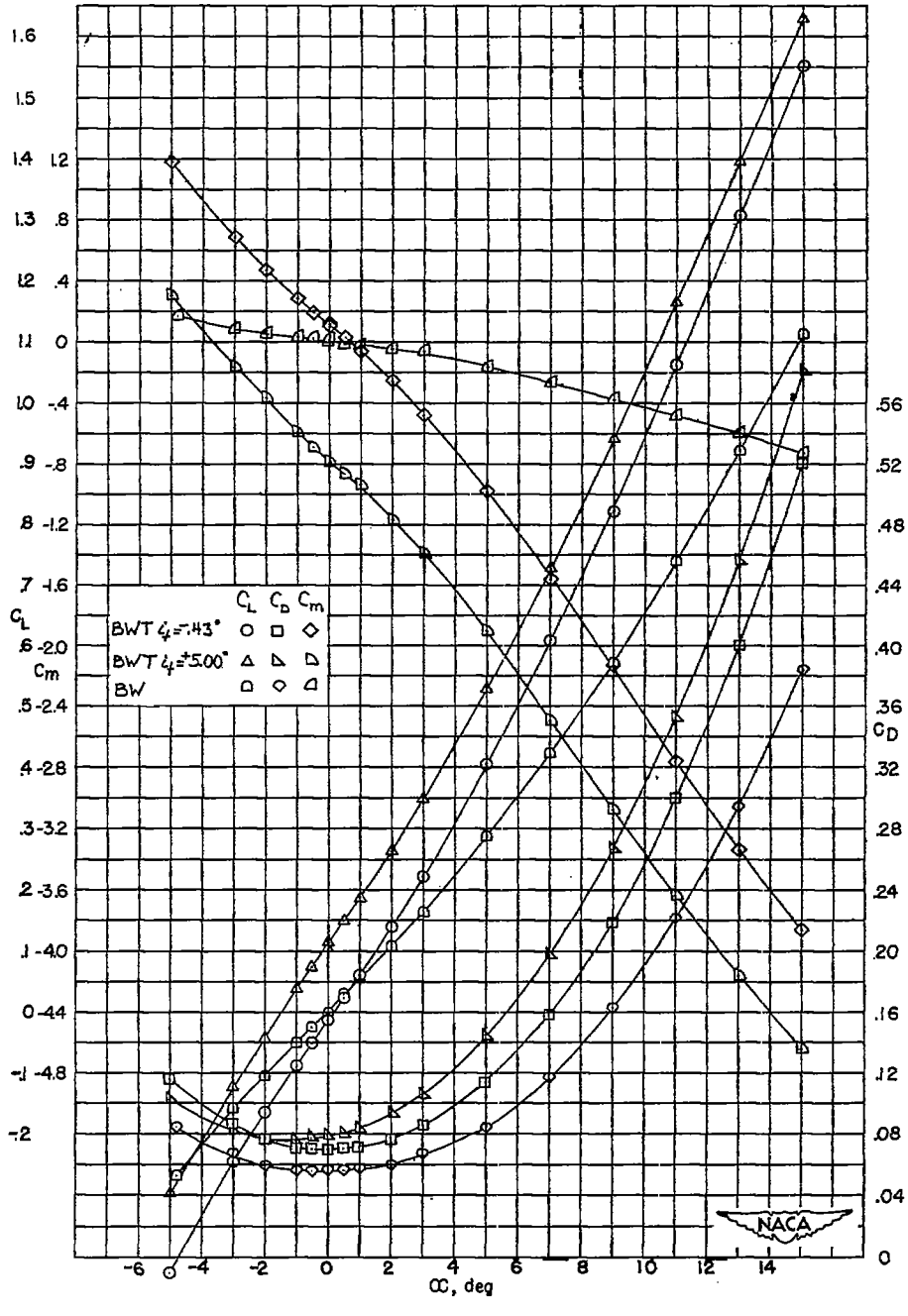

(b) BW_1T_1; wing rearward.

Figure 4.- Continued.

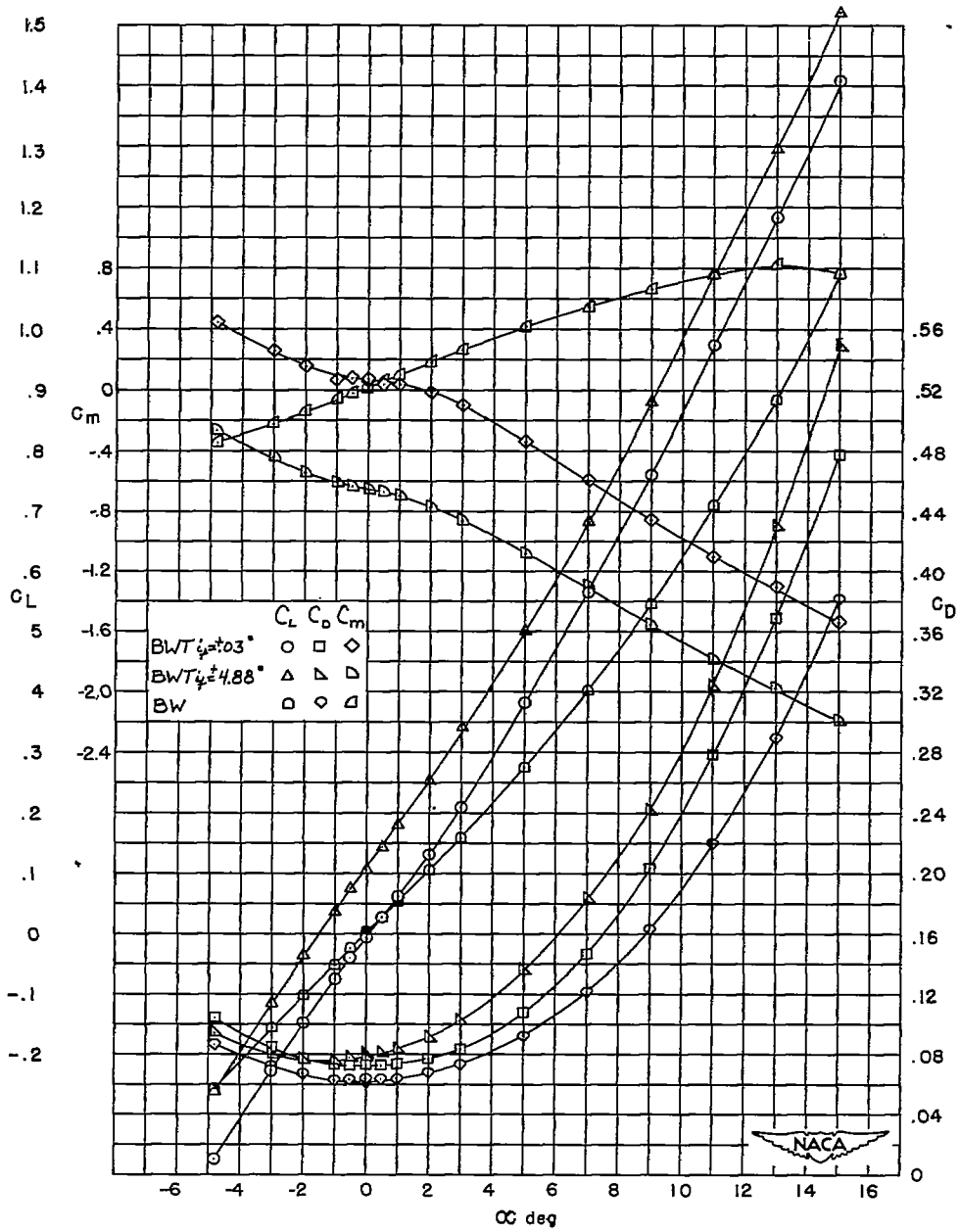

(c) BW_1T_2; wing forward.

Figure 4.- Continued.

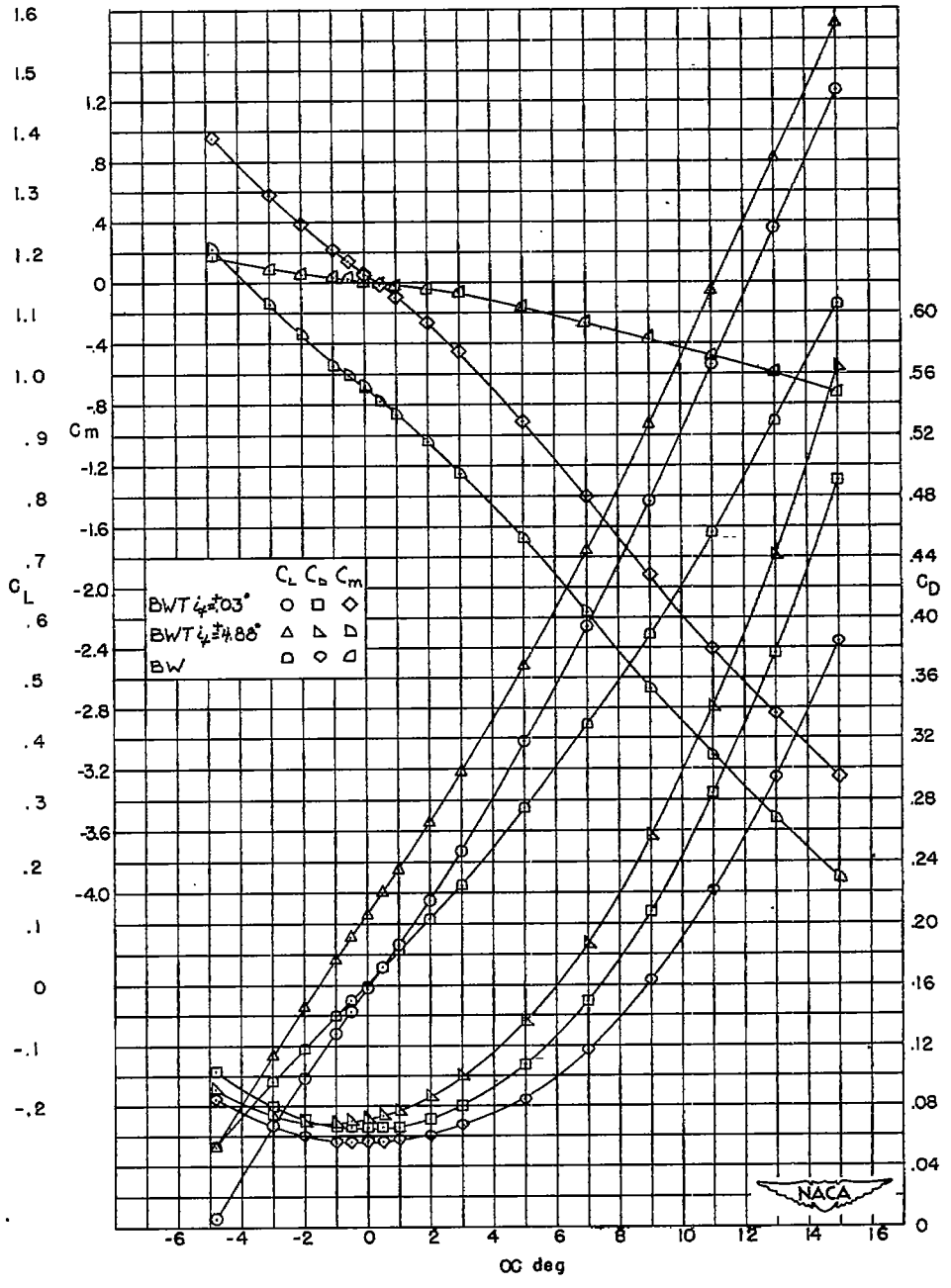

(d) BW_1T_2; wing rearward.

Figure 4.- Continued.

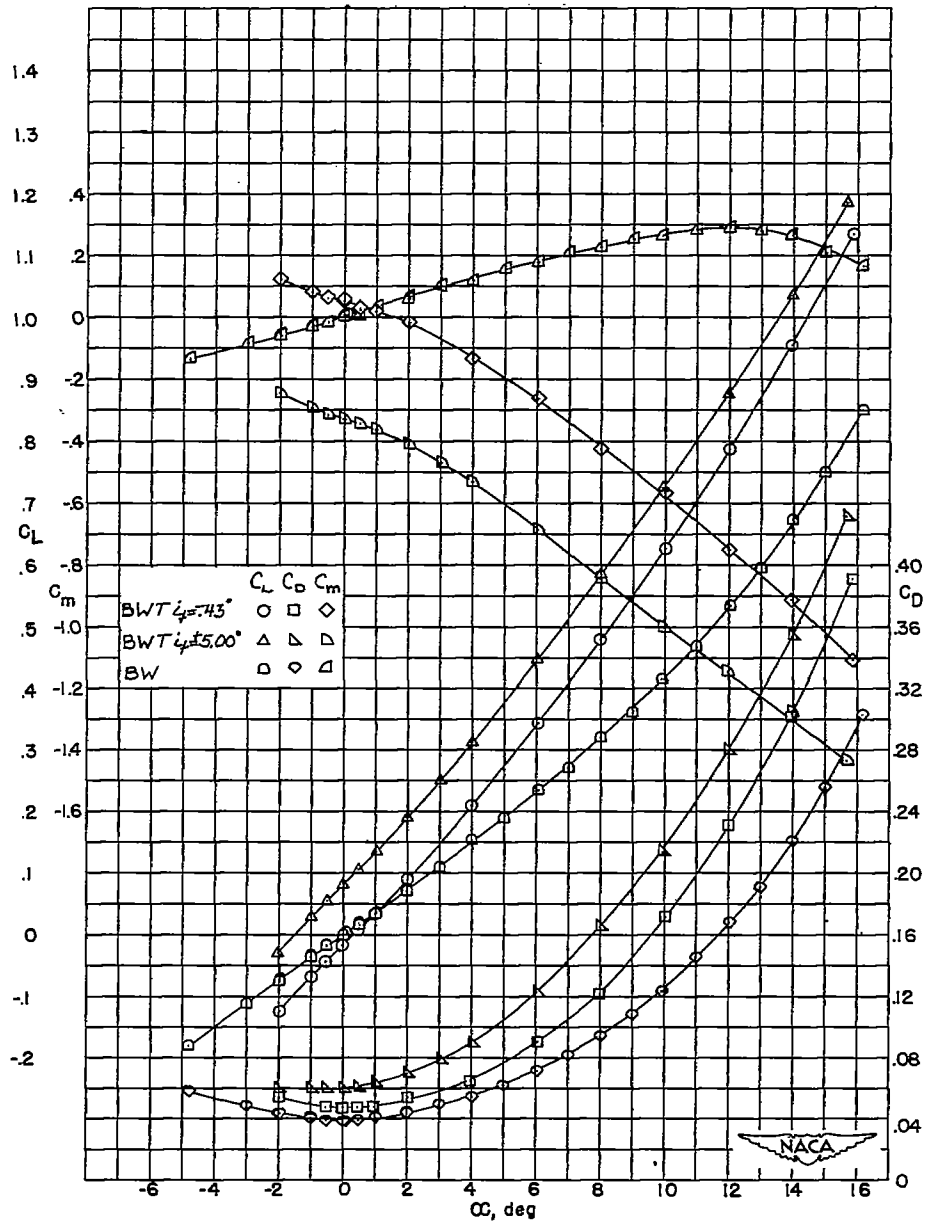

(e) BW_2T_1; wing forward.

Figure 4.- Continued.

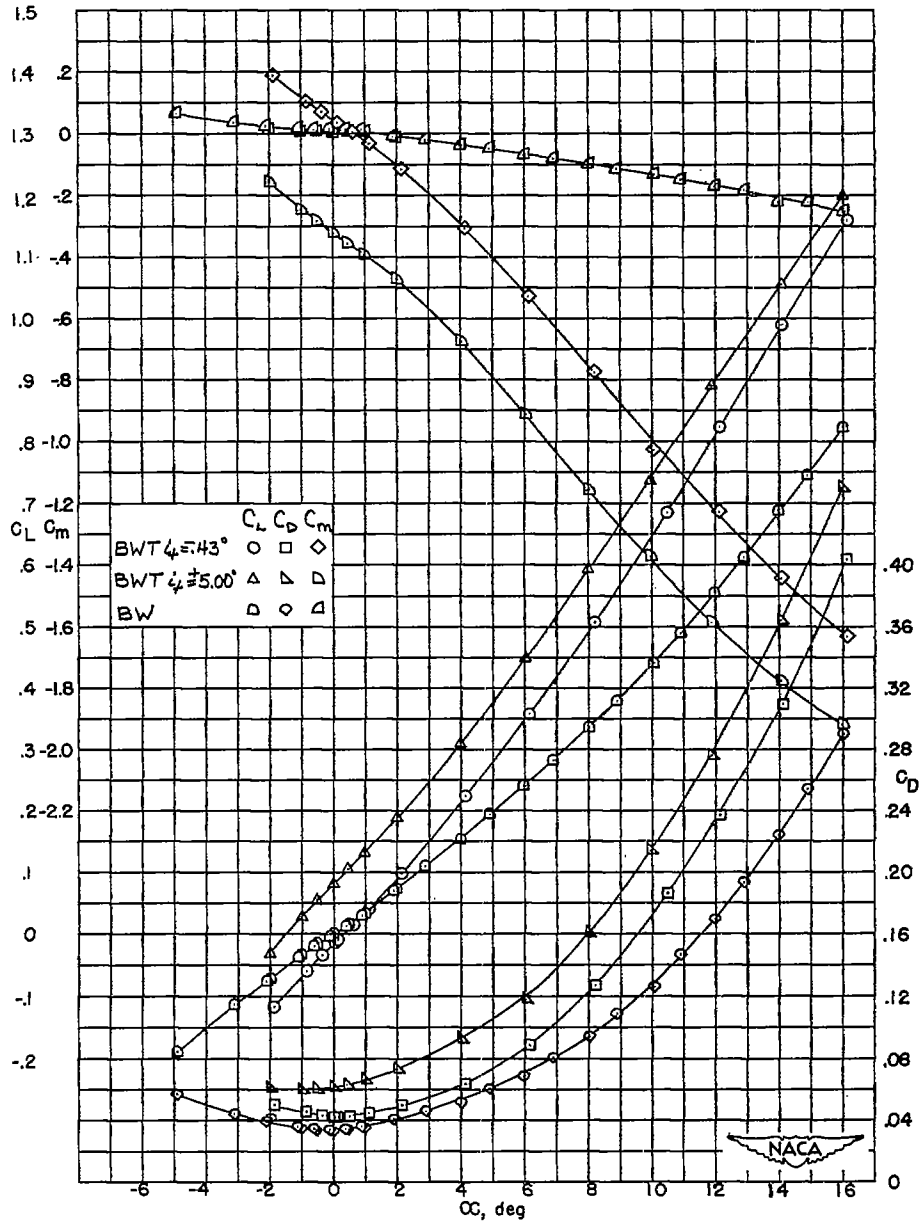

(f) BW_2T_1; wing rearward.

Figure 4.- Continued.

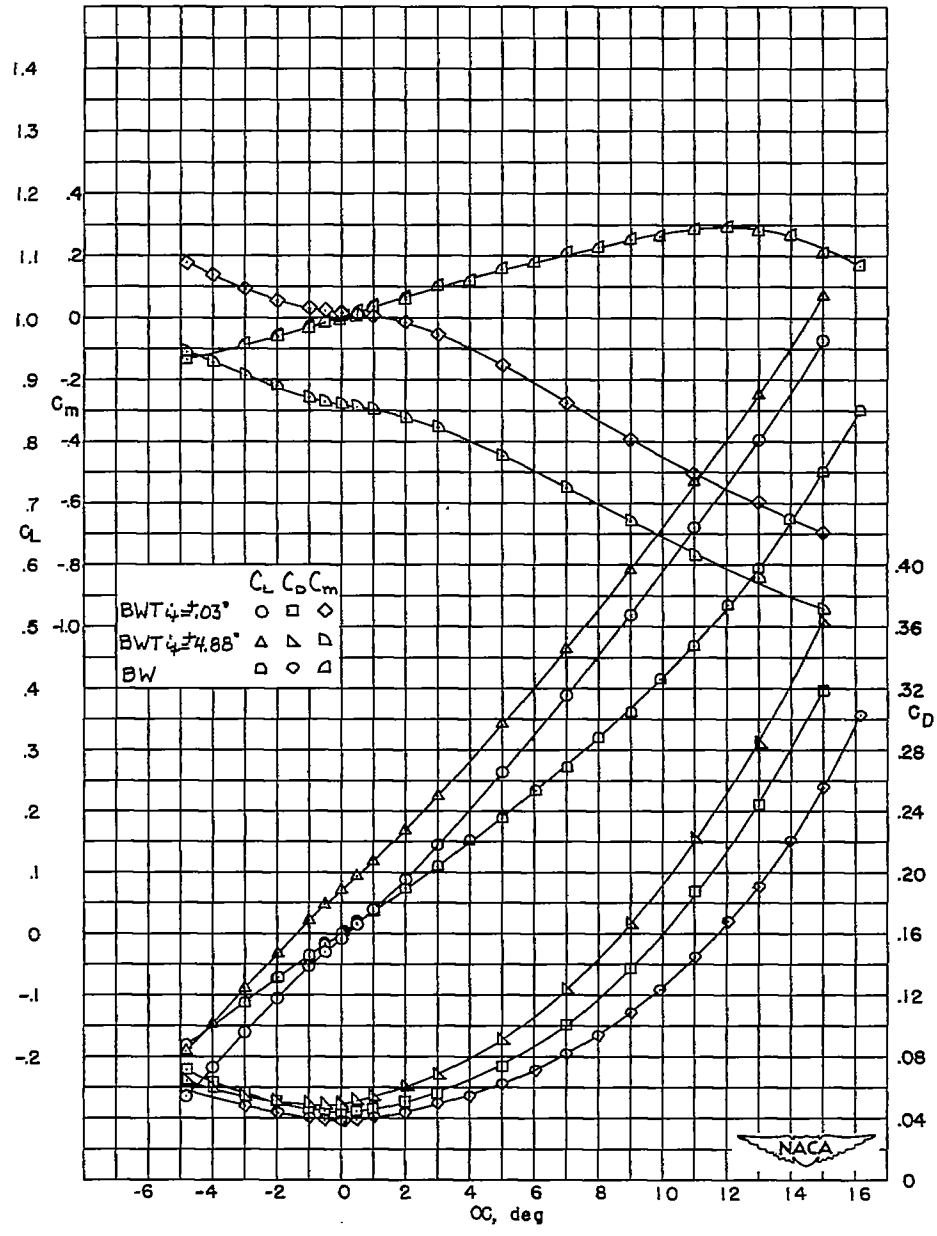

(g) BW_2T_2; wing forward.

Figure 4.- Continued.

[redacted]

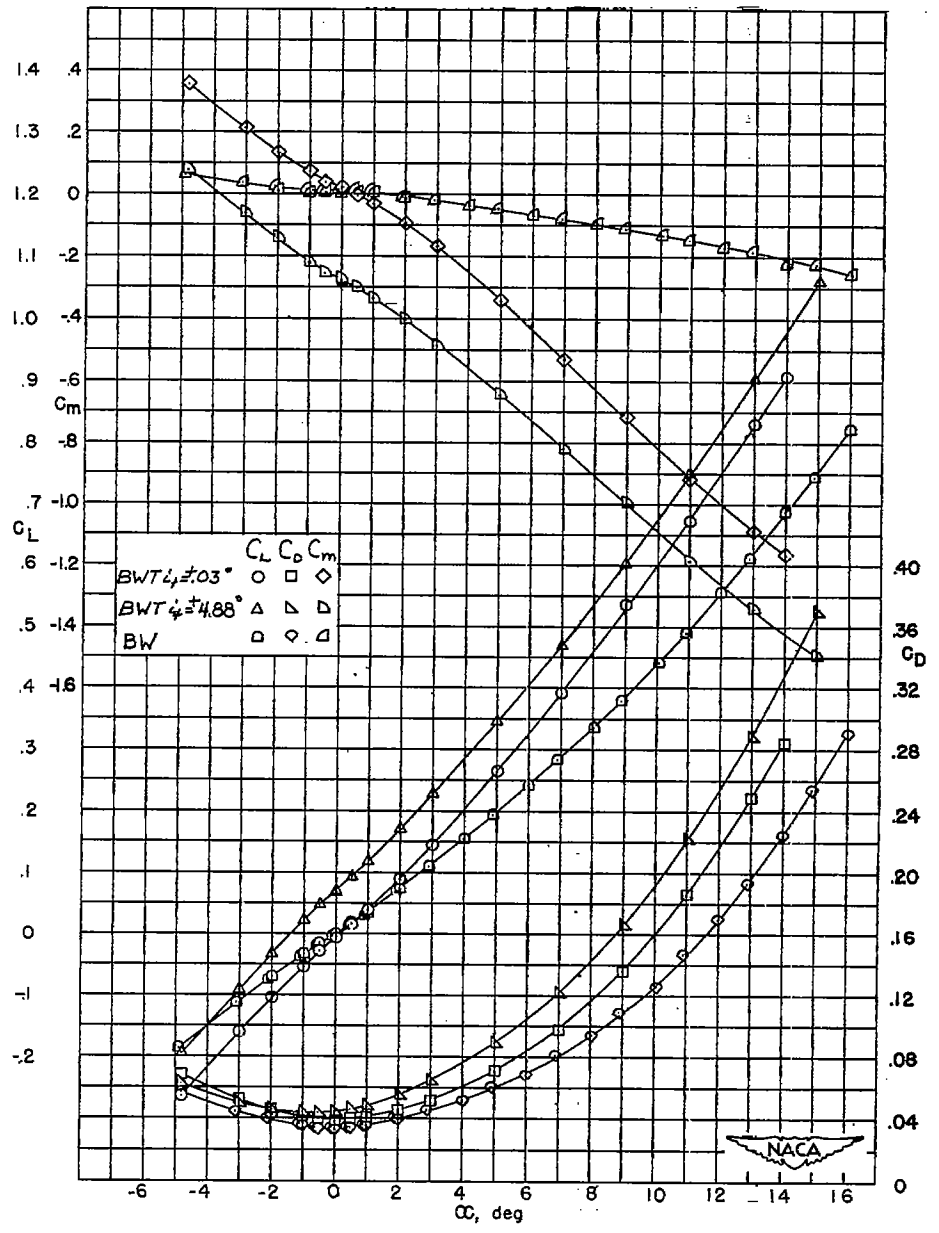

(h) BW_2T_2; wing rearward.

Figure 4.- Continued.

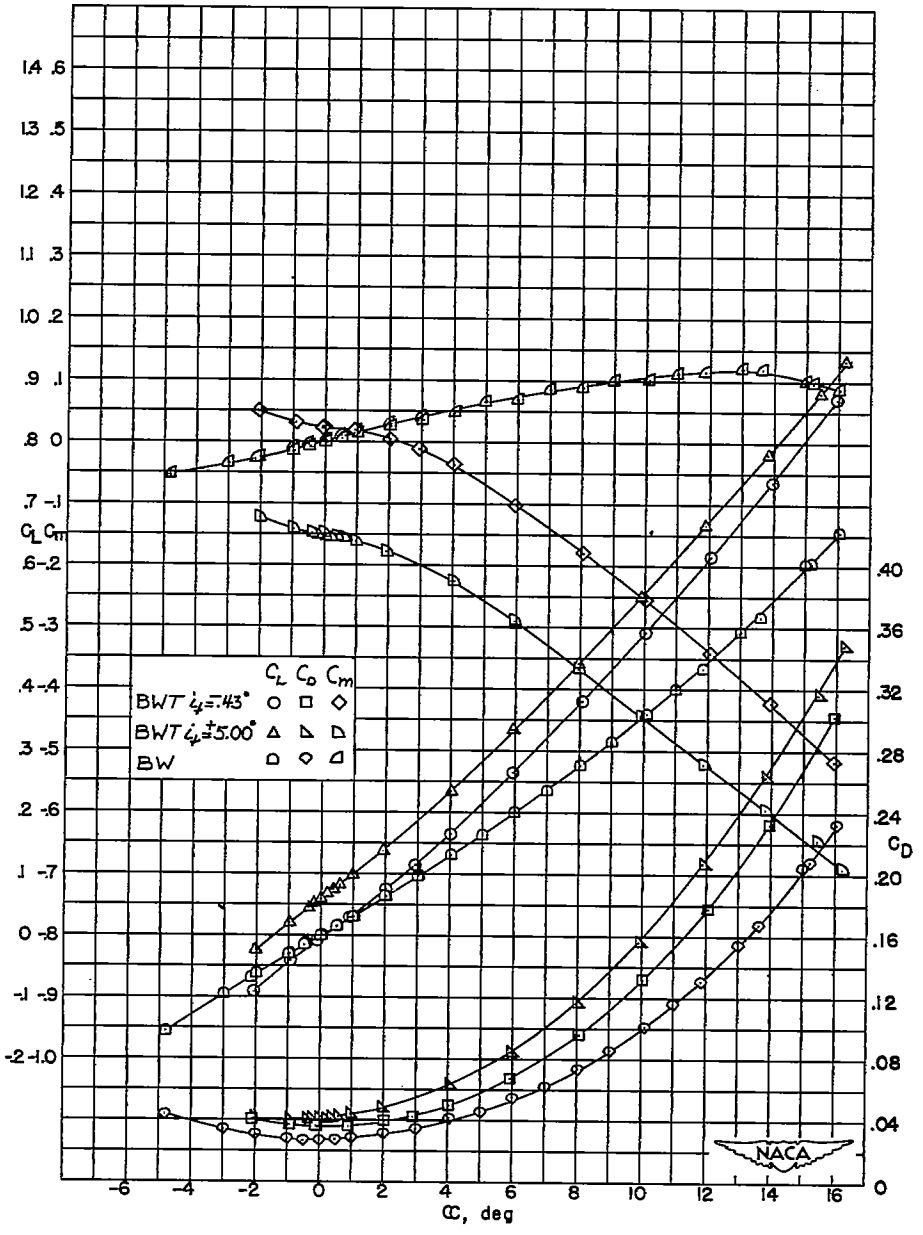

(i) BW_3T_1; wing forward.

Figure 4.- Continued.

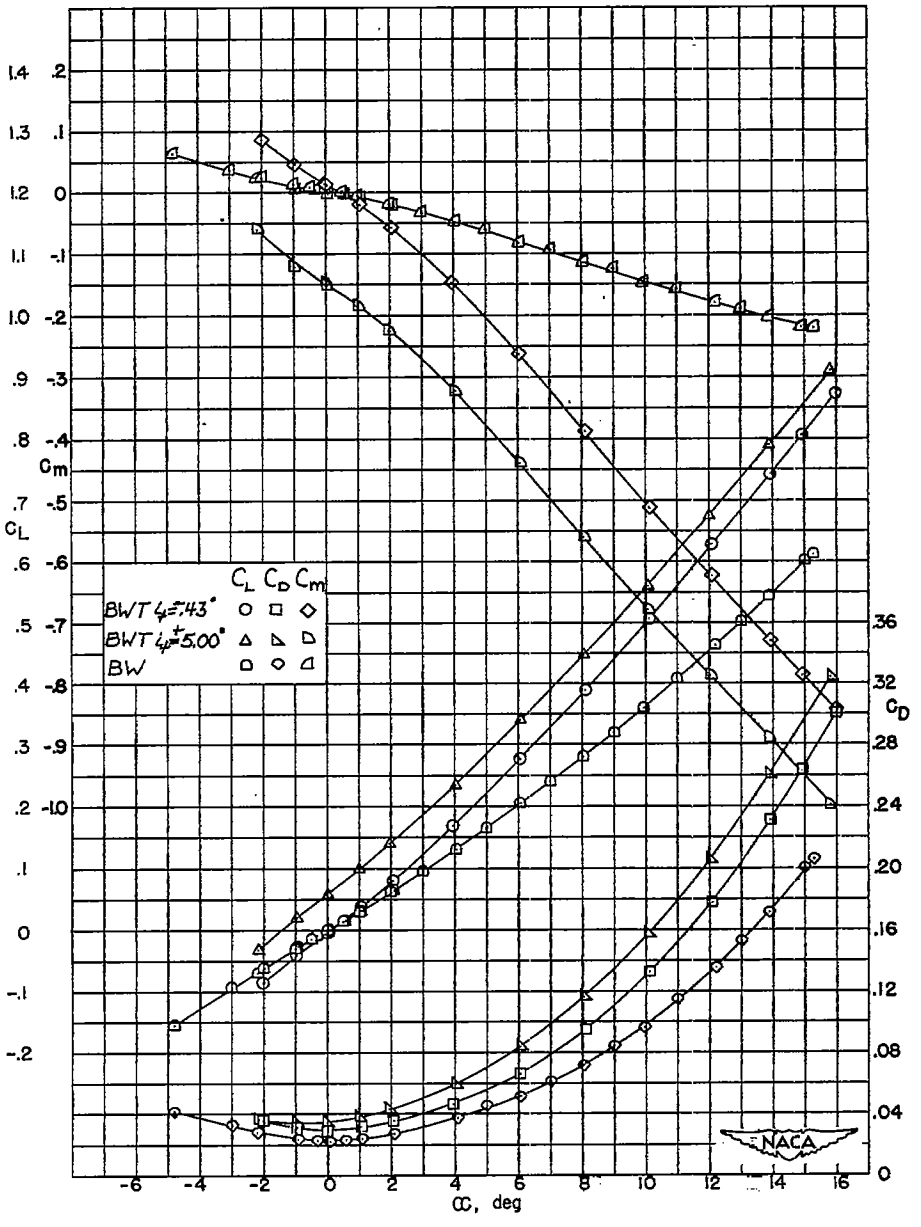

(j) BW_3T_1; wing rearward.

Figure 4.- Continued.

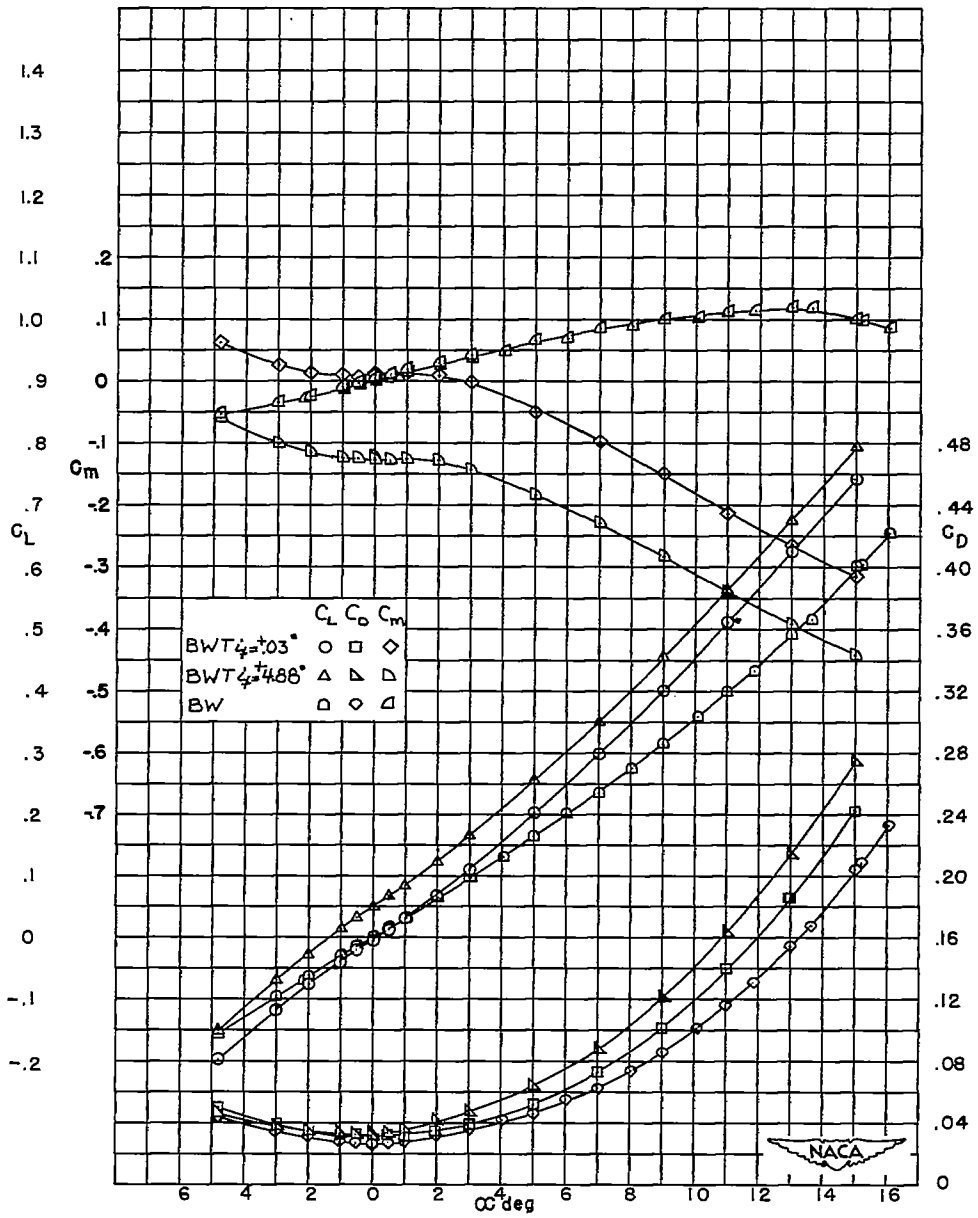

(k) BW_3T_2; wing forward.

Figure 4.- Continued.

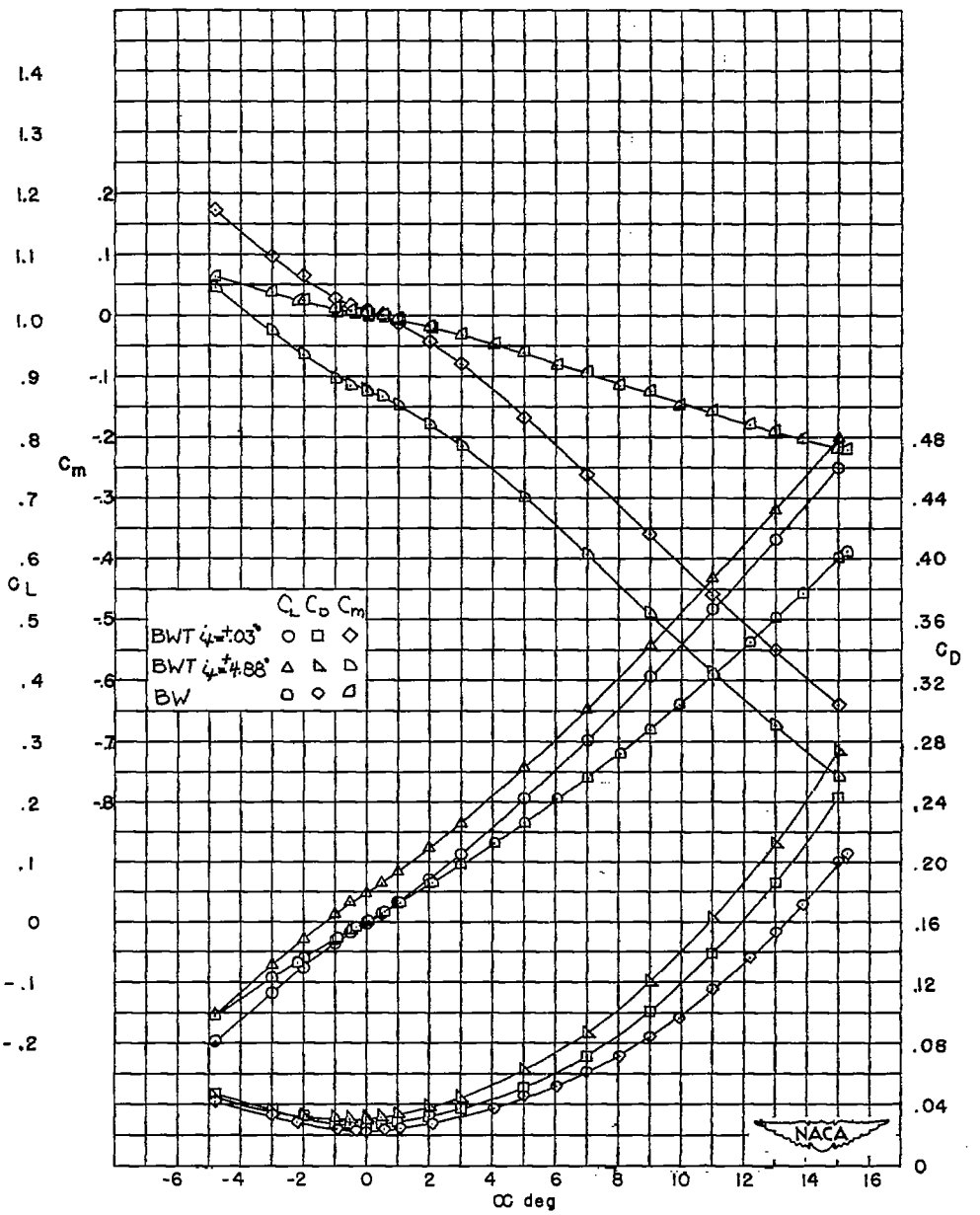

(l) BW_3T_2; wing rearward.

Figure 4.- Continued.

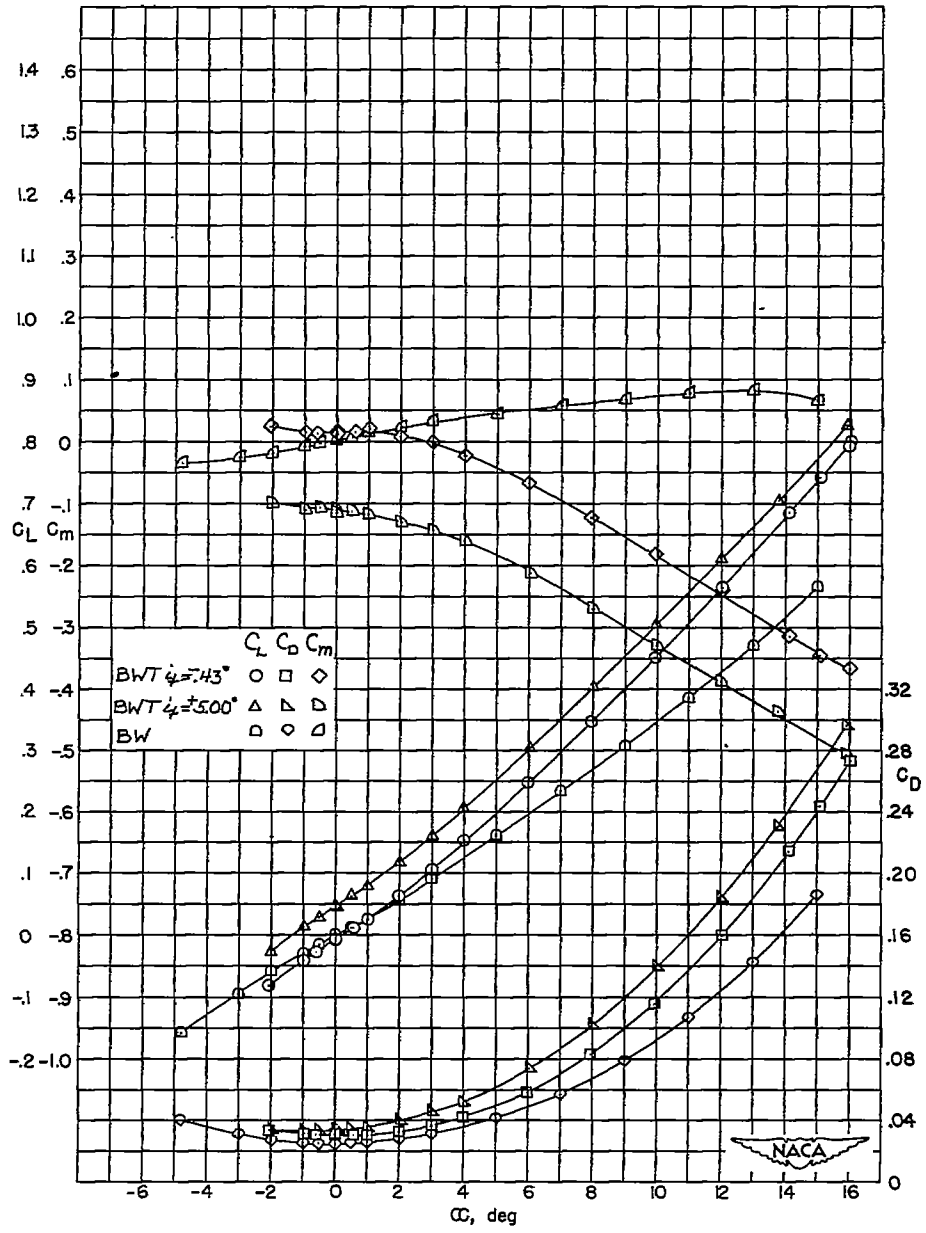

(m) BW_4T_1; wing forward.

Figure 4.- Continued.

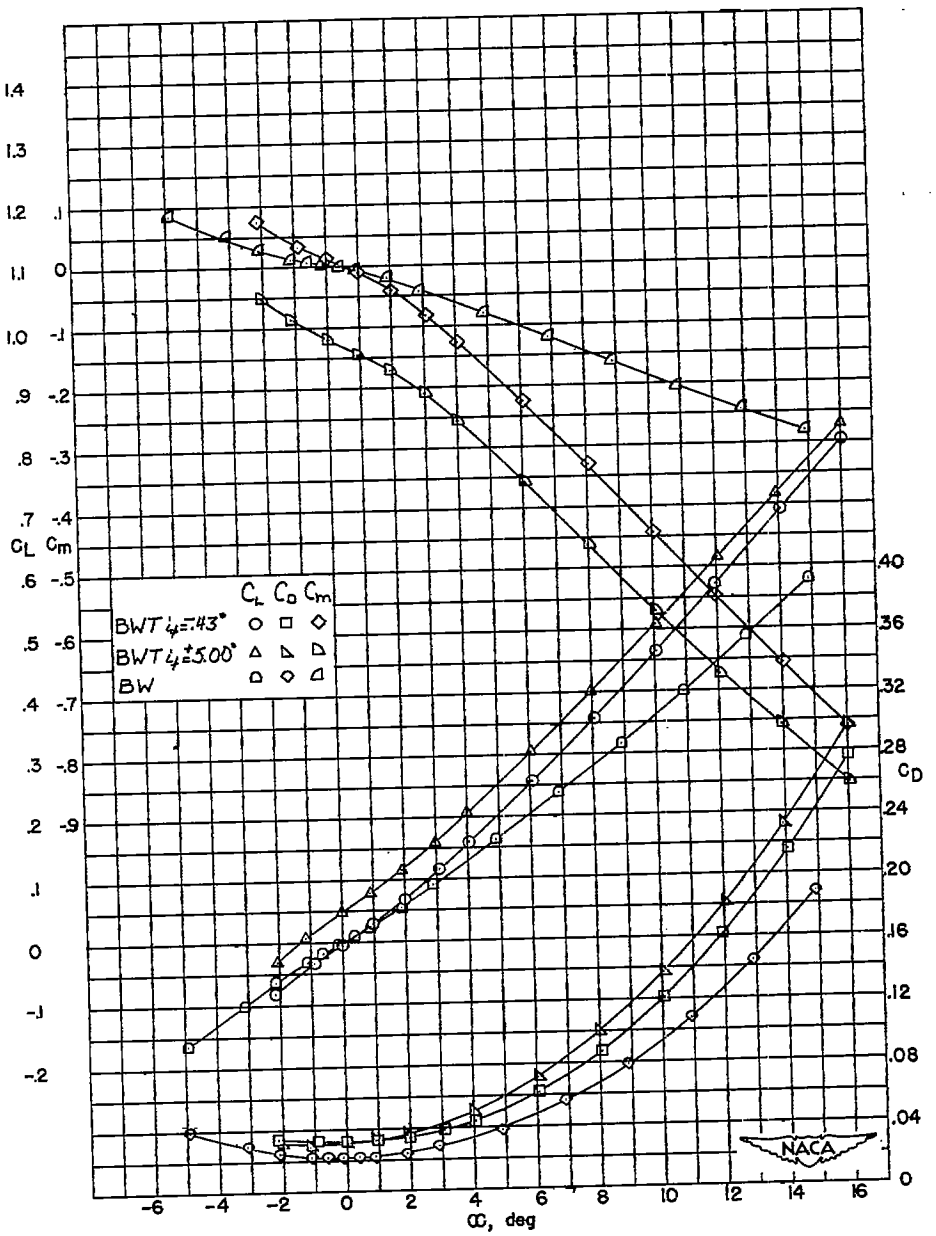

(n) BW_4T_1; wing rearward.

Figure 4.- Continued.

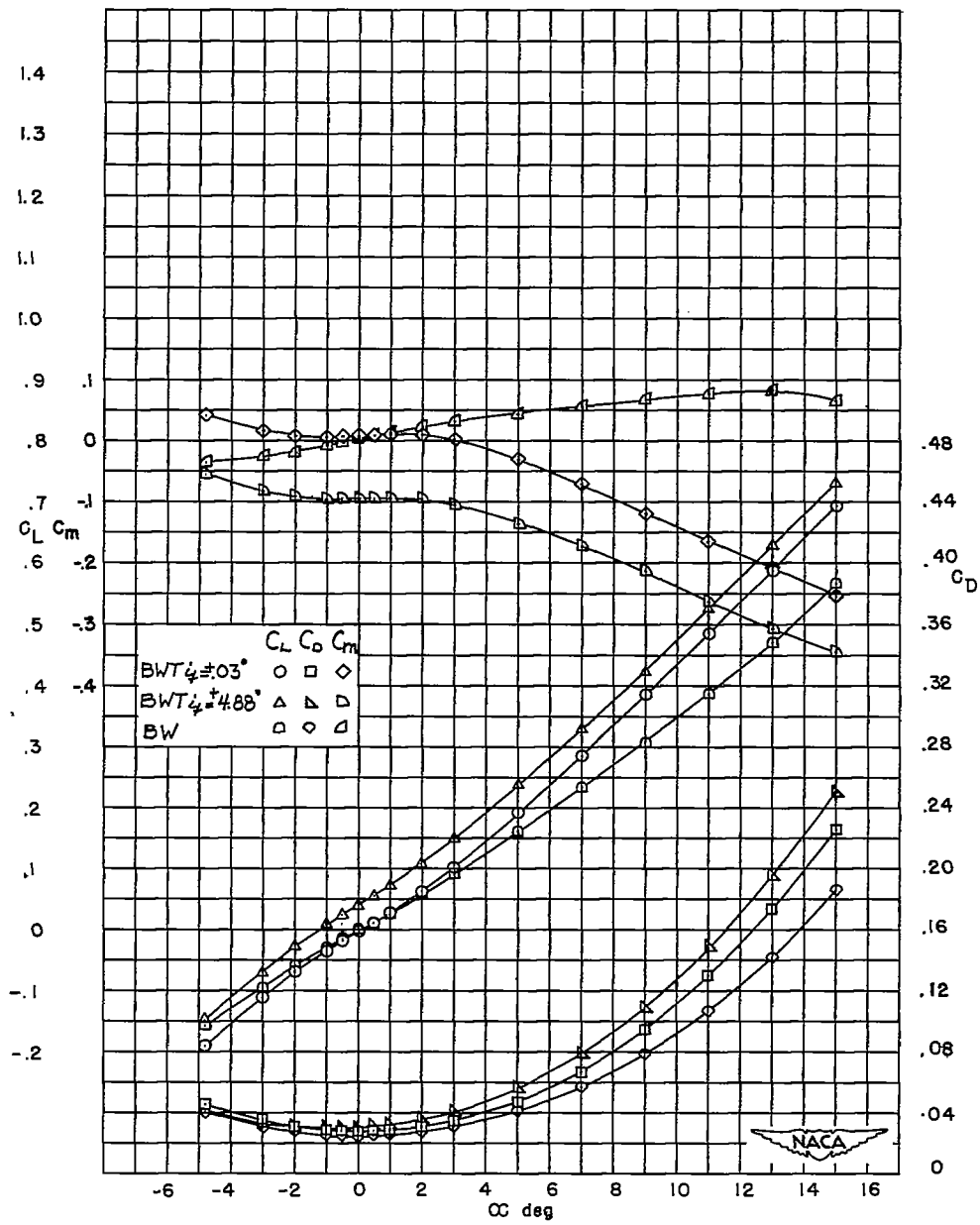

(o) BW_4T_2; wing forward.

Figure 4.- Continued.

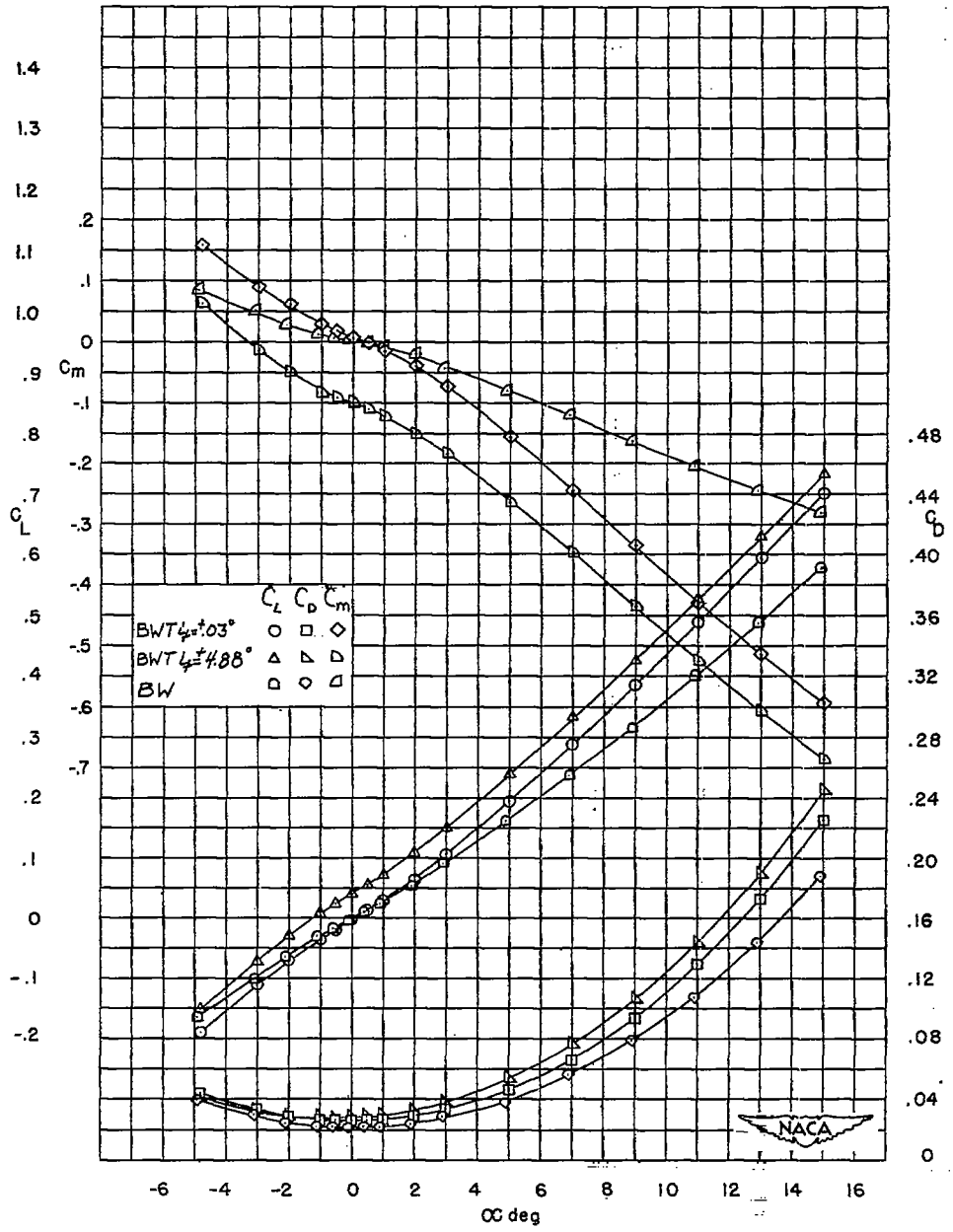

(p) BW_4T_2; wing rearward.

Figure 4.- Concluded.

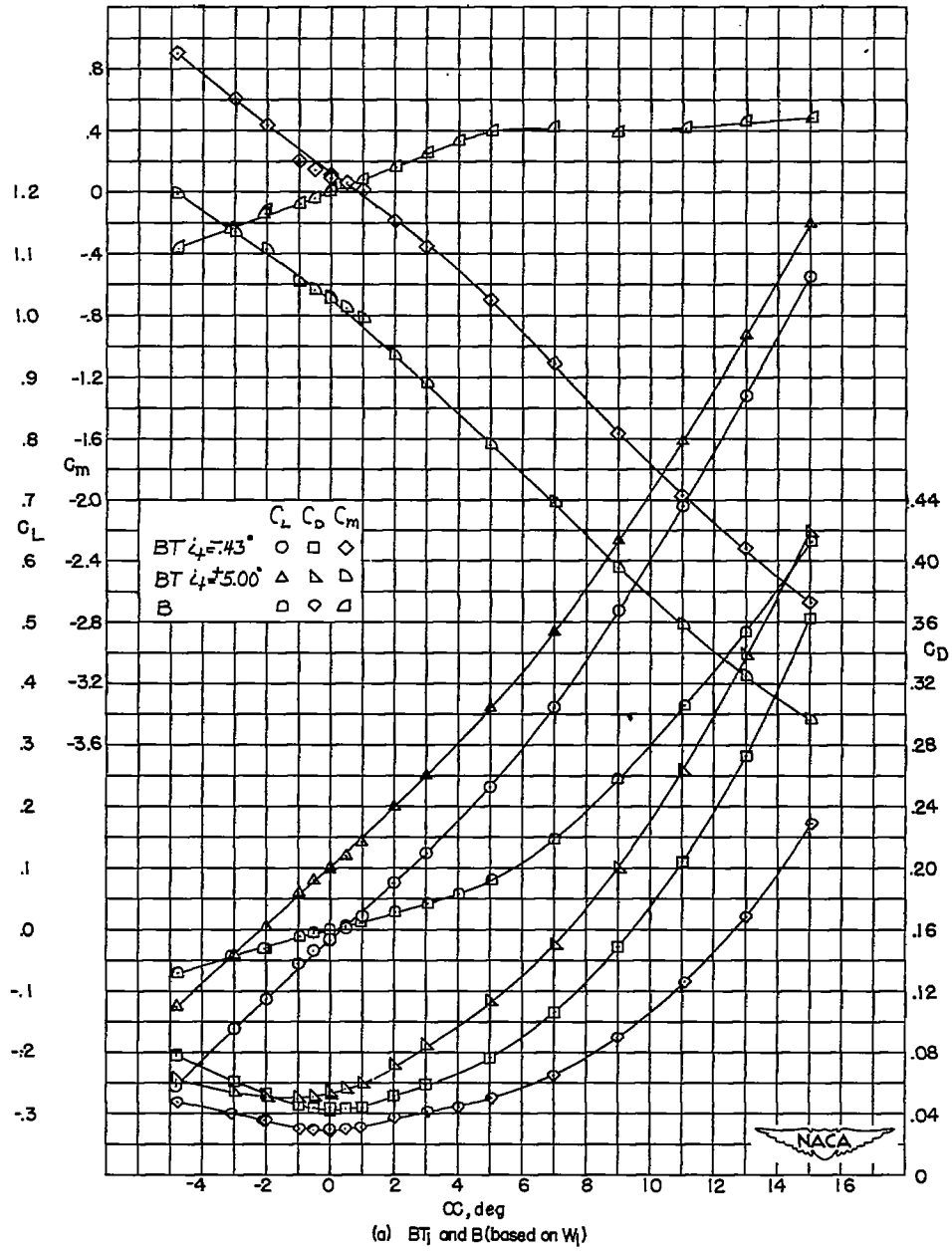

Figure 5.- Aerodynamic characteristics of the BT and B configurations at M = 1.93.

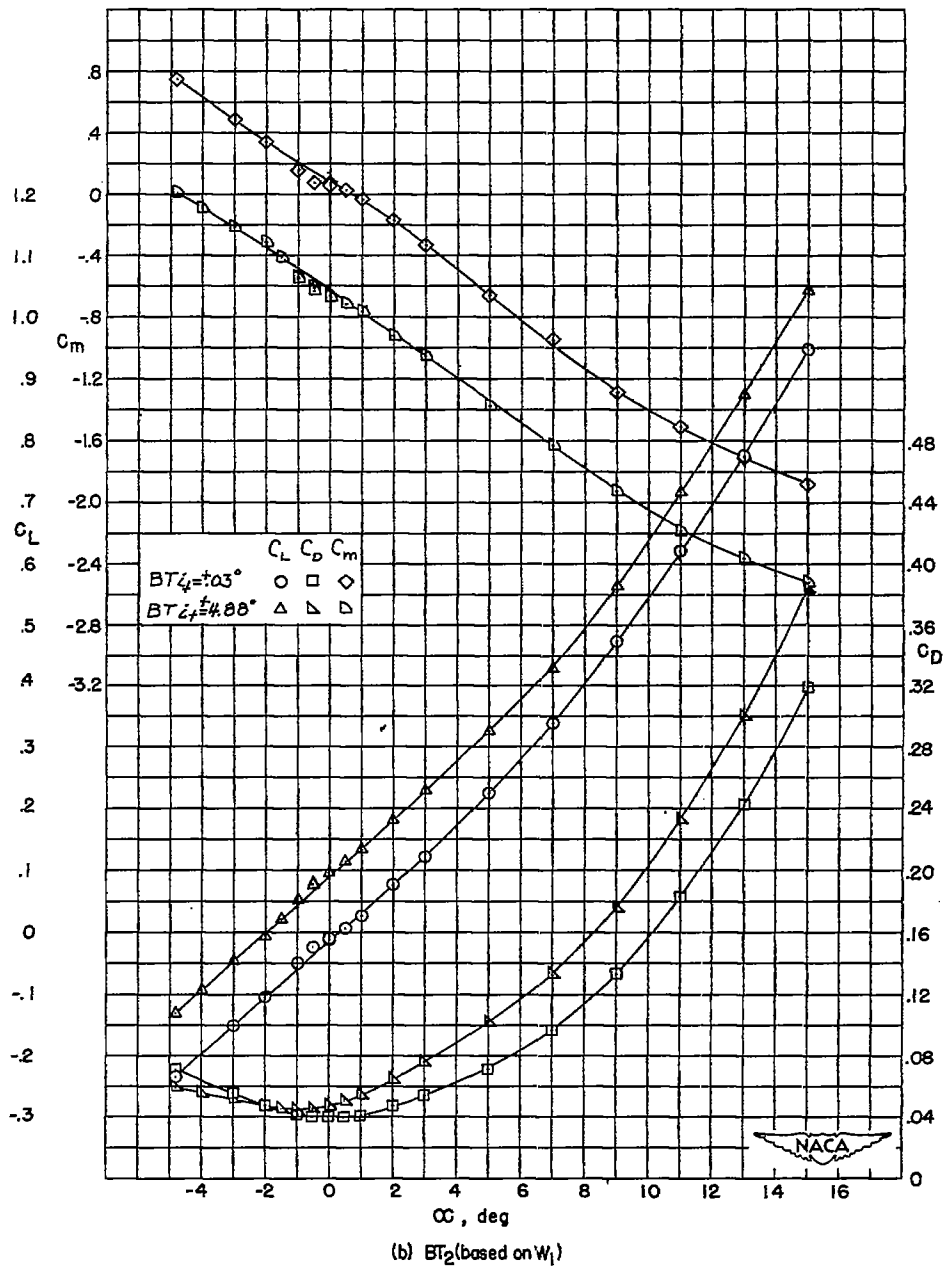

(b) BT_2(based on W_1)

Figure 5.- Continued.

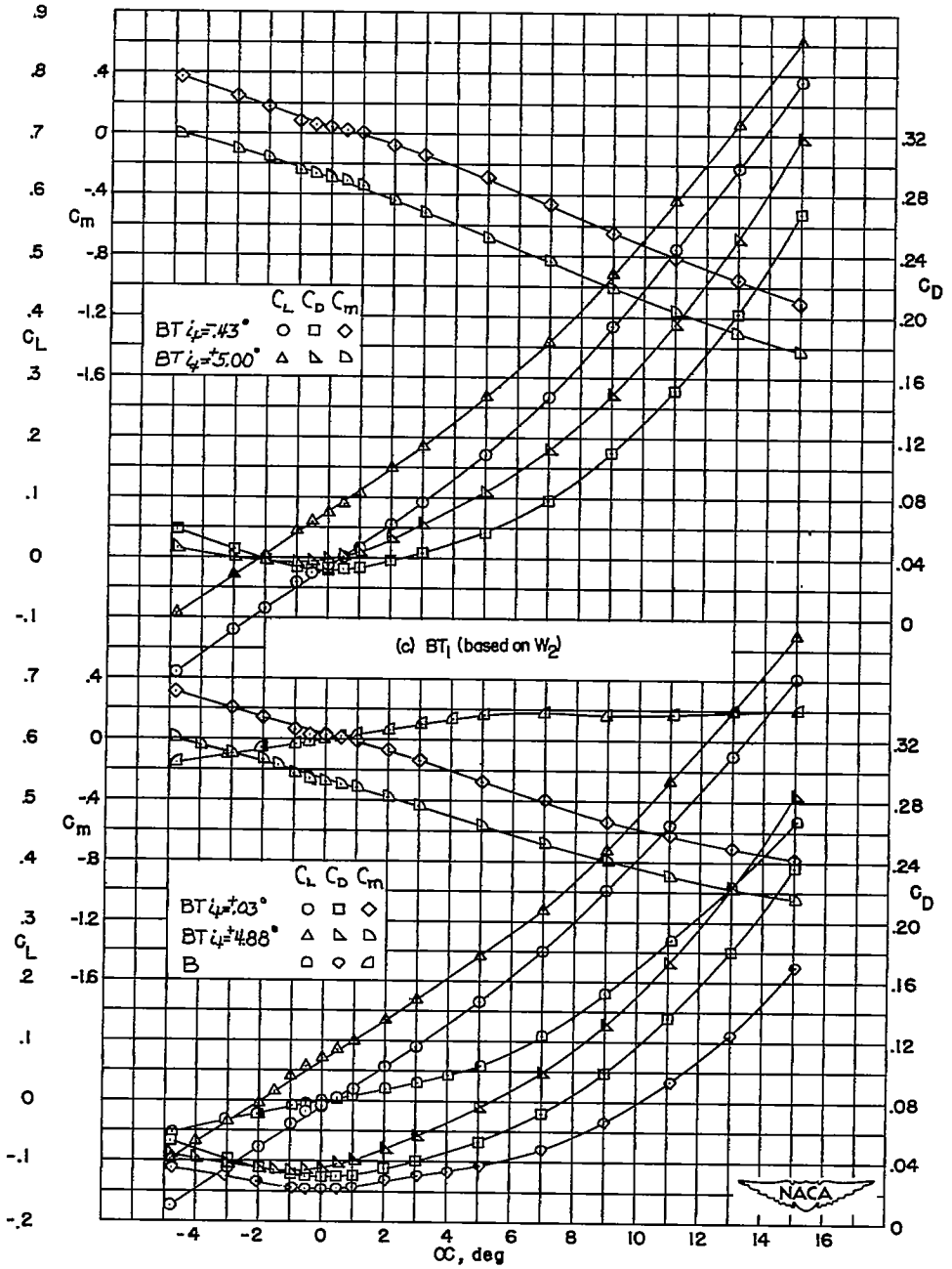

(d) BT_2 and B (based on W_2)

Figure 5.- Continued.

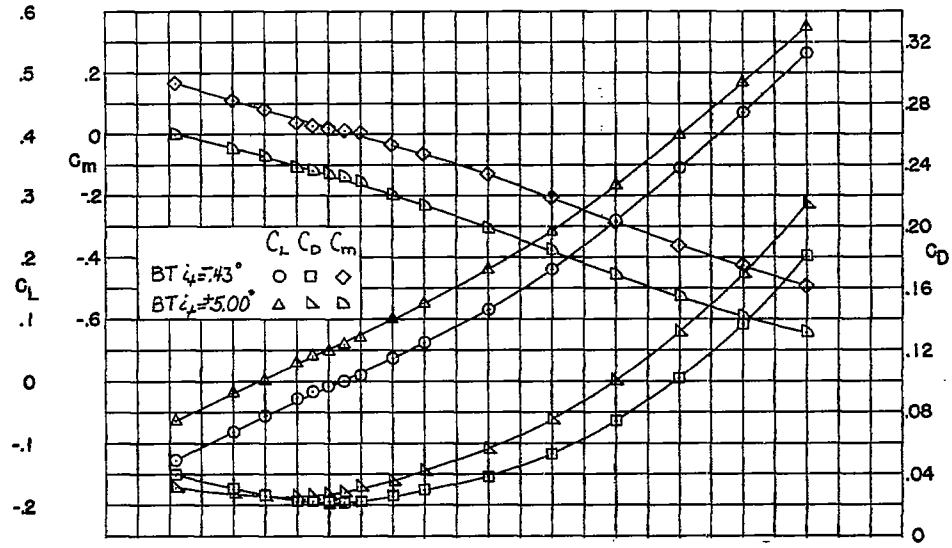

(e) BT_1 (based on W_3)

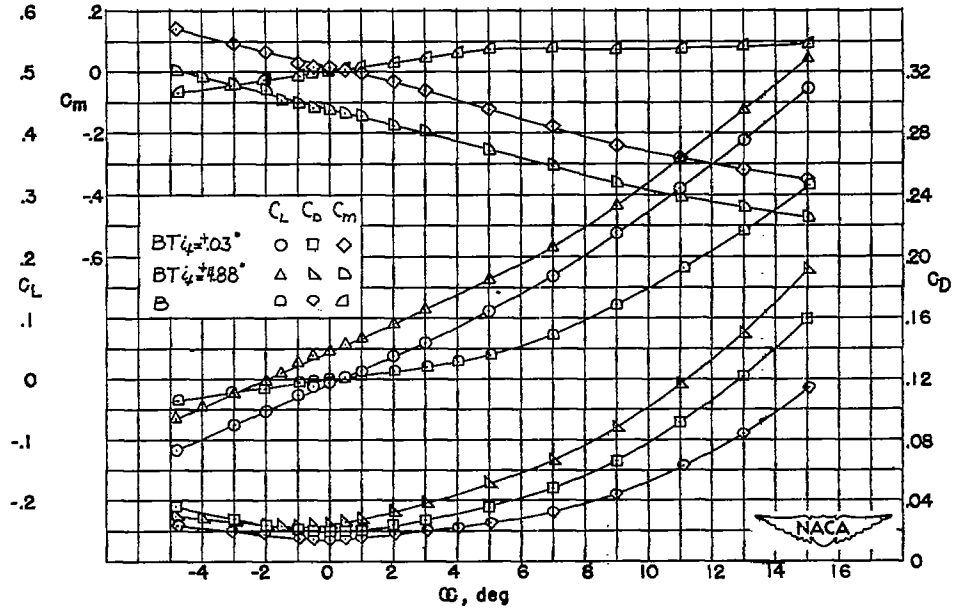

(f) BT_2 and B (based on W_3)

Figure 5.- Continued.

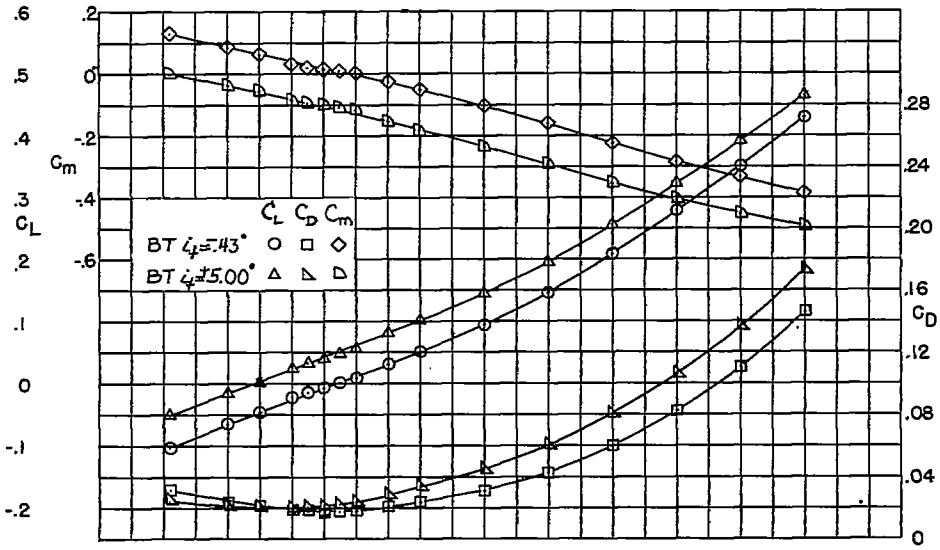

(g) BT_1 (based on W_4)

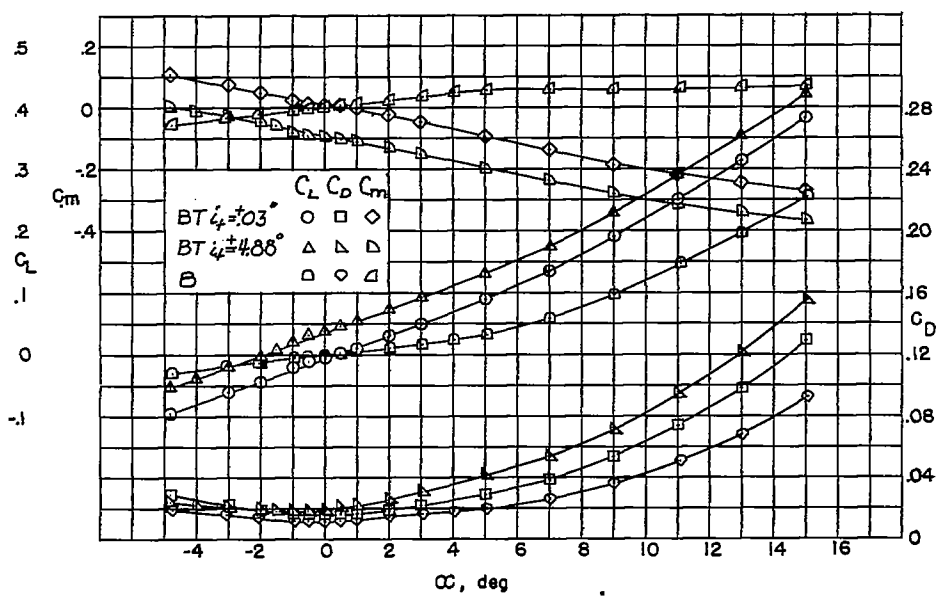

(h) BT_2 and B (based on W_4)

Figure 5.- Concluded.

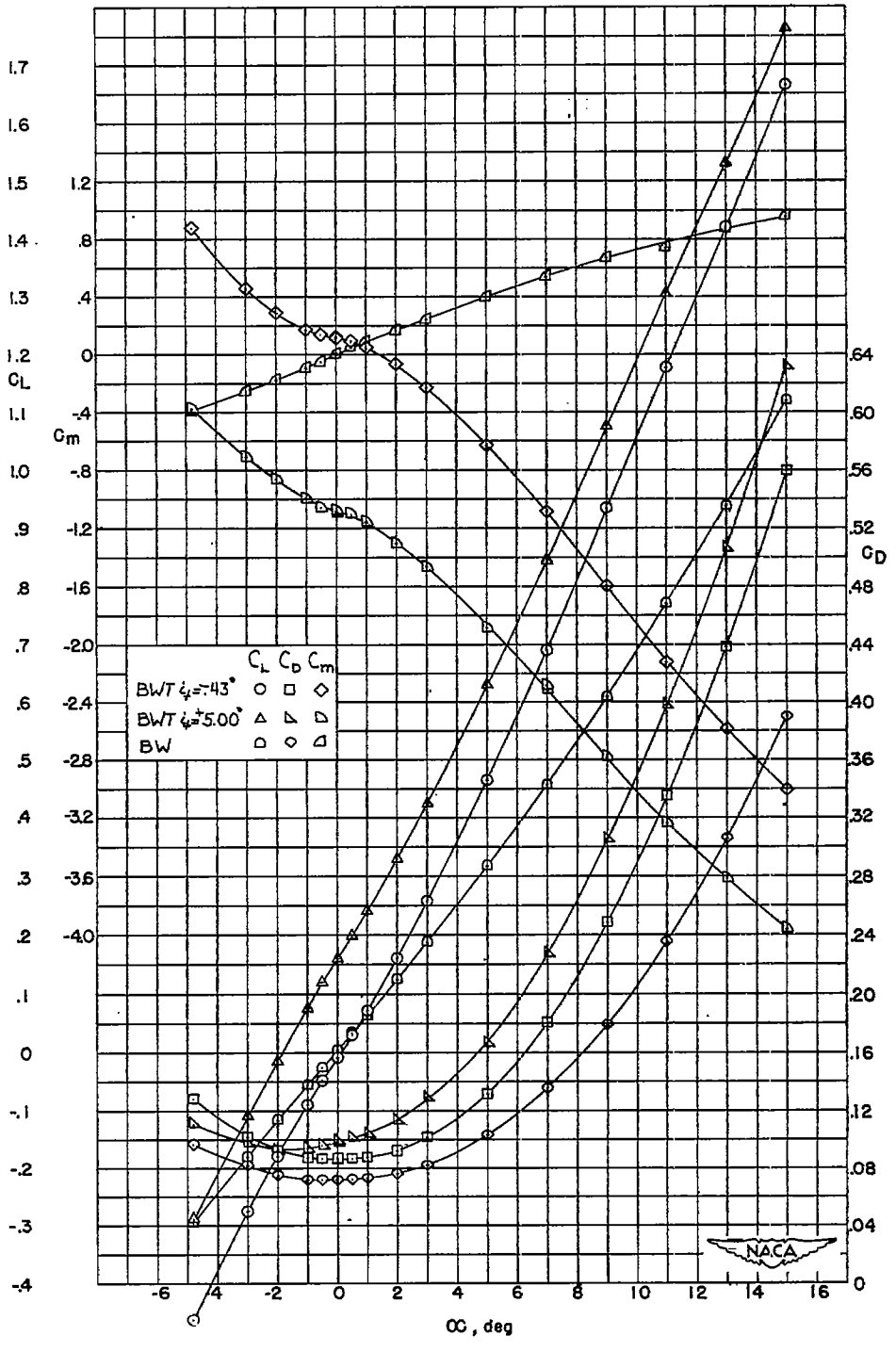

(a) BW_1T_1; wing forward.

Figure 6.- Aerodynamic characteristics of the BWT and BW configurations at M = 1.62.

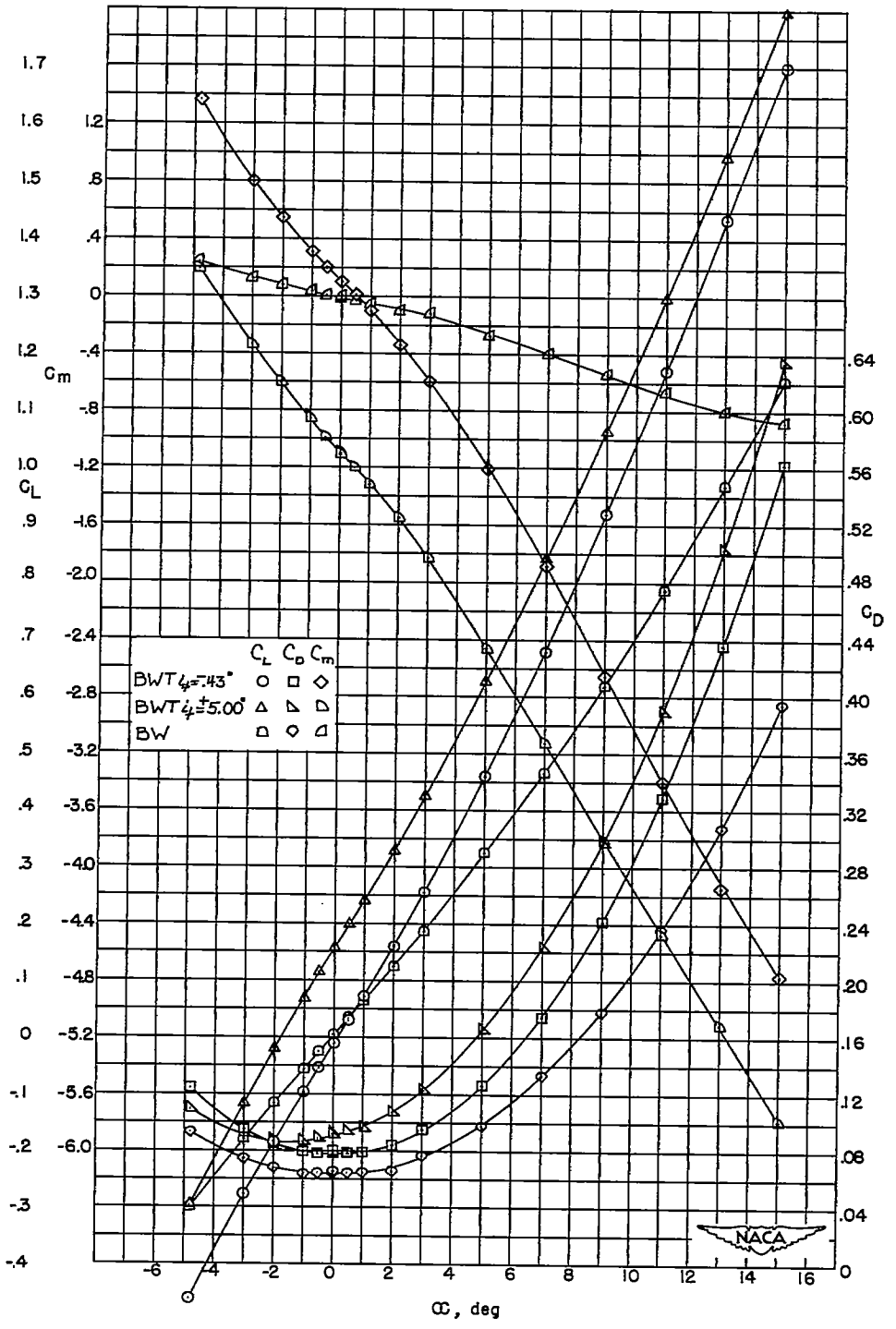

(b) BW_1T_1; wing rearward.

Figure 6.- Continued.

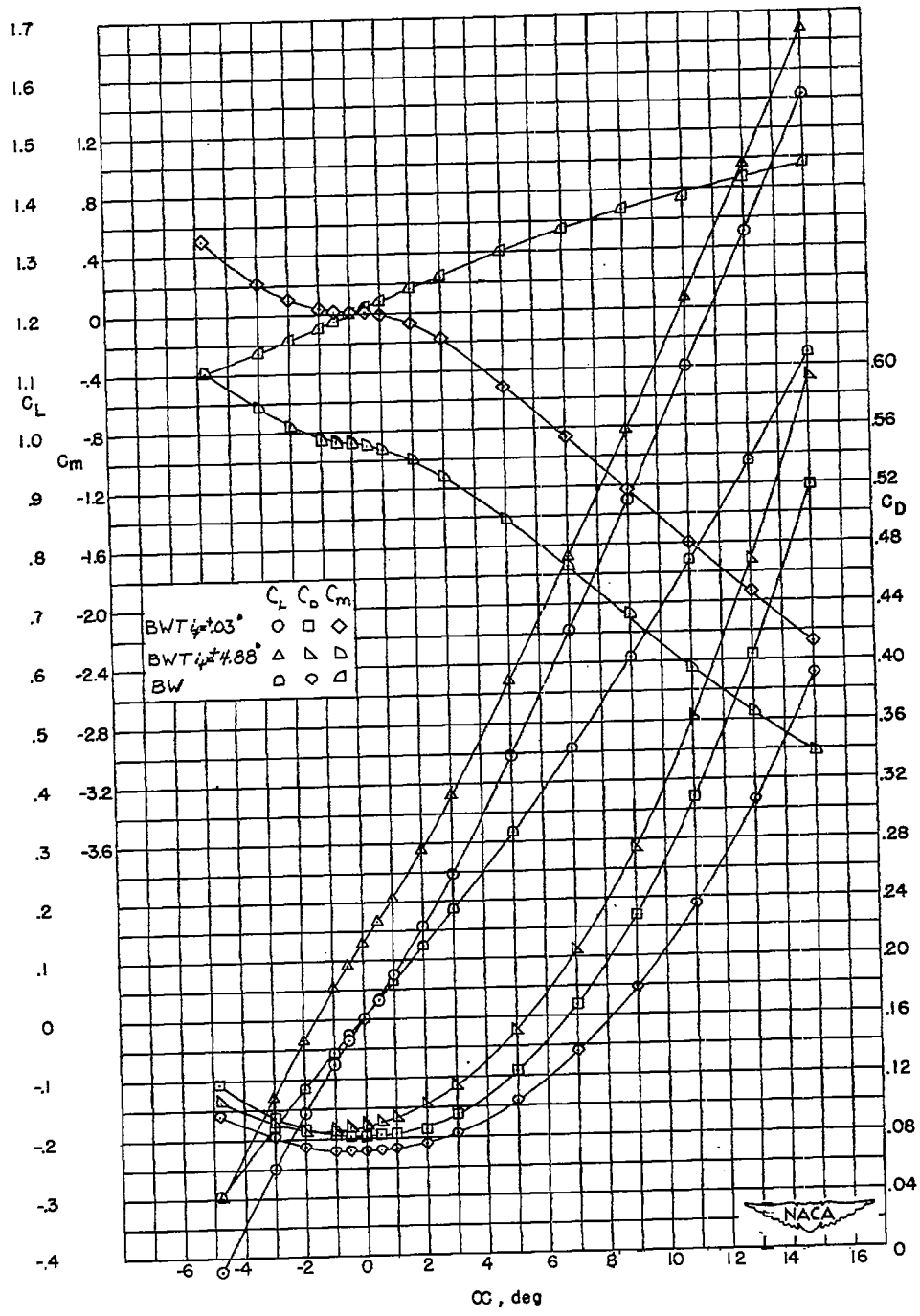

(c) BW_1T_2; wing forward.

Figure 6.- Continued.

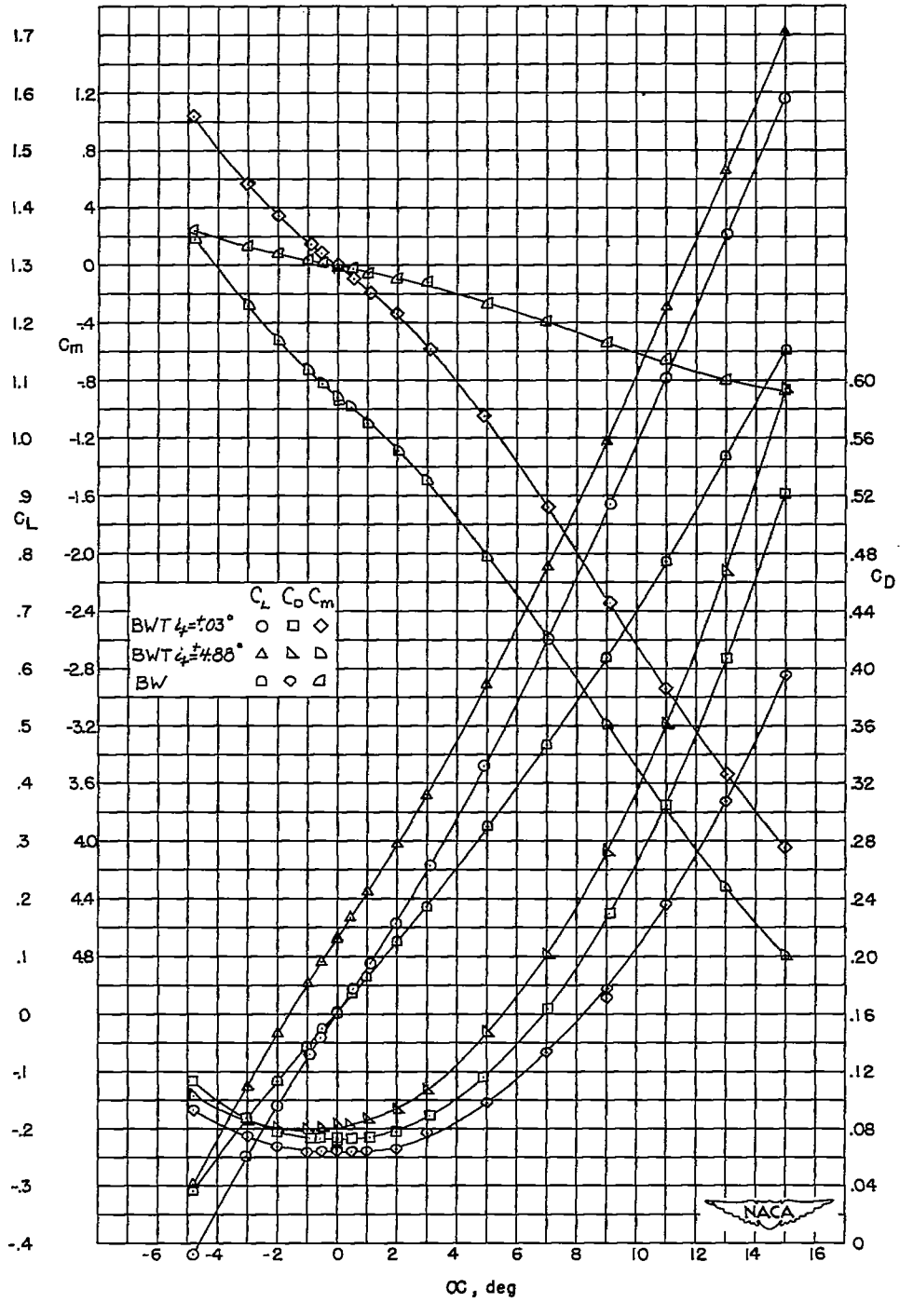

(d) BW_1T_2; wing rearward.

Figure 6.- Continued.

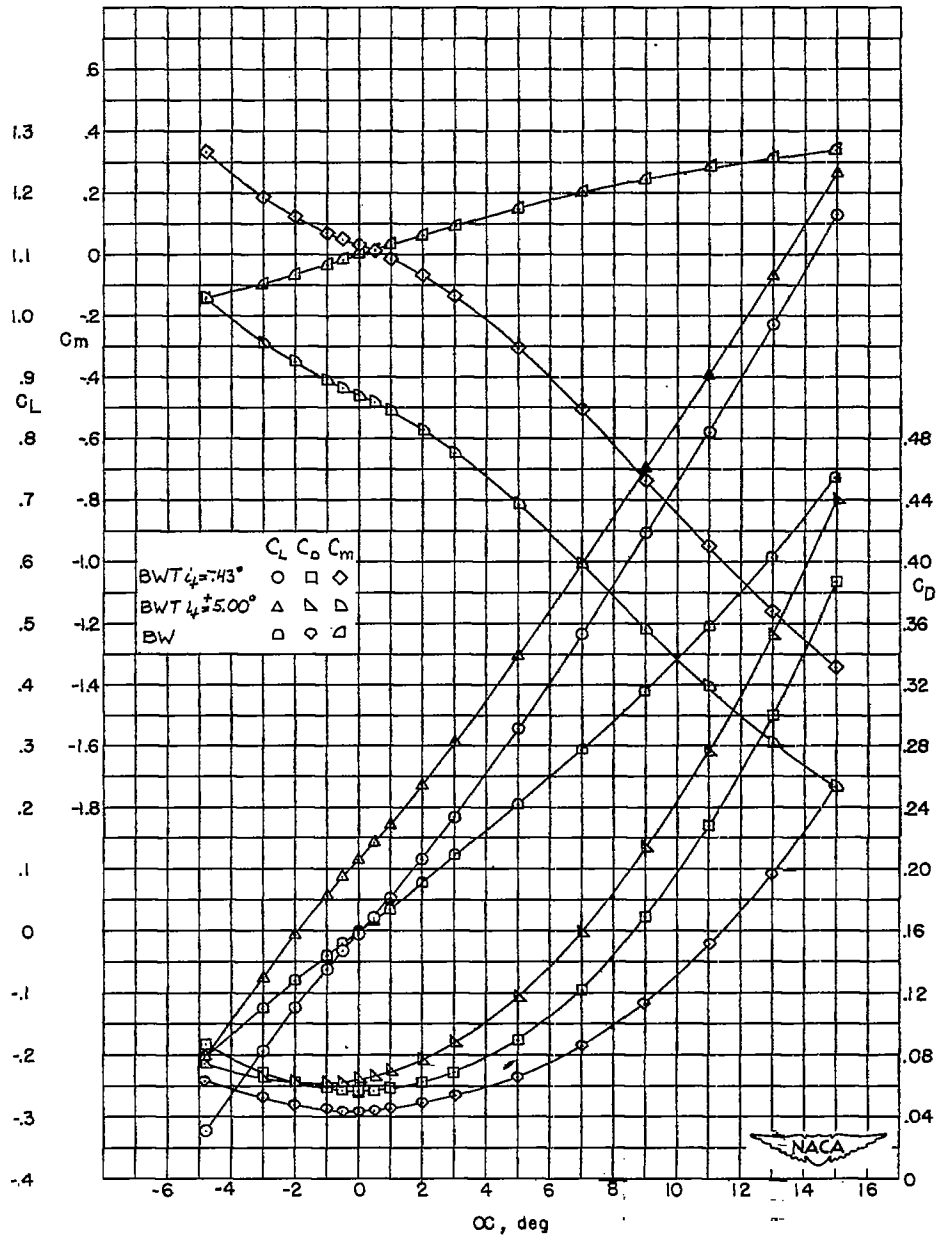

(e) BW_2T_1; wing forward.

Figure 6.- Continued.

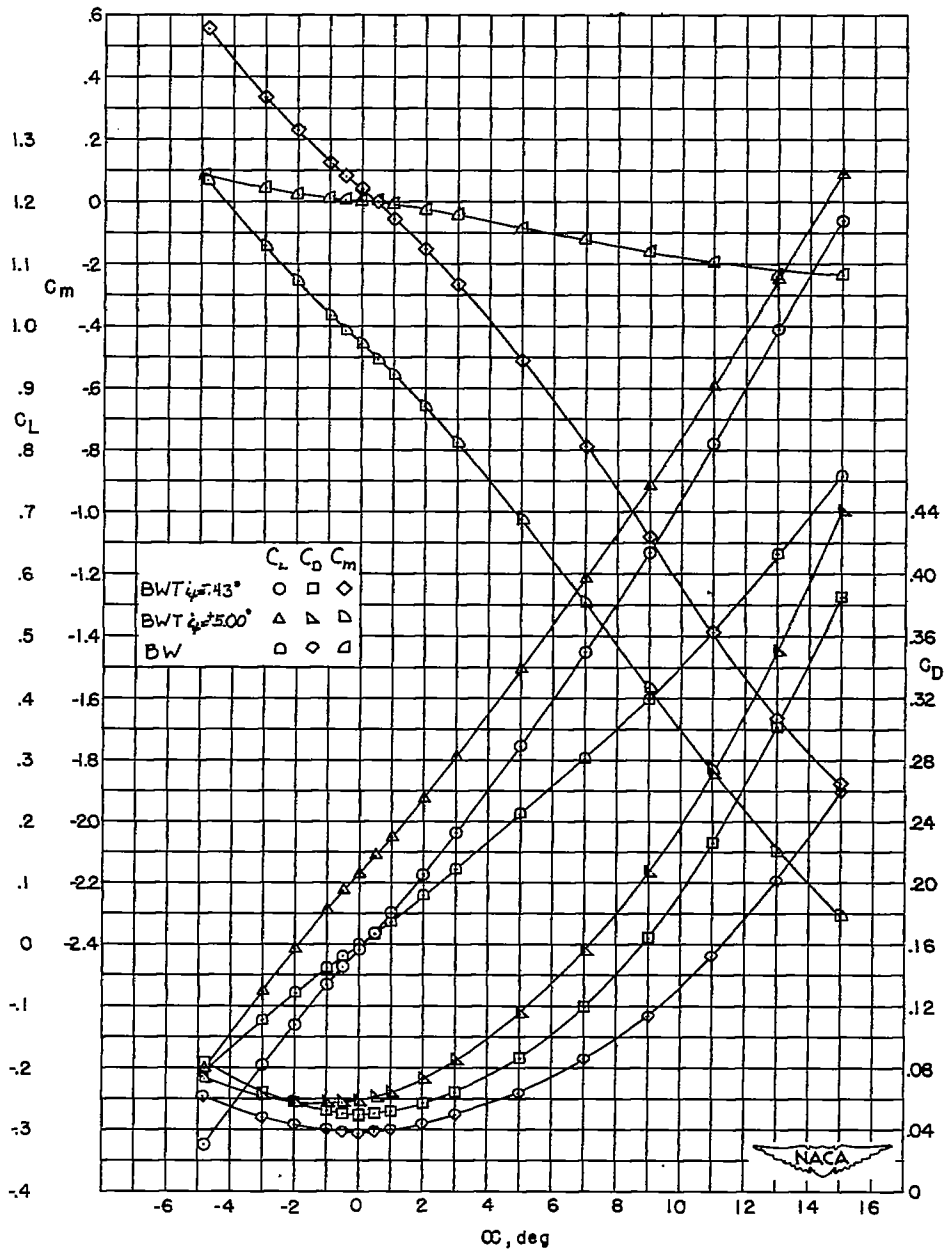

(f) BW_2T_1; wing rearward.

Figure 6.- Continued.

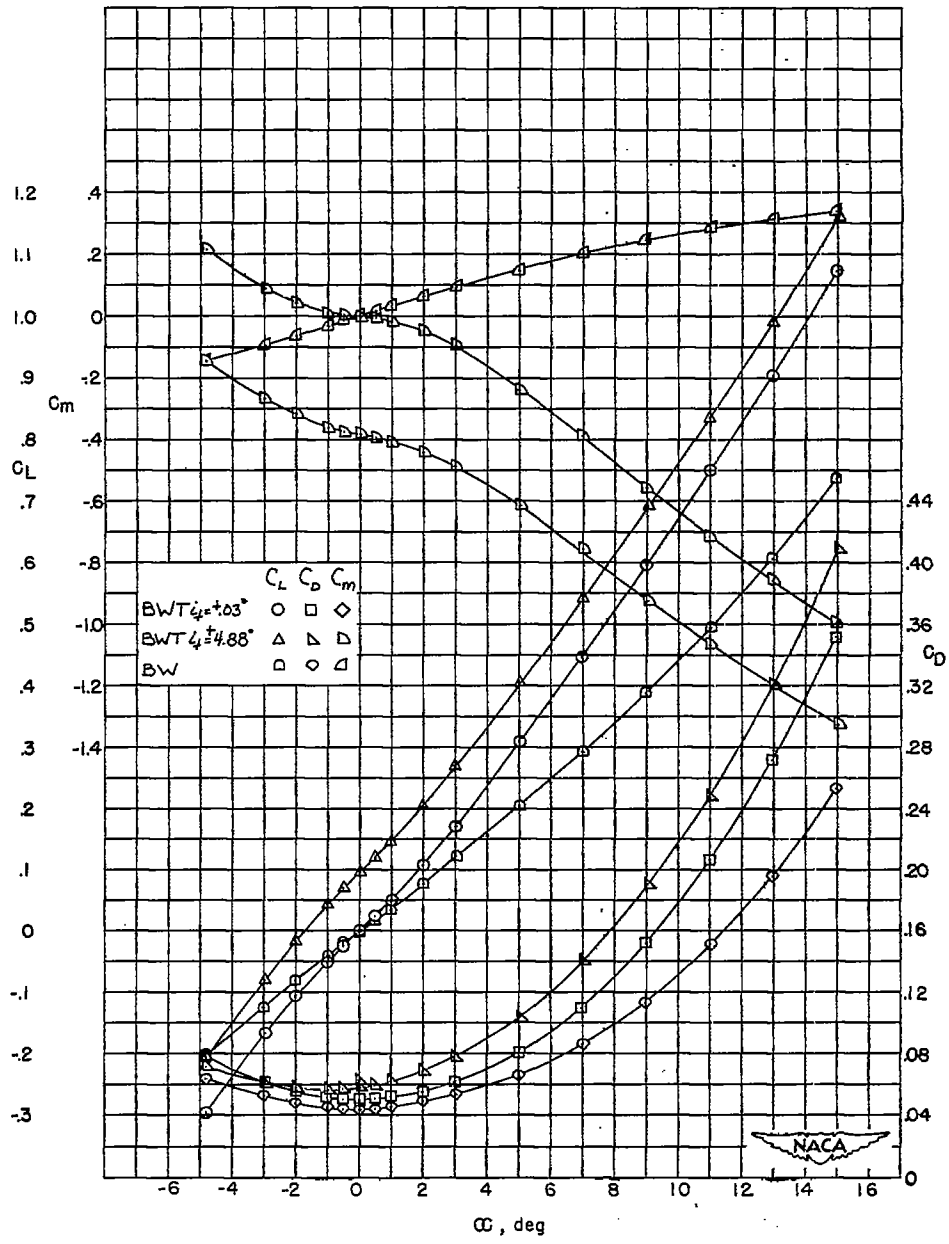

(g) BW_2T_2; wing forward.

Figure 6.- Continued.

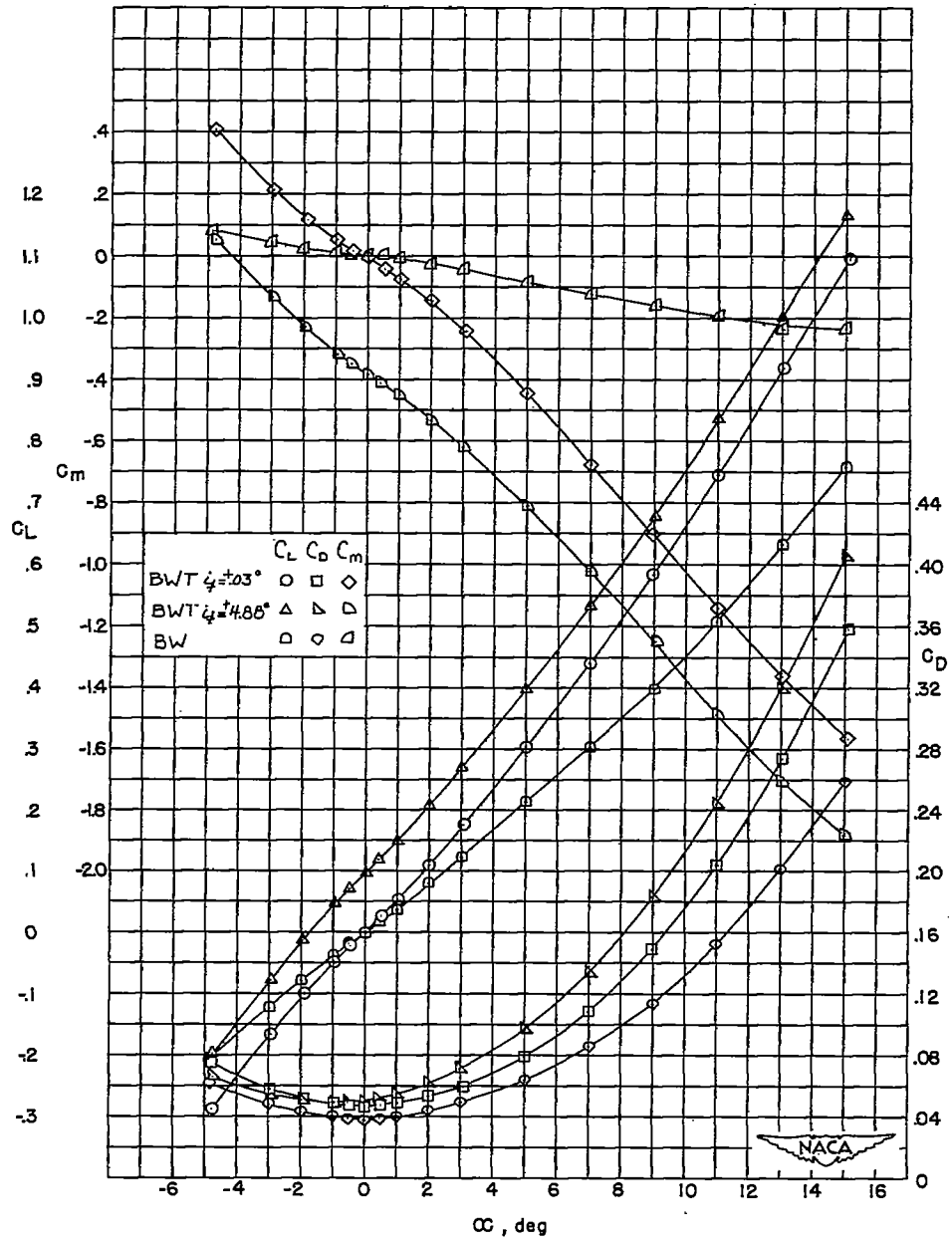

(h) BW_2T_2; wing rearward.

Figure 6.- Continued.

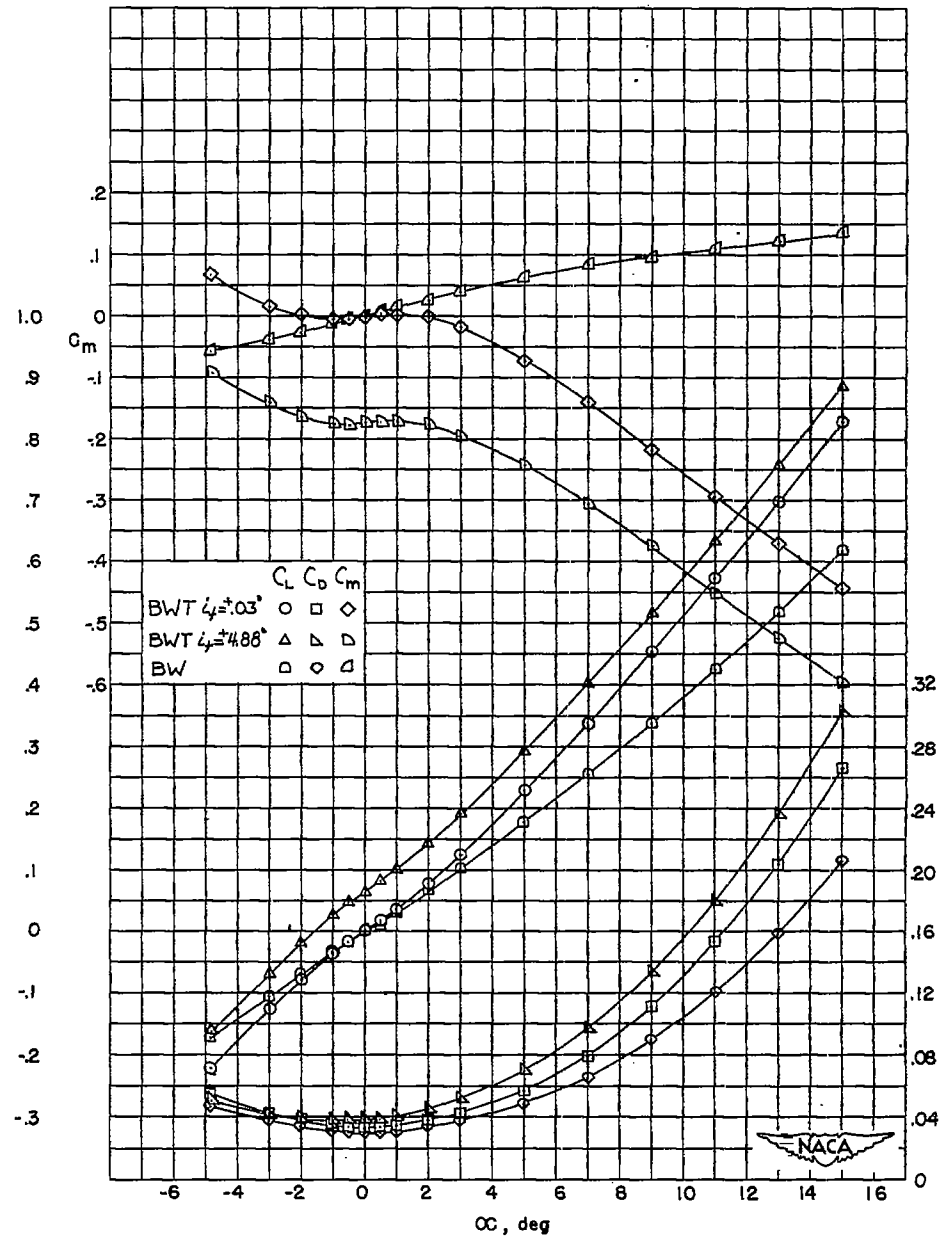

(i) BW_3T_2; wing forward.

Figure 6.- Continued.

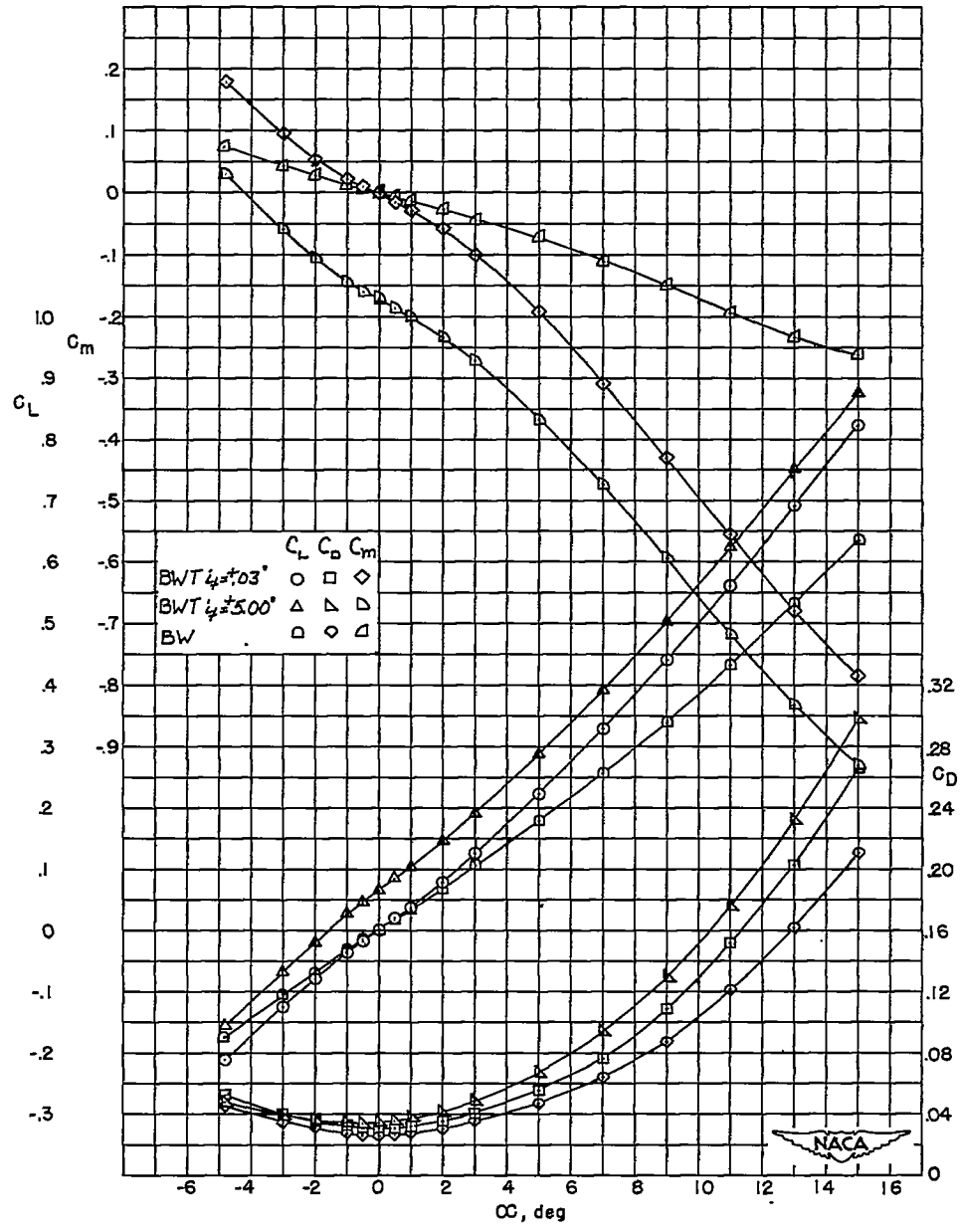

(j) BW_3T_2; wing rearward.

Figure 6.- Concluded.

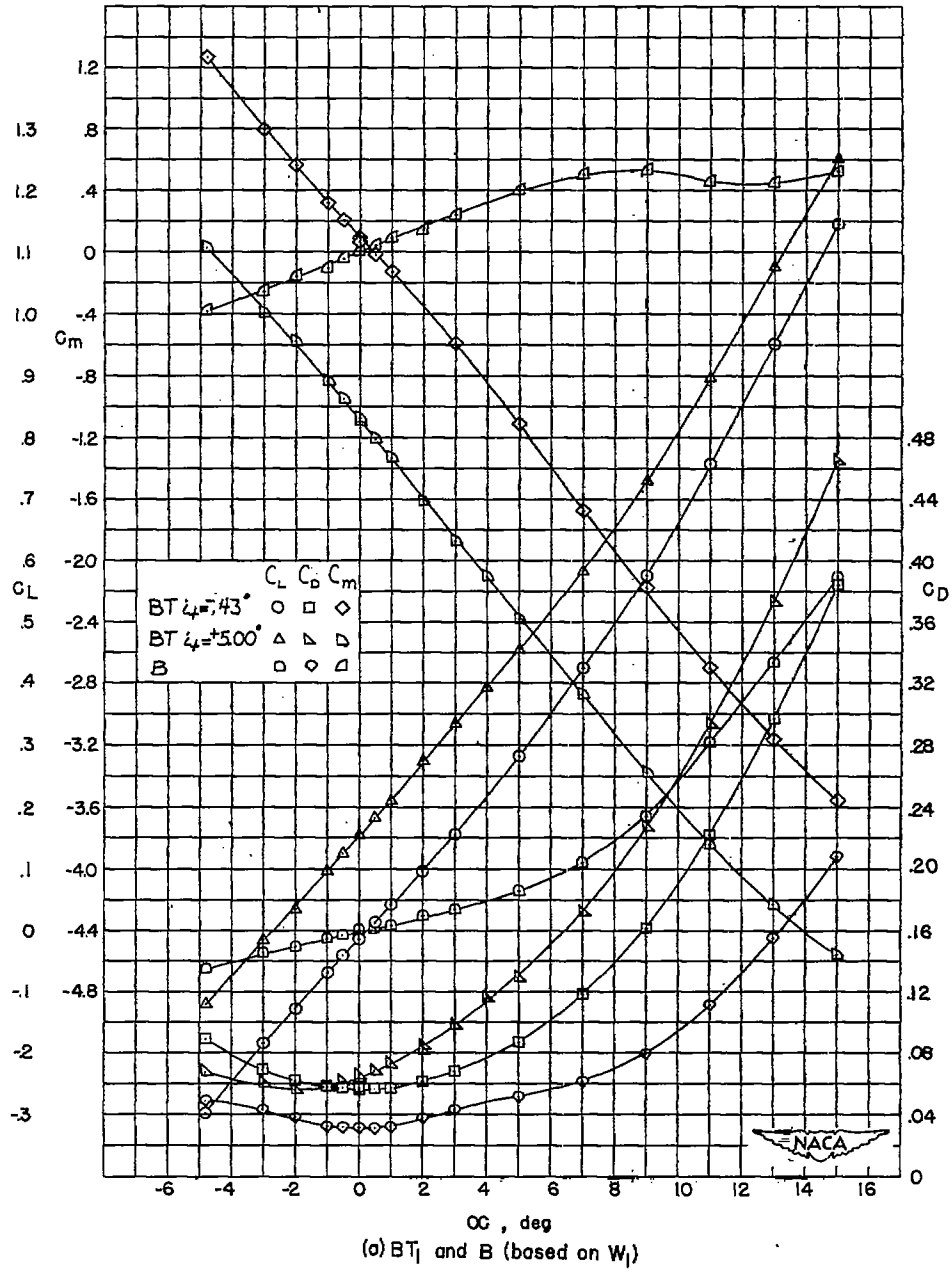

Figure 7.- Aerodynamic characteristics of the BT and B configurations at M = 1.62.

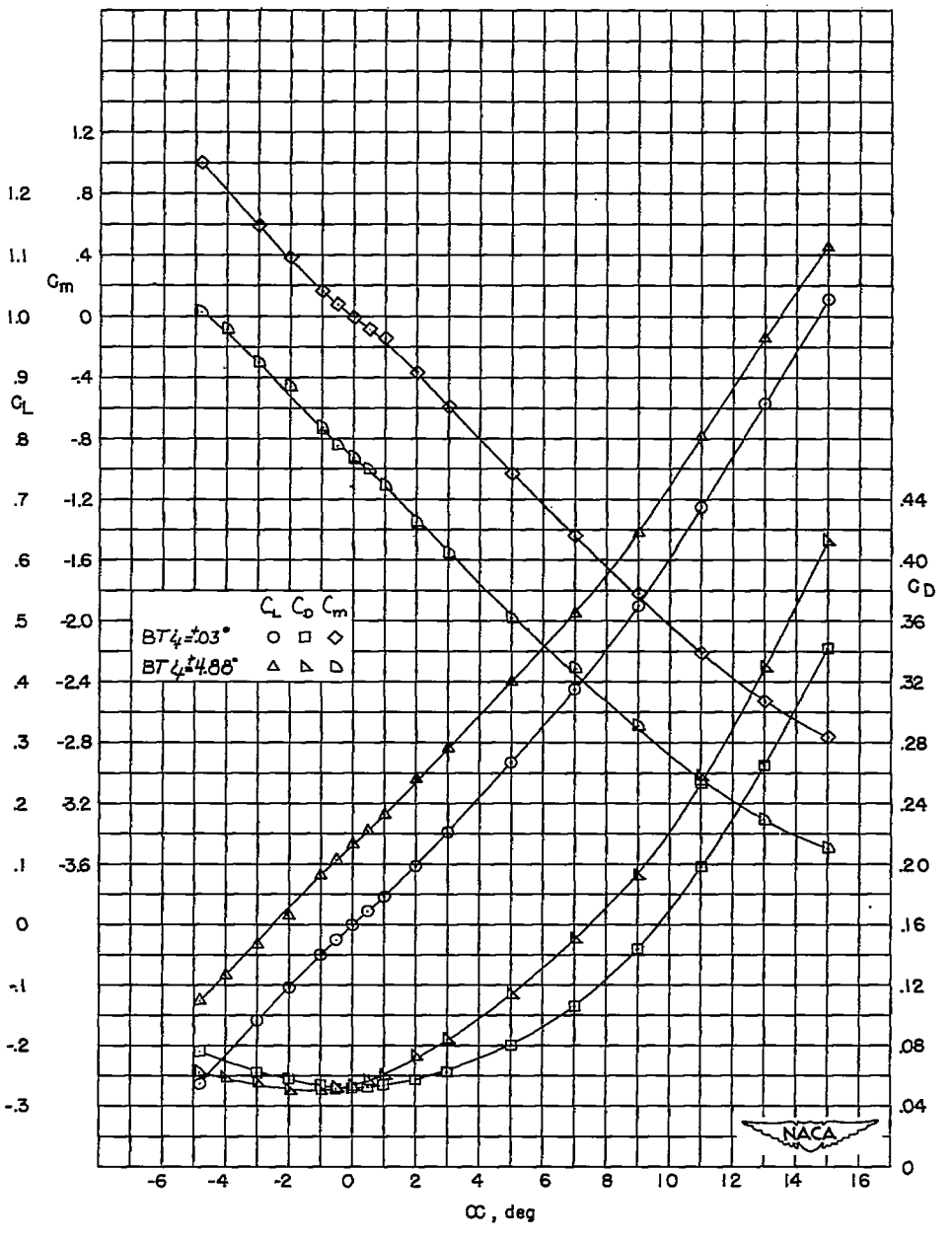

(b) BT_2 (based on W_1)

Figure 7.- Continued.

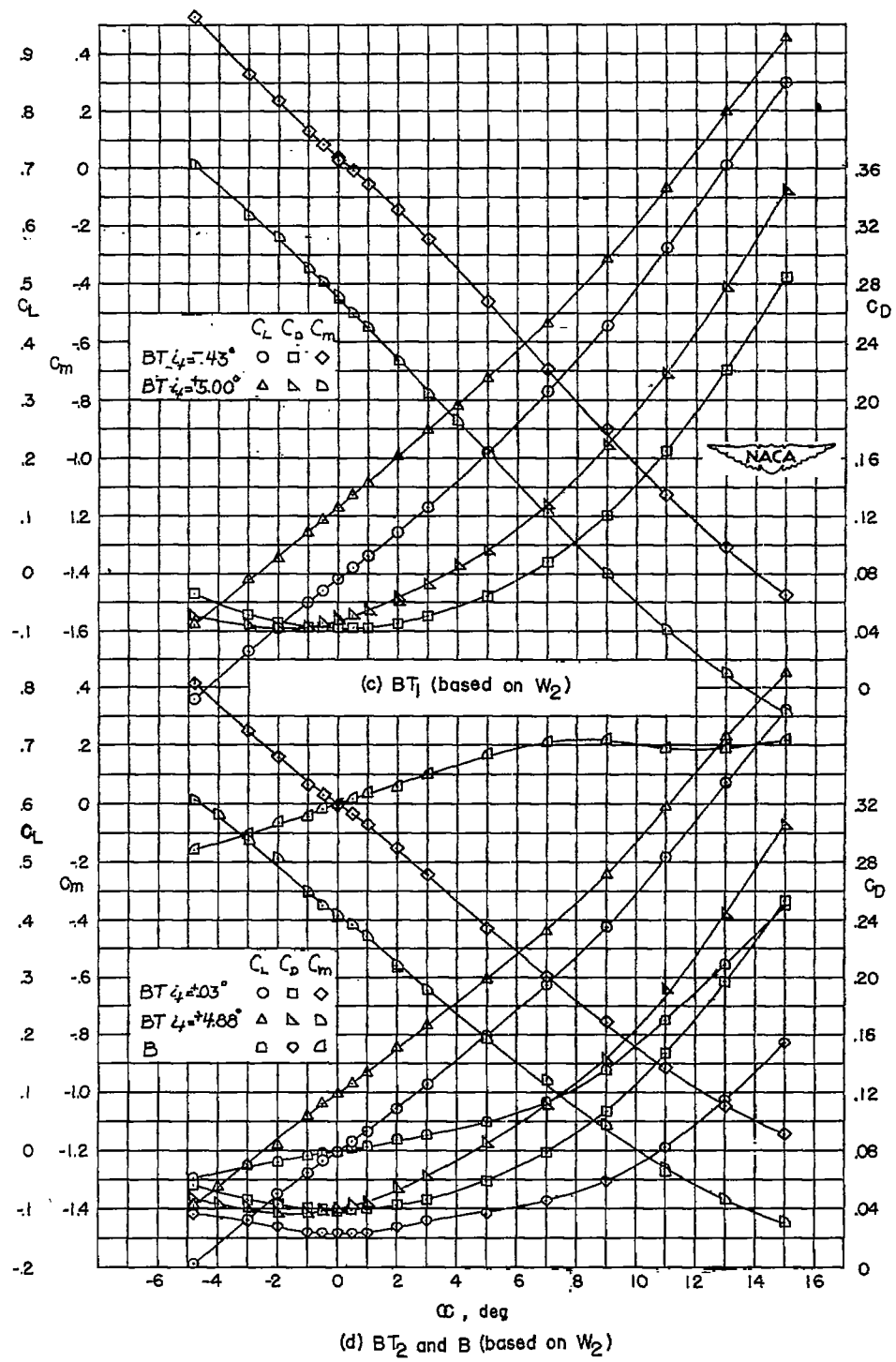

Figure 7.- Continued.

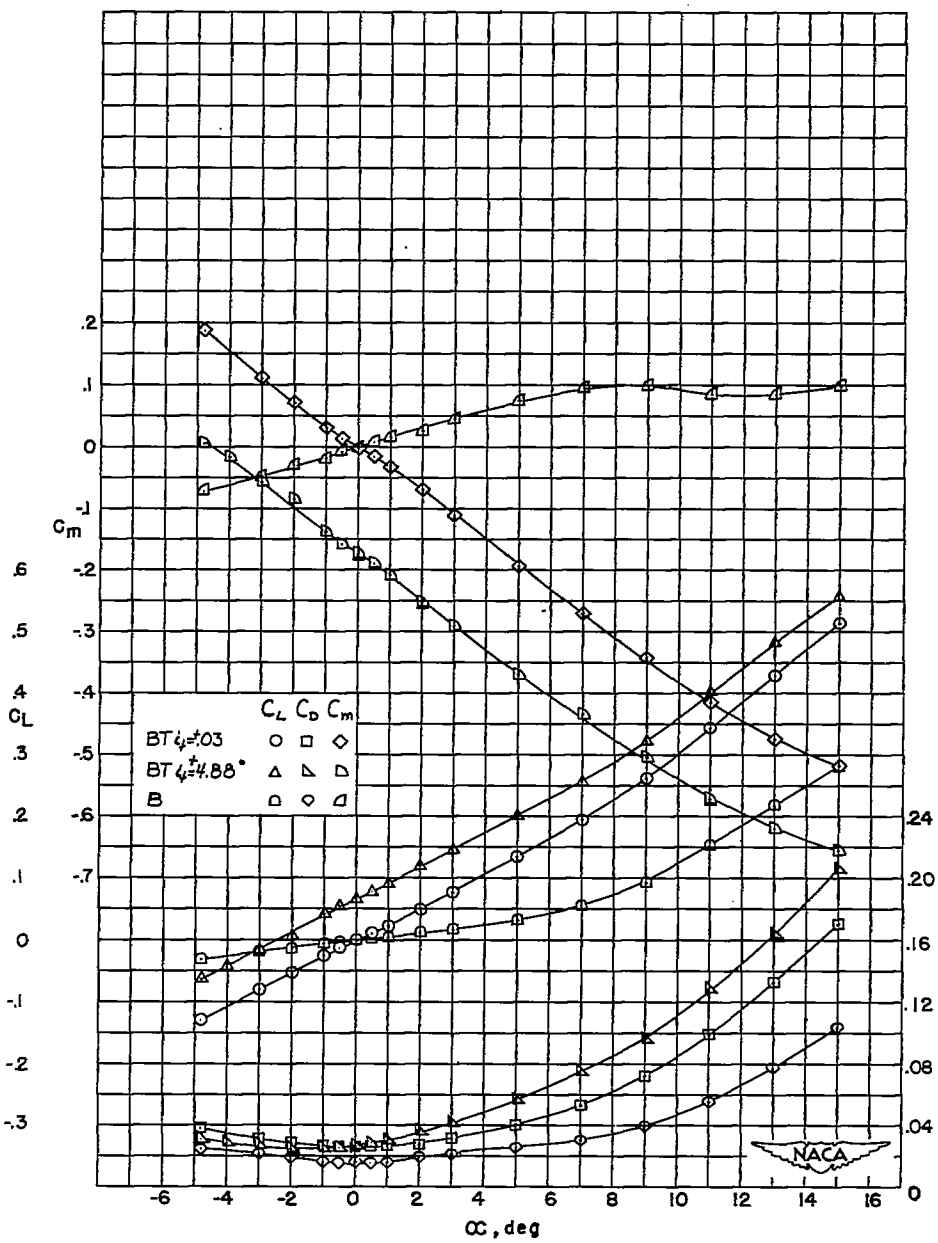

(e) BT_2 and B (based on W_3)

Figure 7.- Concluded.

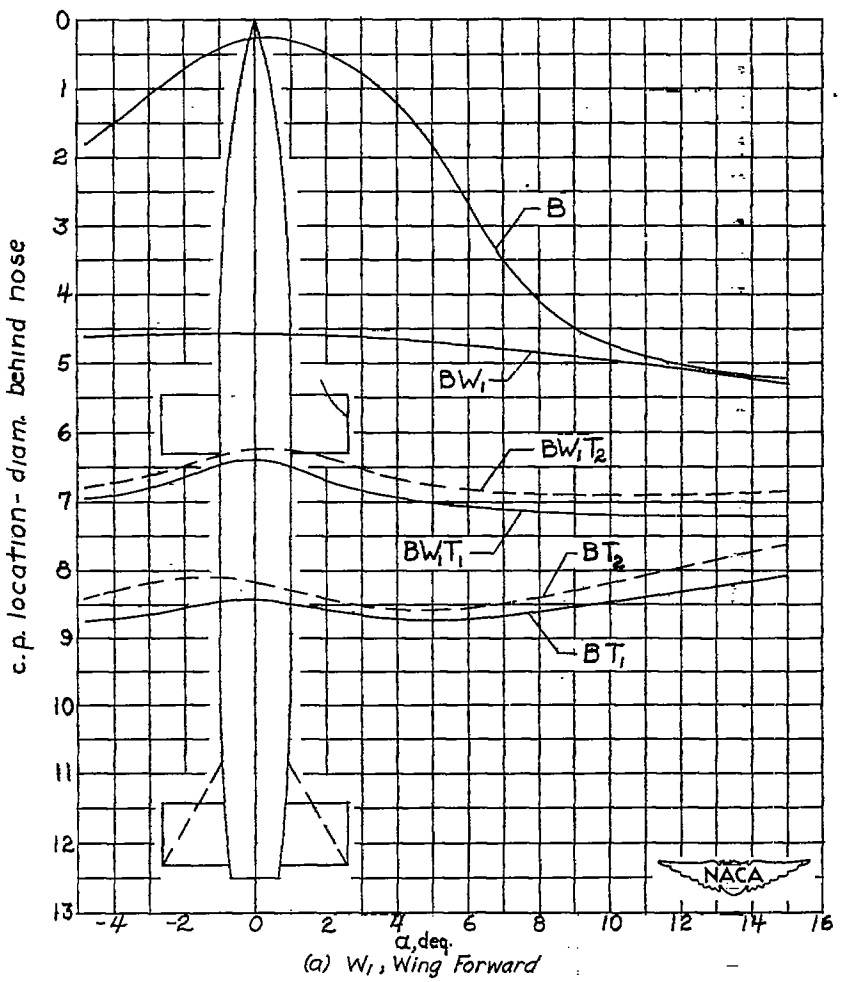

Figure 8.- Variation of center-of-pressure with angle of attack for all configurations. M = 1.93.

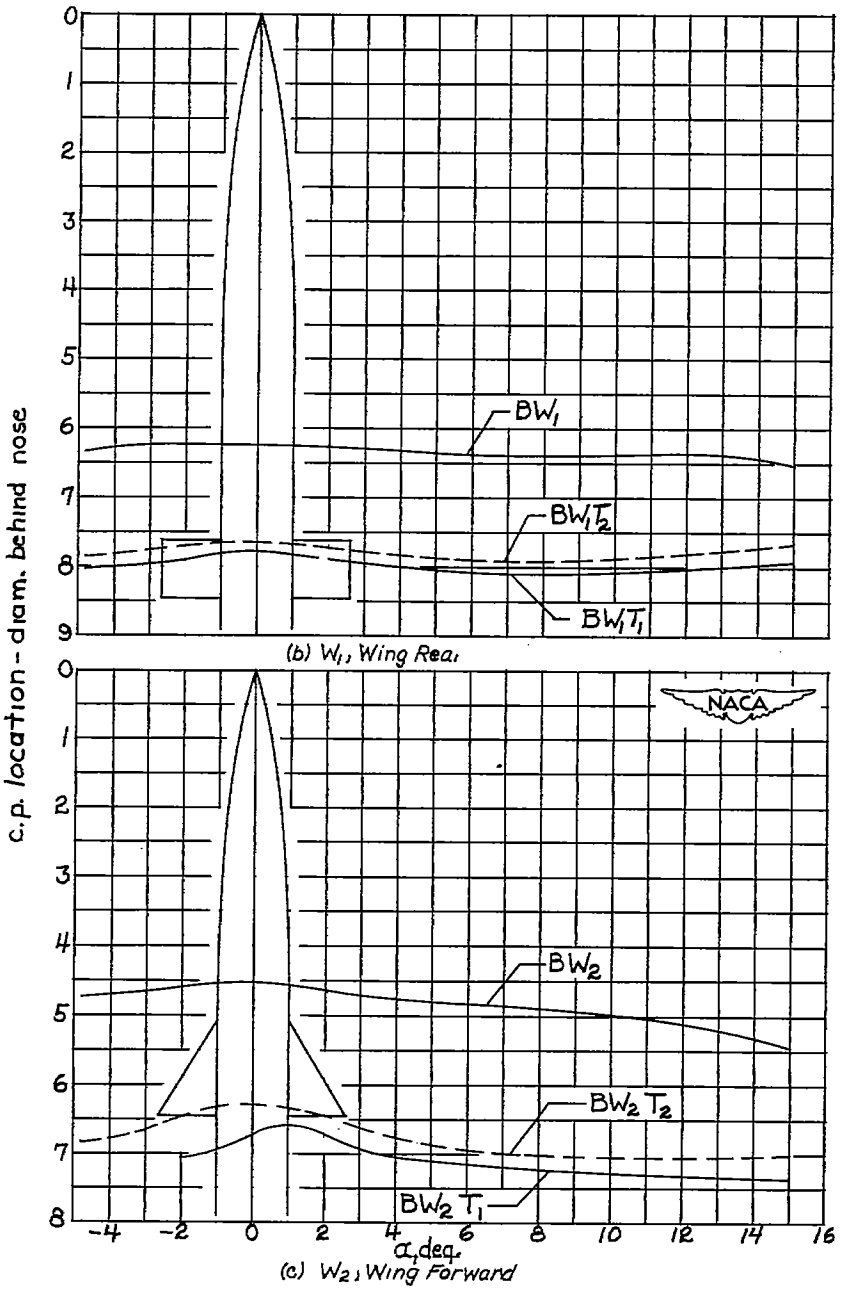

Figure 8.- Continued.

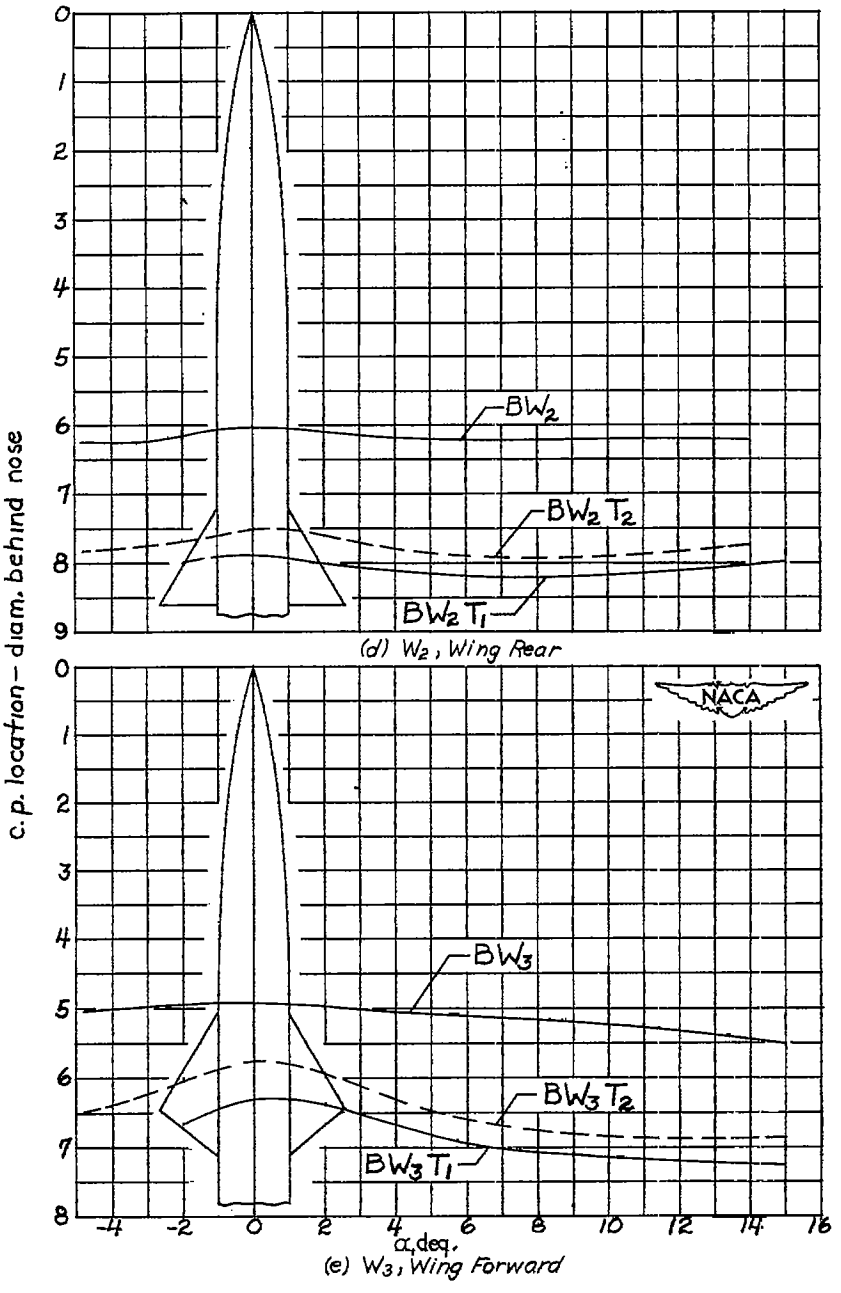

Figure 8.- Continued.

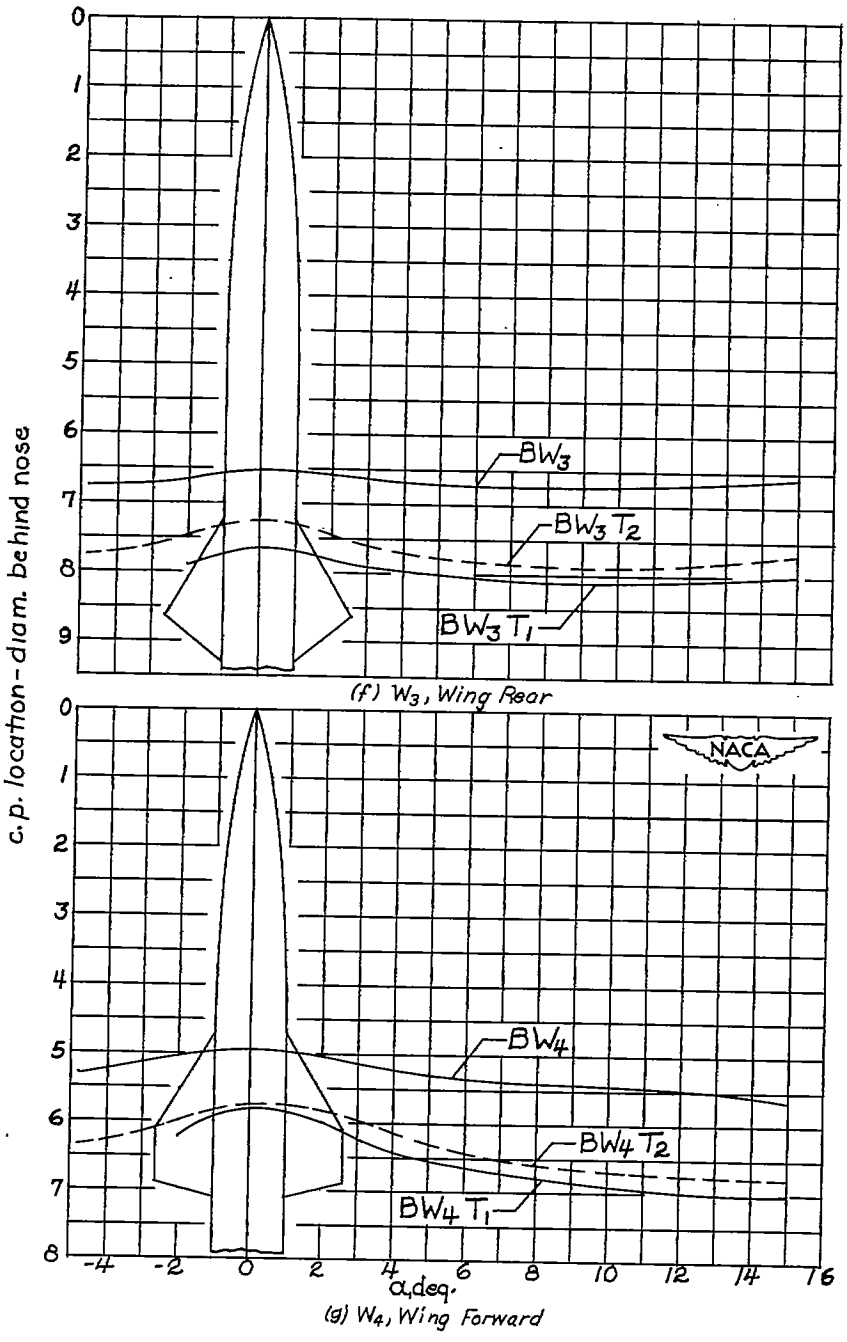

Figure 8.- Continued.

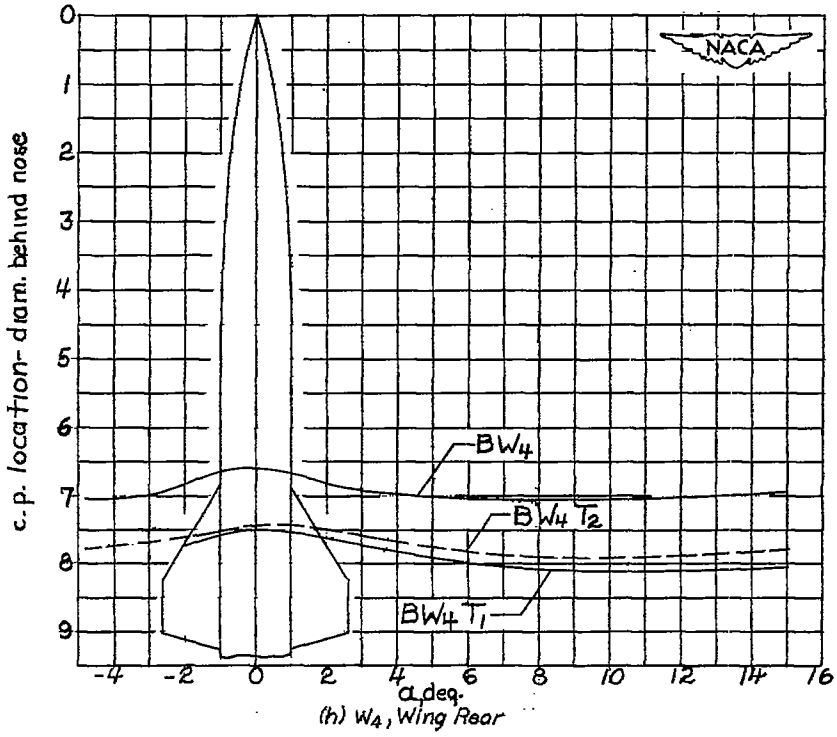

Figure 8.- Concluded.

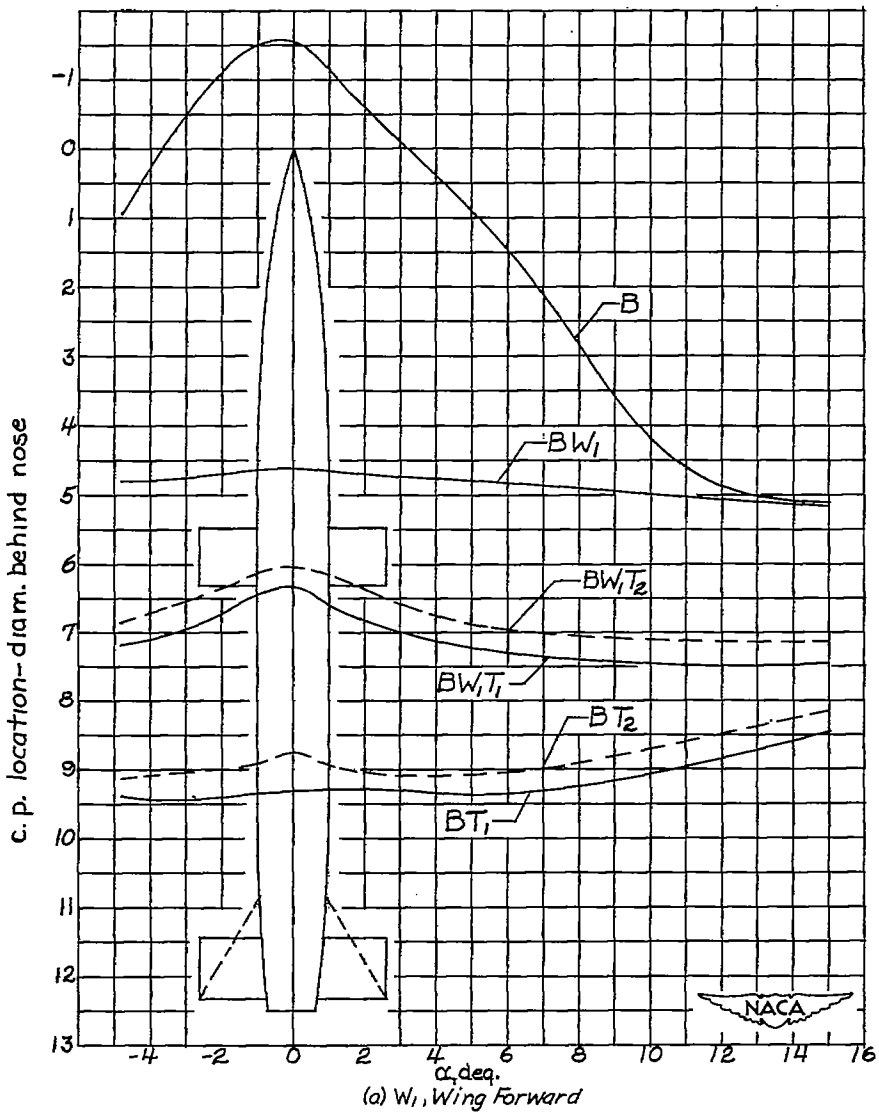

Figure 9.- Variation of center-of-pressure with angle of attack for all configurations. M = 1.62.

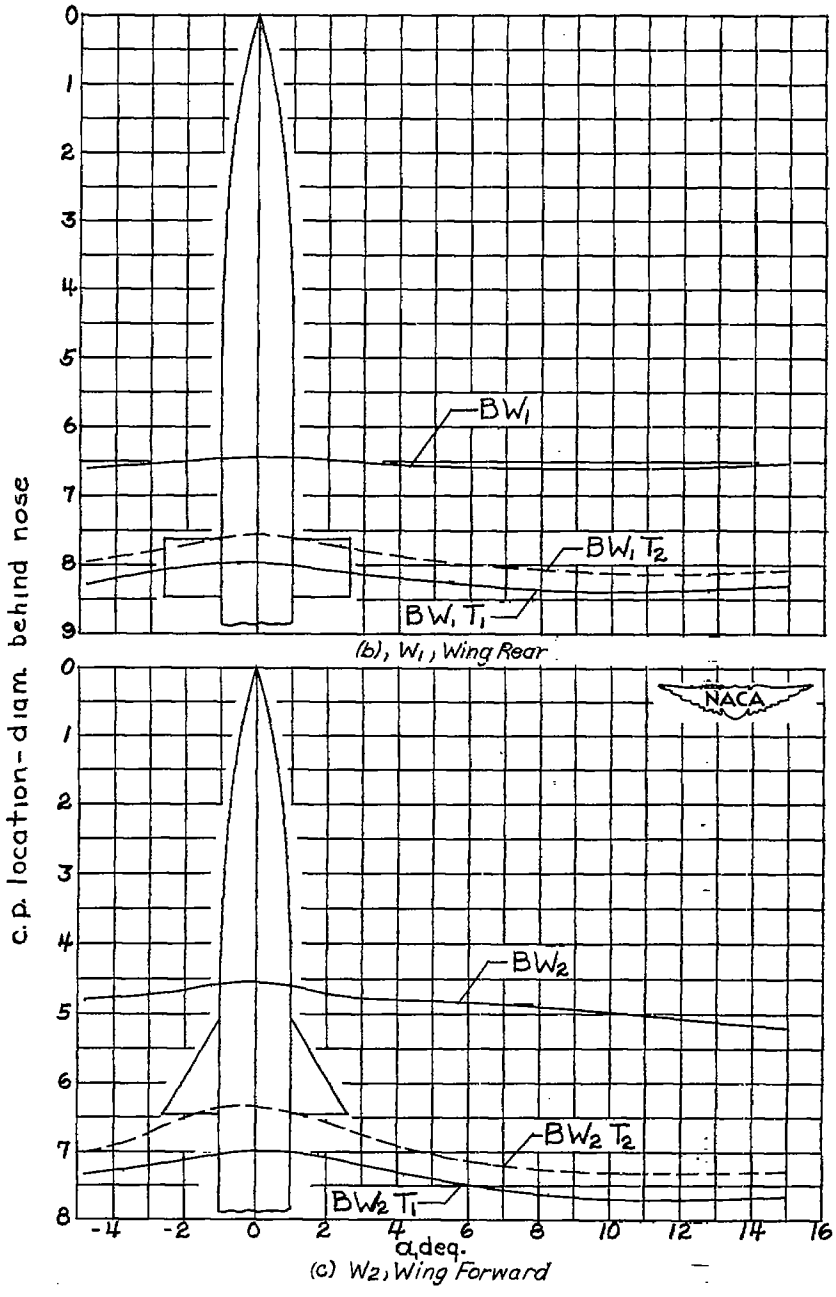

Figure 9.- Continued.

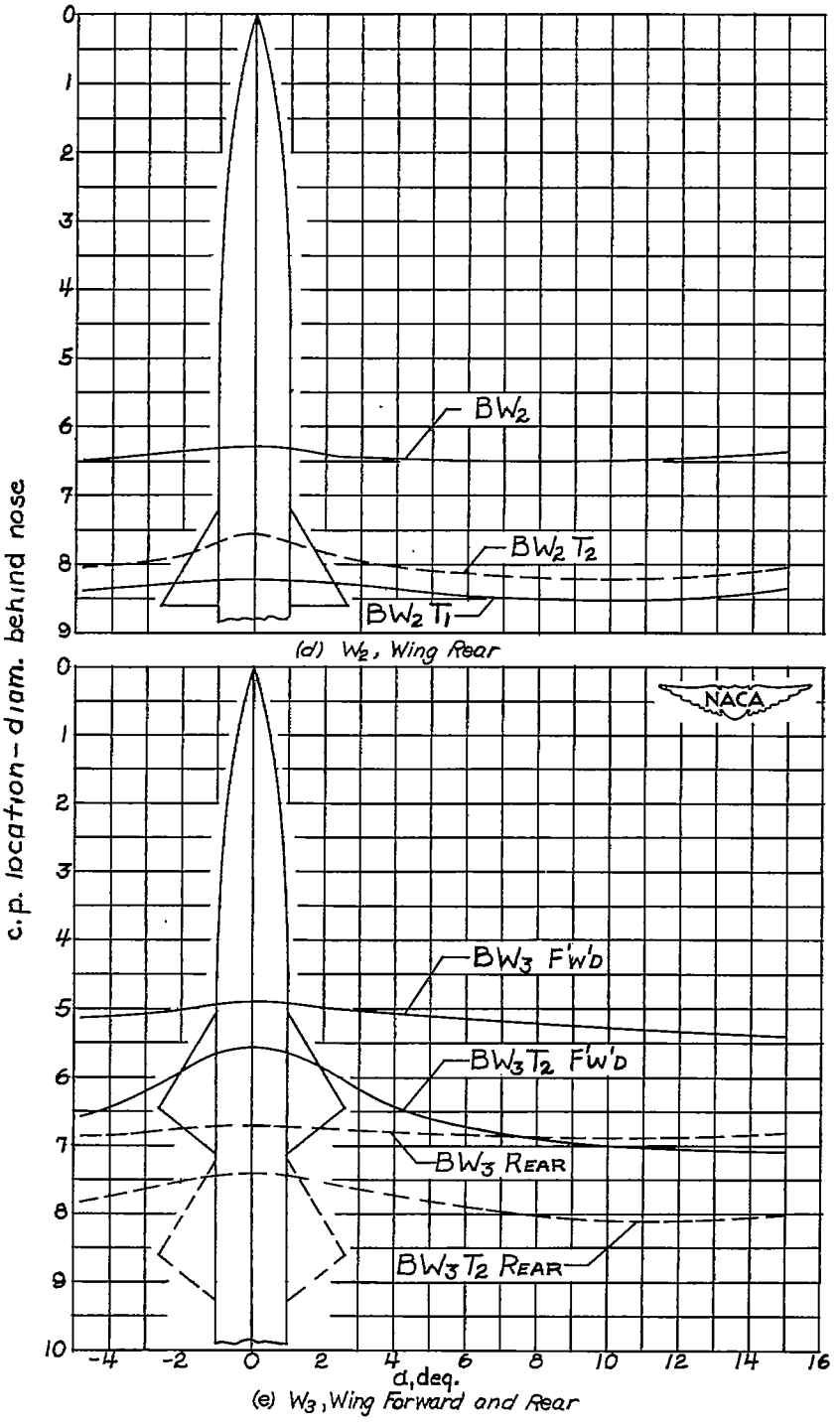

Figure 9.- Concluded.

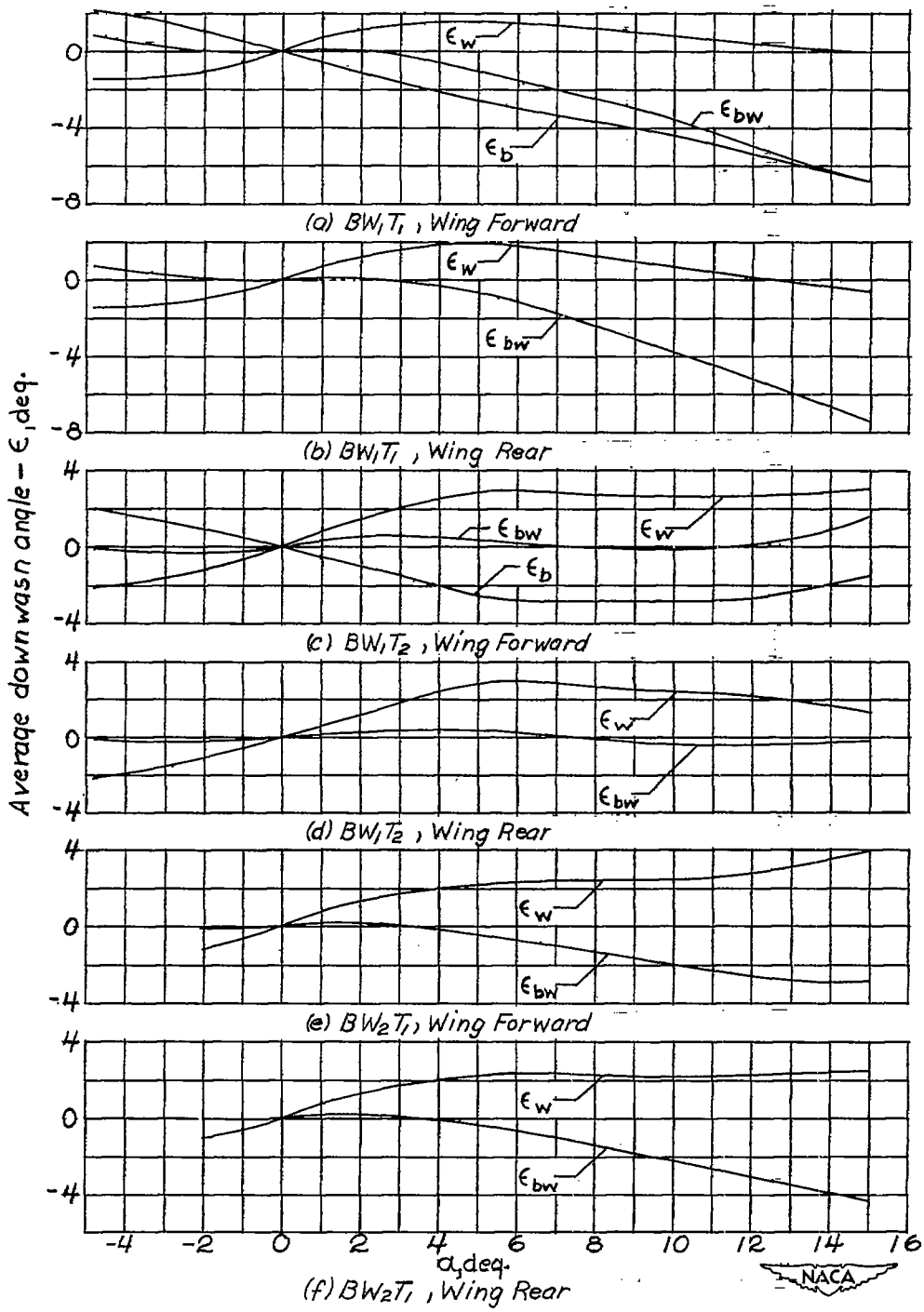

Figure 10.- Variation of average downwash angles with angle of attack. M = 1.93.

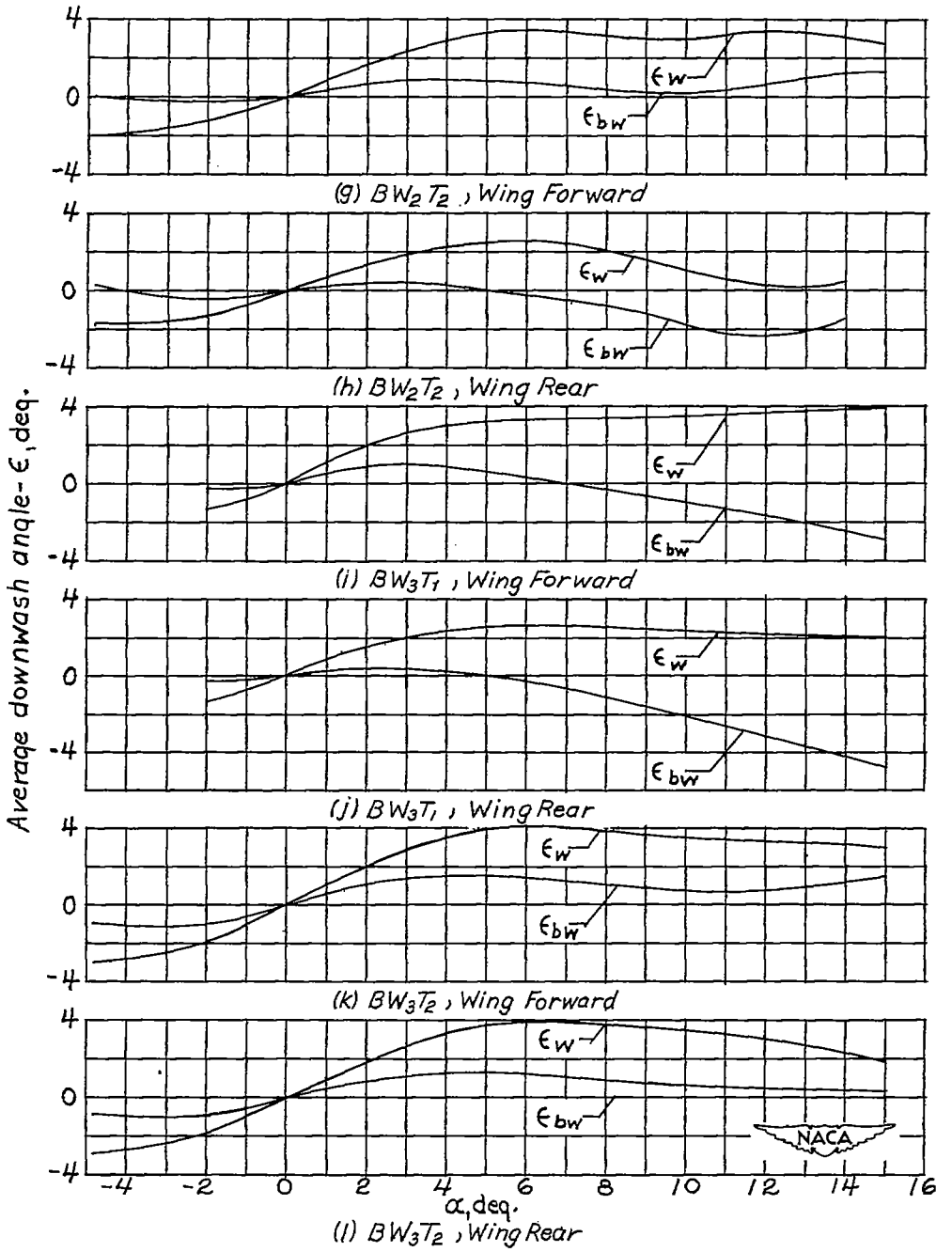

Figure 10.- Continued.

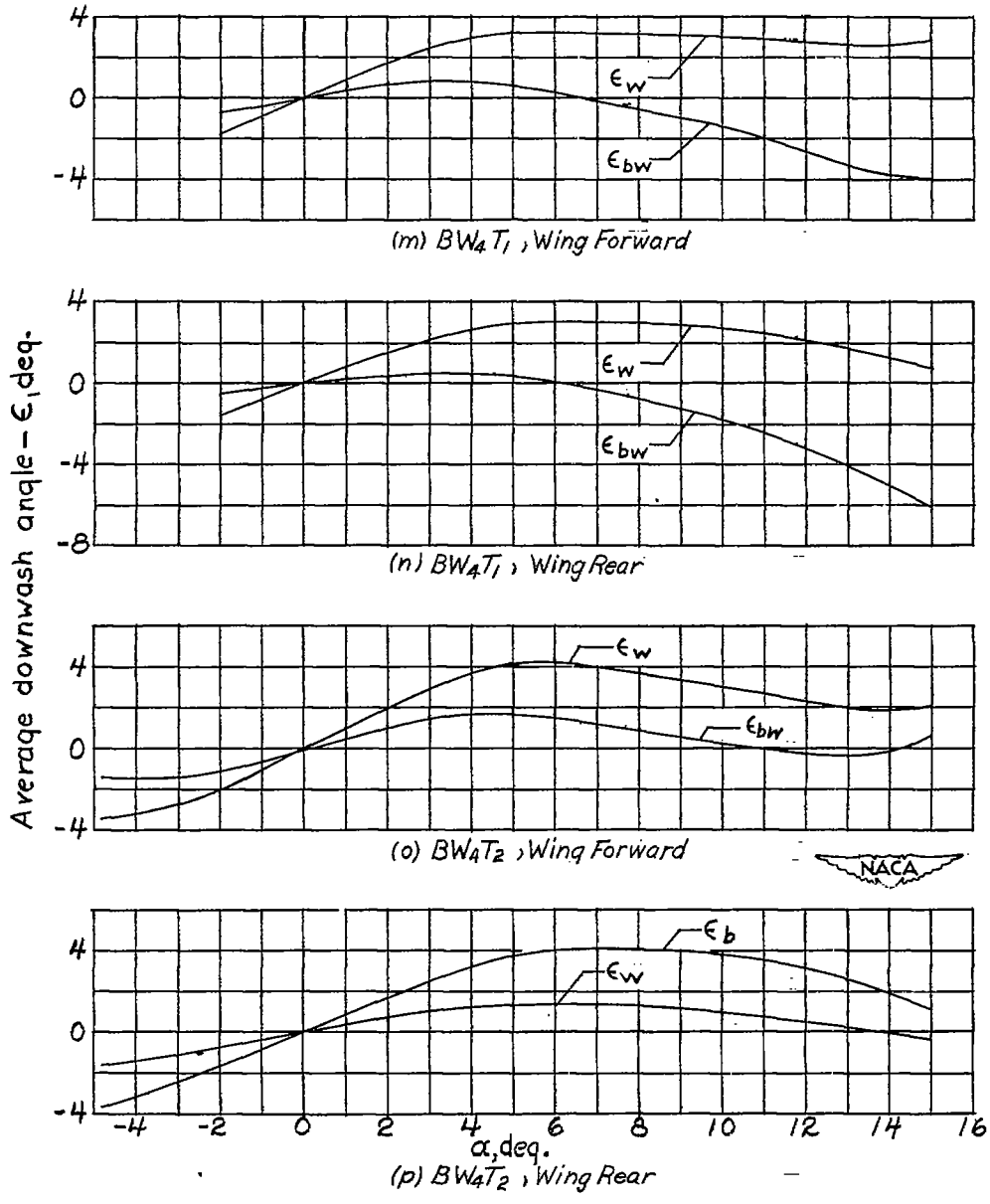

Figure 10.- Concluded.

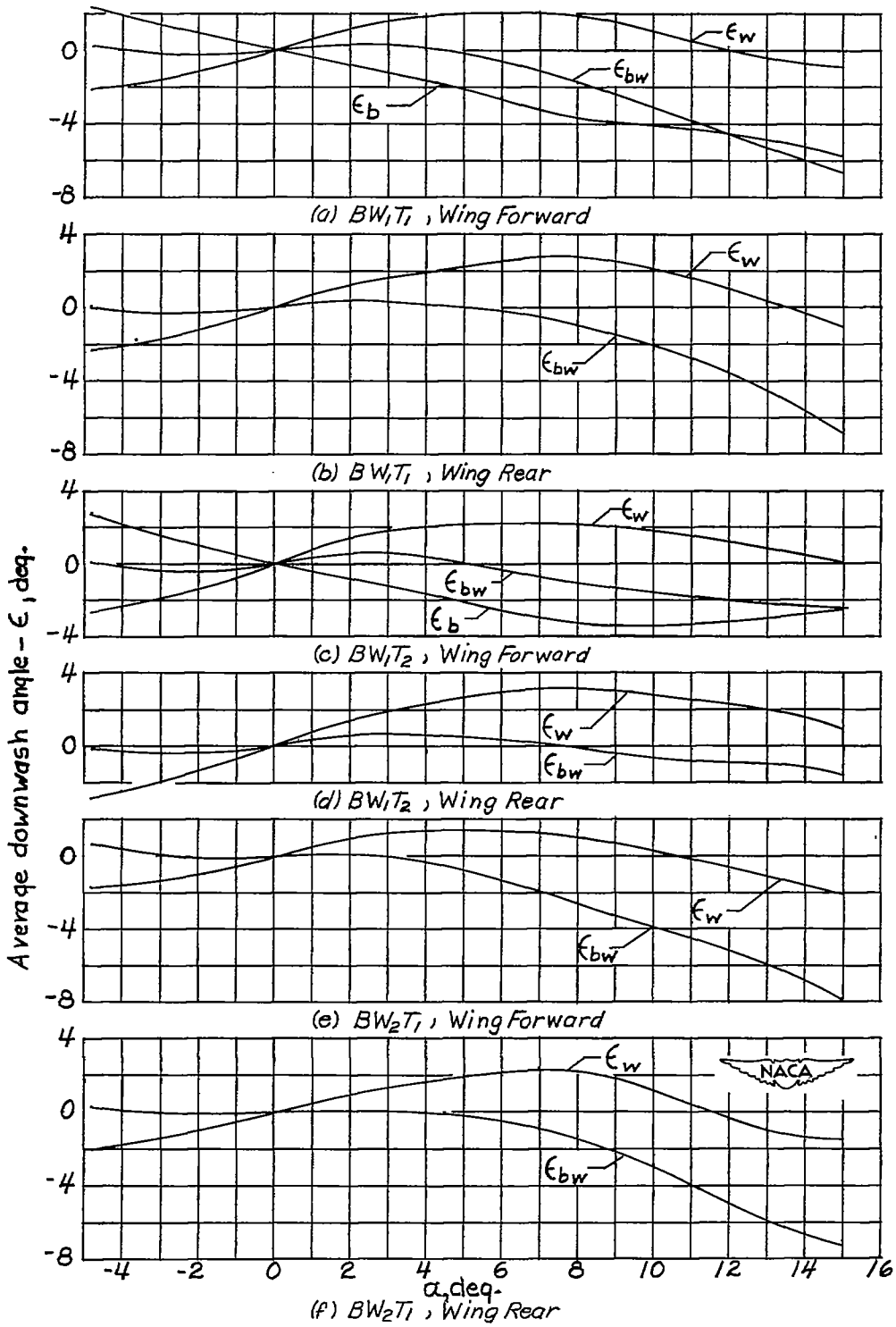

Figure 11.- Variation of average downwash angles with angle of attack. M = 1.62.

[redacted]

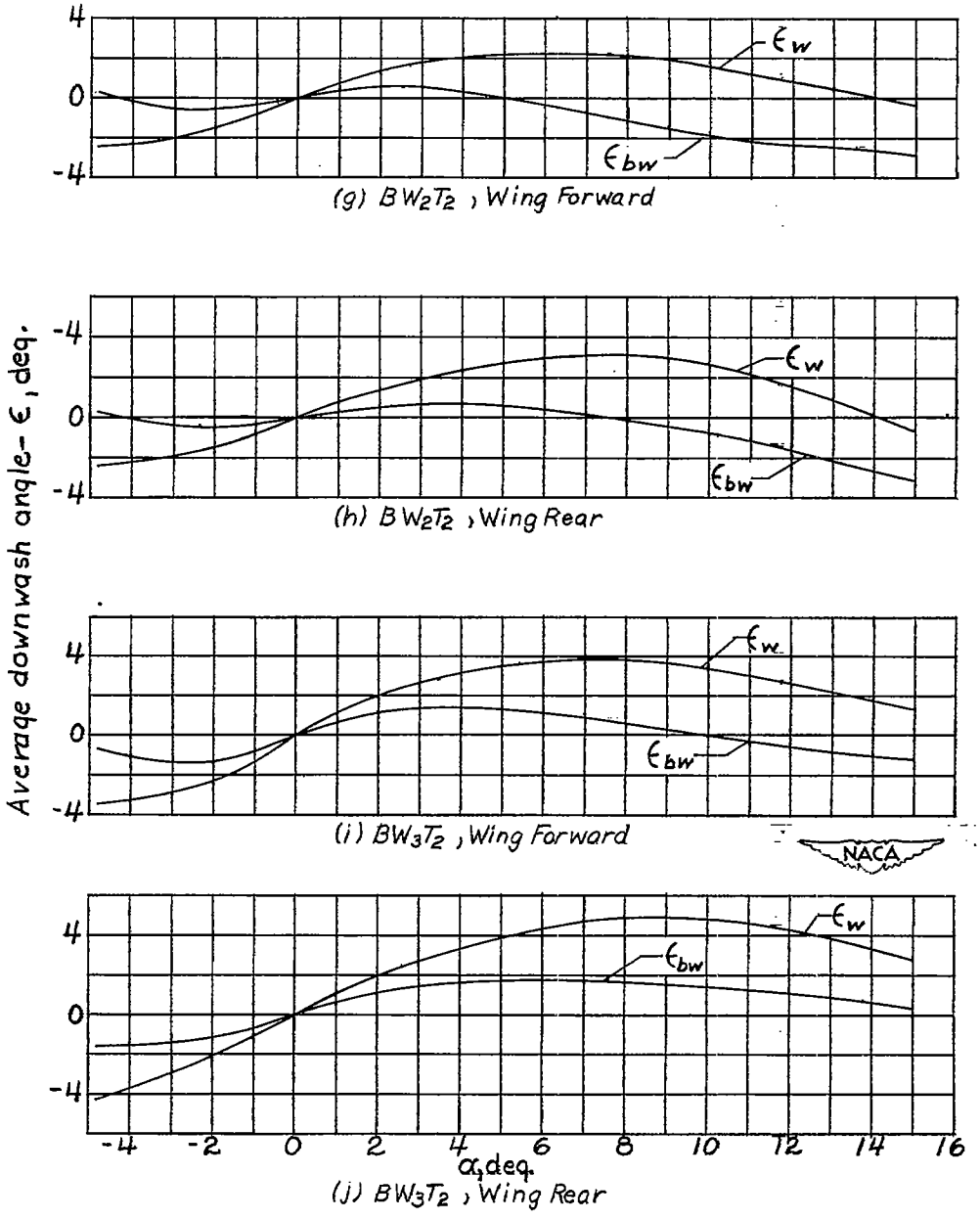

Figure 11.- Concluded.

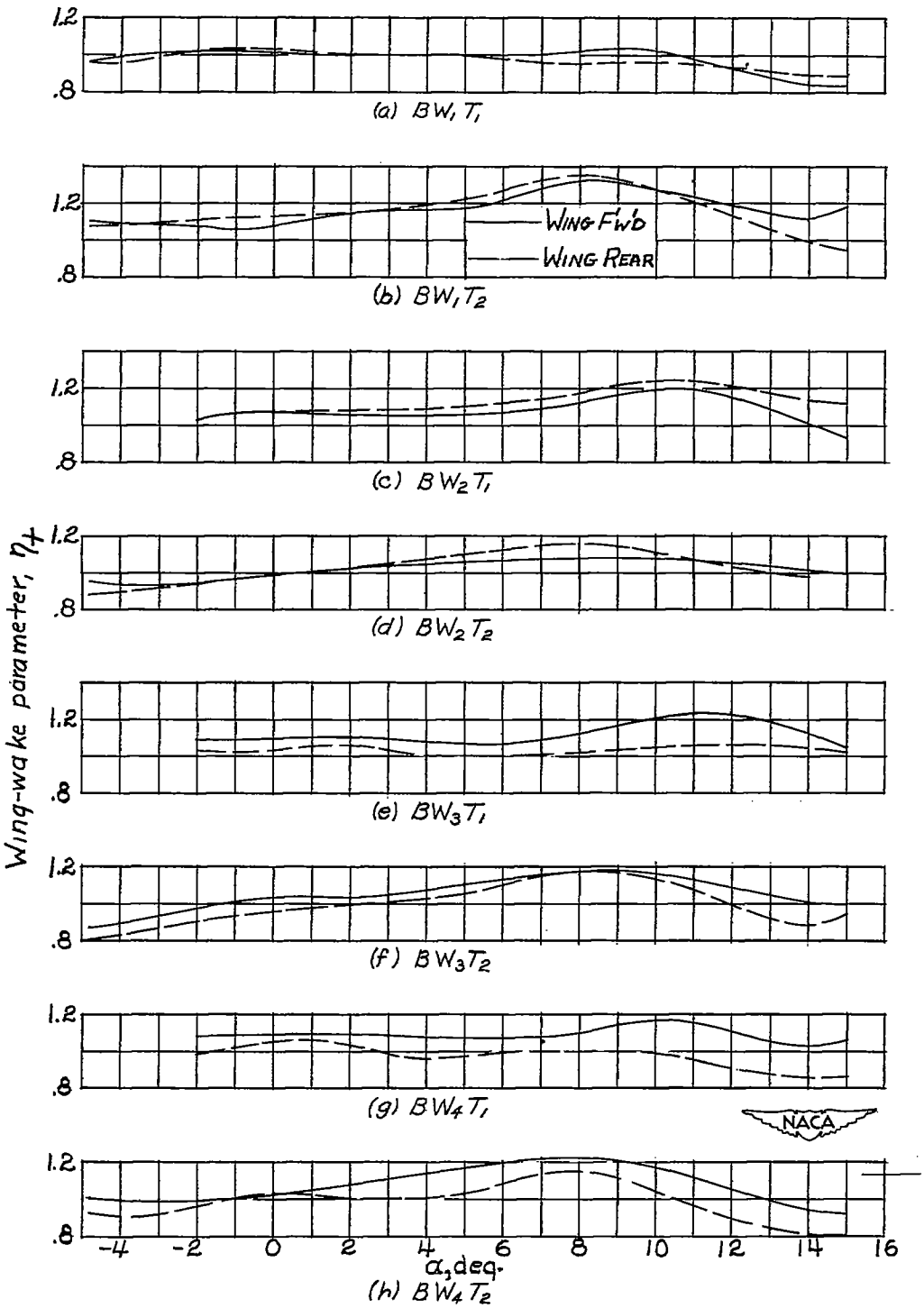

Figure 12.- Variation of wing-wake parameter η_t with angle of attack. M = 1.93.

[redacted]

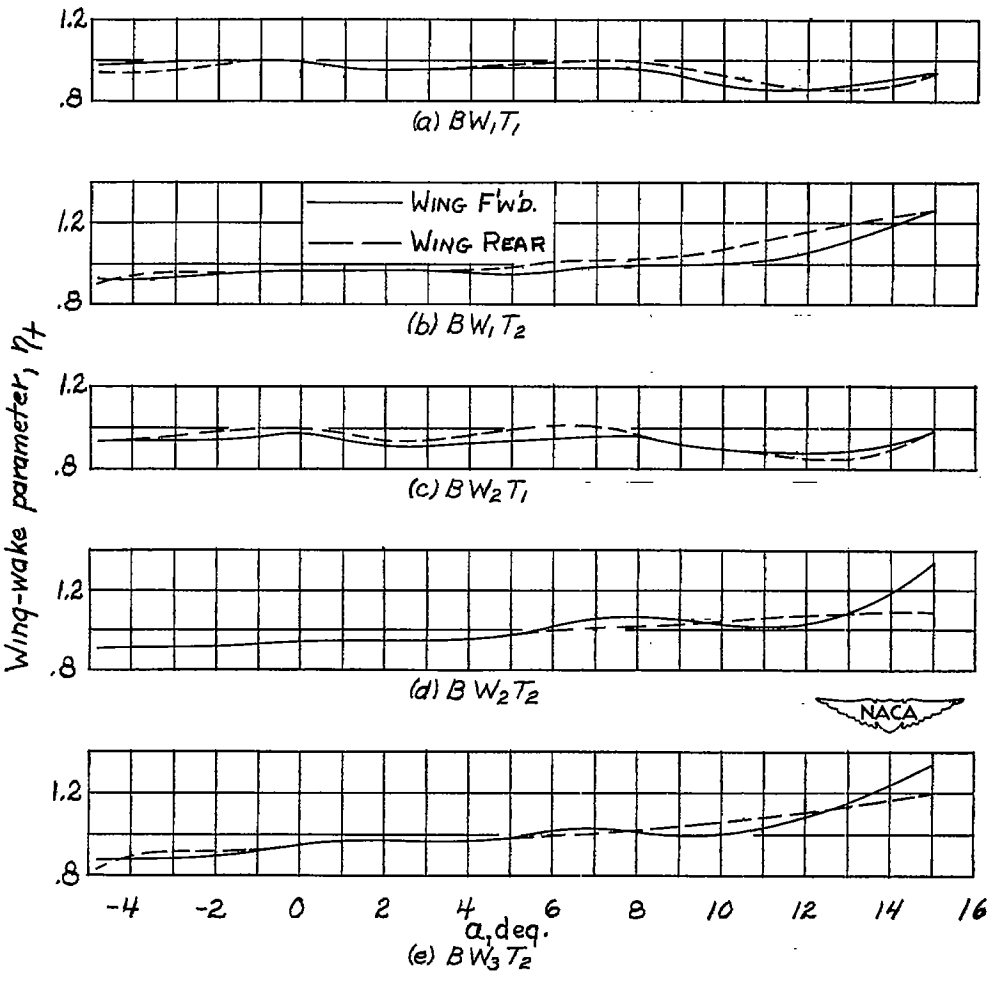

Figure 13.- Variation of wing-wake parameter η_t with angle of attack. M = 1.62.

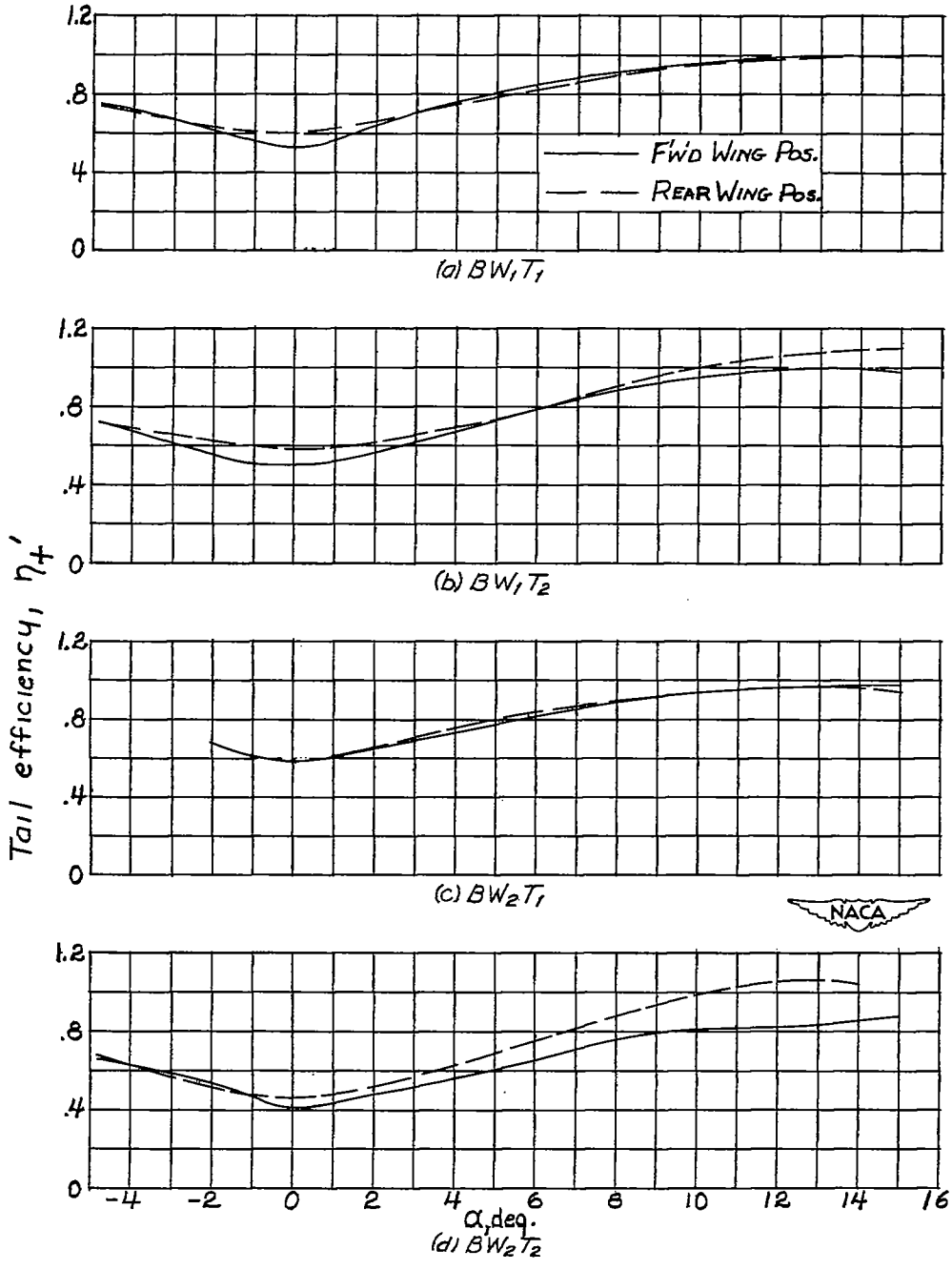

Figure 14.- Variation of tail efficiency η_t' with angle of attack. M = 1.93.

[redacted]

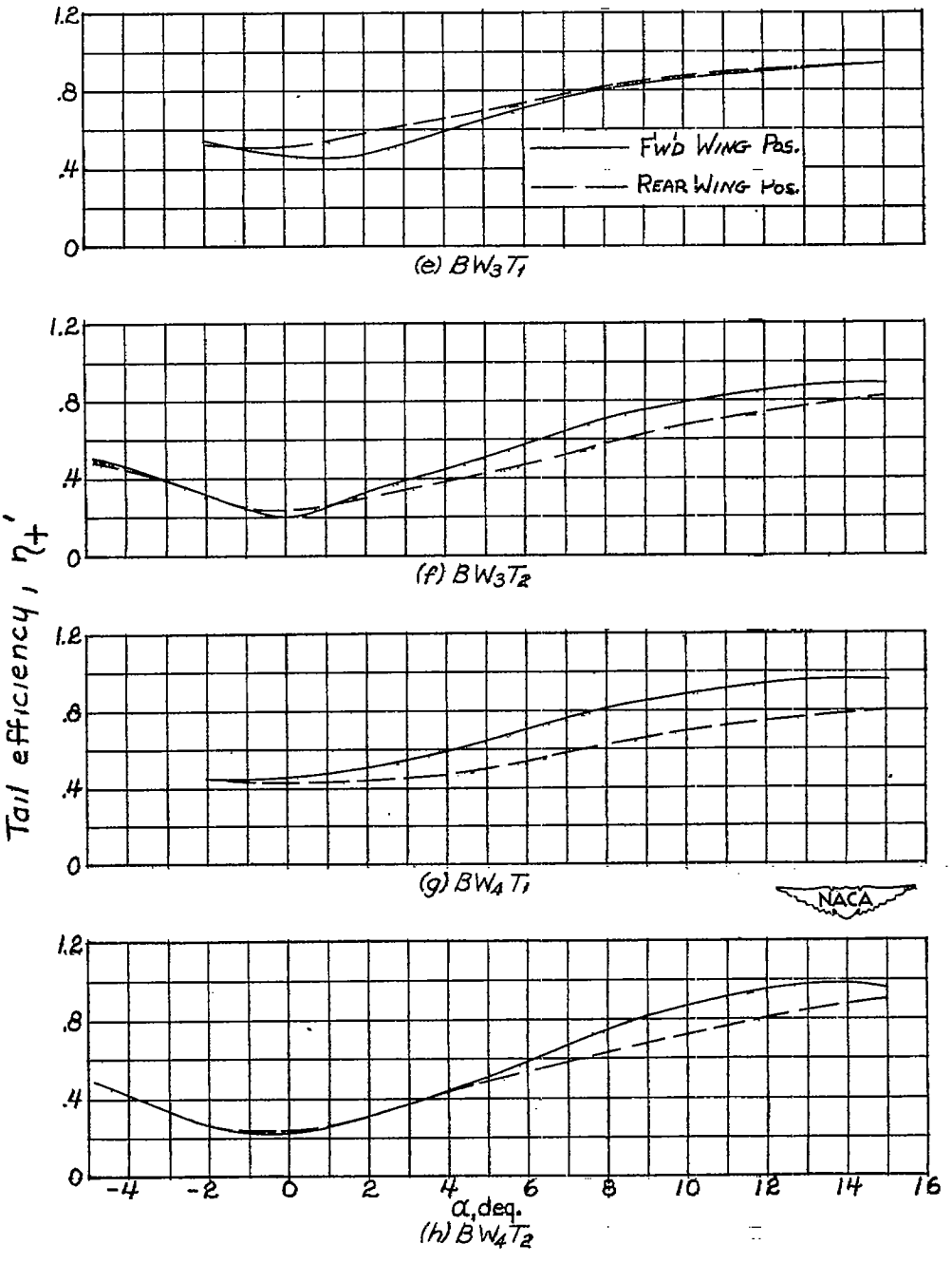

Figure 14.- Concluded.

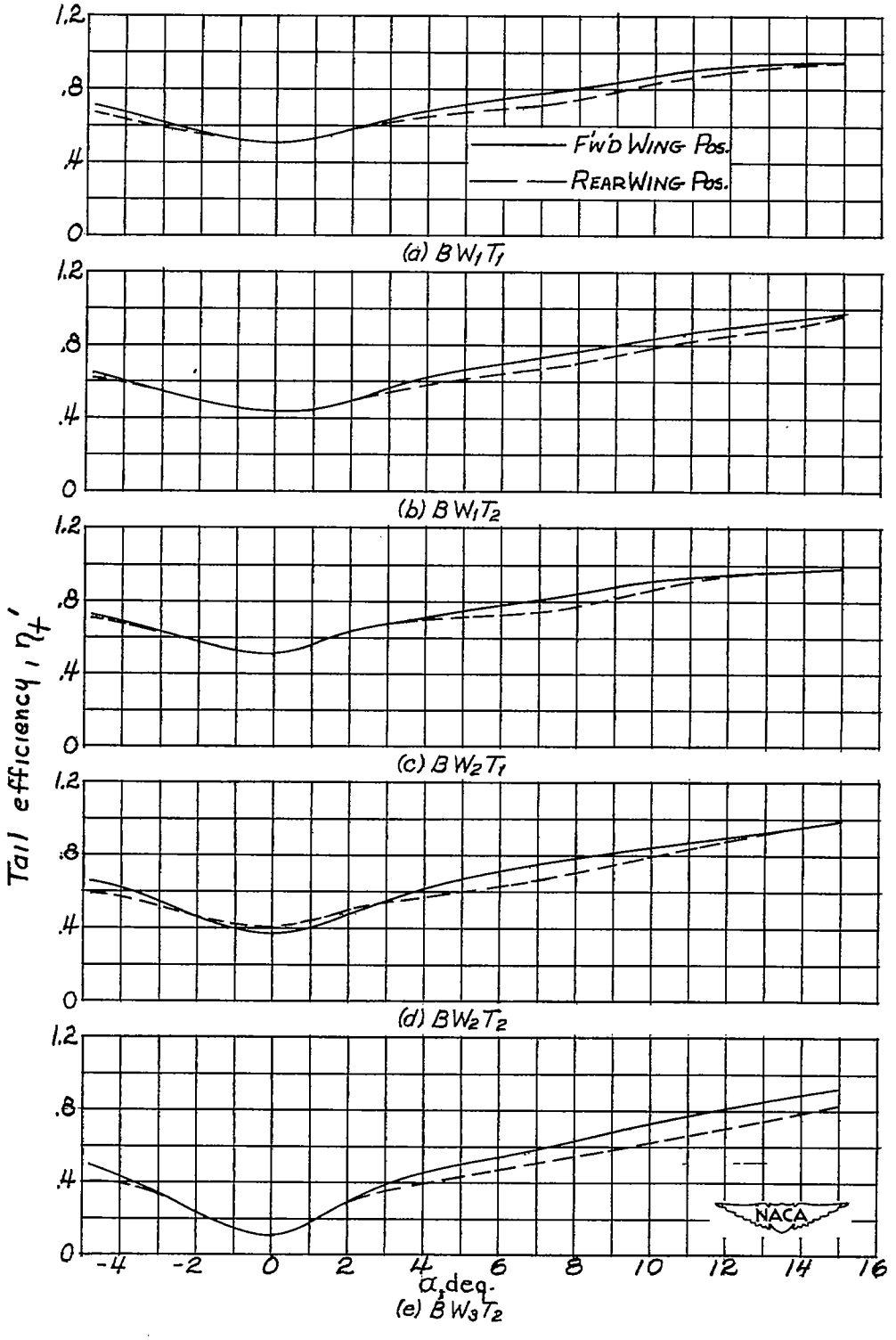

Figure 15.- Variation of tail efficiency η_t' with angle of attack. M = 1.62.